The Dissertation Committee for John David Wind Certifies that this is the approved version of the following dissertation:

Improving Polyimide Membrane Resistance to Carbon Dioxide Plasticization in Natural Gas Separations

Committee:

Donald R. Paul, Supervisor

William J. Koros, Co-Supervisor

Keith P. Johnston

Claudia Staudt-Bickel

Stephen E. Webber

C. Grant Willson

Improving Polyimide Membrane Resistance to Carbon Dioxide Plasticization in Natural Gas Separations

by

John David Wind, B.S.Ch.E., M.S.E.

Dissertation

Presented to the Faculty of the Graduate School of

The University of Texas at Austin

in Partial Fulfillment

of the Requirements

for the Degree of

Doctor of Philosophy

The University of Texas at Austin

December 2002

Dedication

To My Family and Shiva

Acknowledgements

I would like to sincerely thank Dr. Koros for his enthusiasm, support, and dedication towards my development as a researcher. He puts a tremendous amount of effort into providing opportunities for students to lean and grow. Even though his schedule is usually booked with activities, he always seems to find time for students to discuss new ideas, troubleshoot problems, and to critique papers and presentations. I have a much better understanding of the value in "telling a story" when presenting research results, due to his mentoring. I hope to carry his energy and positive attitude with me in my future endeavors.

Dr. Paul has also been an influential mentor to me over the last two years. His attention to detail and logical approach towards problem solving have had a significant impact on my critical thinking abilities. Being a member of his research group gave me a broader perspective on polymer science.

I also appreciate the rest of my committee's assistance with this project. Working with Dr. Staudt-Bickel over three summers has been valuable, especially in understanding the chemistry of membranes. It's a lot of fun to work with someone who has such a positive attitude. In addition, Dr. Willson and members of his research group (in particular Michael Stewart and Gerard Schmid) have been helpful with IR spectroscopy and molecular modeling. Collaboration with

Steve Sirard, Dr. Johnston, and Dr. Green on the *in-situ* spectroscopic ellipsometry has been very educational and productive. I would also like to thank Dr. Webber for serving on my committee and for teaching a good course on macromolecular science. Andreas Taubert and Dr. Winey at the University of Pennsylvania have been excellent collaborators on the ionomer characterization.

Members of the Koros research group have been great to work with and I have enjoyed becoming friends with them. Ryan Burns is an outstanding lab partner and friend, someone who puts a lot of effort into doing things right. His sense of humor and interest in a wide variety of subjects help to make work fun and interesting. De Vu is one of the most generous people I have known, always willing to help anybody out. I especially appreciate his help with computer issues. Rajiv Mahajan also provided good technical insight and good conversations. Finally, I would like to thank Channing Chen, Shilpa Damle, Randy Rife, Vonda Totten, T Stockman, Jim Smitherman, Kevin Haynes, and Keisha Steel.

Austin has been a wonderful place to spend the last four years. Shiva has been my best friend and I look forward to our future together. The EWRE gang (Matt, Caroline, Julie, Dave, Craig, Steph, Misti, Eddie, and many others), C. Moore, John and Shannon Sanchez, Ben Rathsack, Andrew Jamieson, Ward and Amy Engbrecht, Zen Mogri, Shilpa Damle, and Rhutesh Shah have been great friends. I'll miss the music, food, intramural games, Dialogue for Peace, and general wackiness of Austin…it's been a very good time!

Improving Polyimide Membrane Resistance to Carbon Dioxide Plasticization in Natural Gas Separations

Publication No._____

John David Wind, Ph.D.

The University of Texas at Austin, 2002

Supervisors: William J. Koros and Donald R. Paul

Polyimide membranes have been widely applied for gas separations due to their attractive permeability, selectivity, and processing characteristics. Their use for natural gas and hydrocarbon separations is limited by plasticization-induced selectivity losses in feeds with significant partial pressures of CO_2 and C_3+ hydrocarbons. This project focuses on understanding CO_2-induced plasticization of polyimide membranes and how it can be controlled by thermal annealing and crosslinking.

Covalent and ionic crosslinking are investigated as approaches for suppressing plasticization, while retaining attractive transport properties. A novel covalent crosslinking protocol has been developed, which offers significant advantages over the traditional post-treatment that was initially used. The two-step crosslinking treatment allows for spectroscopic characterization of the reaction yields in the monoesterification and transesterification reactions. These crosslinking reactions occur at temperatures well below the glass transition and no

additives are required in the casting solution, making the approach attractive for the eventual production of asymmetric hollow fibers.

The ionically crosslinked membranes are not as stable against CO_2 plasticization as the covalently crosslinked materials. By varying the ionic crosslinking density, the effects on long-term sorption and permeation at high CO_2 pressures were investigated. From STEM images, it does not appear that heterogeneity in the ion distribution is the cause of the membrane plasticization.

With covalent crosslinking, the copolymer composition, crosslinking agent, and thermal treatment are important factors in determining the final membrane transport properties. The crosslinking reaction is accompanied by a heat treatment that can also lead to stabilization of aromatic polyimides. These effects were decoupled by systematic variations in the polymer structure and thermal treatment.

In a plasticized membrane, the sorption, diffusion, and swelling processes are all interdependent. The key to controlling plasticization is to control the membrane swelling, since this is related to the increase in polymer chain segmental mobility facilitated by the CO_2 sorption. Mixed gas separations demonstrate the non-ideal factors that must be accounted for when modeling membrane performance over a wide range of pressures. The separation performance at practically relevant feed conditions is intrinsically better *and* more stable than the commercial polymeric membranes currently used for natural gas separations.

Table of Contents

List of Tables

List of Figures

Chapter 1: Introduction

1.1 GLASSY POLYMER GAS SEPARATION MEMBRANE APPLICATIONS

Gas separation membrane systems have been widely utilized due to their simplicity, modular nature, and attractive economics compared to more traditional separation technologies such as pressure swing adsorption (PSA) and cryogenic distillation. A comprehensive review of membrane formation, module design, and applications is given by Fleming and Koros [1].

Monsanto installed the first large-scale membrane systems (polysulfone) for hydrogen recovery from ammonia purge gas and refinery tail gas streams in the early 1980's. Air separation systems to produce 95-99% N_2 were introduced in the late 1980's. These systems produce N_2 for inerting fuel tanks, controlled atmosphere packaging for produce, and many other applications.

Membranes are also used for natural gas purification (CO_2, H_2O, H_2S removal), mainly with cellulose acetate polymers. However, these materials only have CO_2/CH_4 selectivities of 12 to 15 under typical operating conditions [2], well below the low-pressure mixed gas selectivity of ~ 30 for dense membranes with zero permeate pressure [3]. Much of the decline in performance is due to plasticization of the membrane by CO_2 and heavy hydrocarbons. The development of stable membranes with CO_2/CH_4 selectivities of 40 would significantly enhance the competitive position of membranes relative to alternate technologies such as amine scrubbing [2].

1.2 NATURAL GAS PROCESSING

Natural gas is the fastest growing primary energy source throughout the world and its use is projected to increase 75% by 2020 from the 2002 level [4]. Natural gas is a very versatile feedstock, since it can be converted into a variety of

products such as methanol, syngas (CO/H_2), and synthetic crude oil and diesel via Fisher-Tropsch catalysis. It is also a cleaner burning fuel than coal or fuel oils for power plants and home heating, thus reducing sulfur oxide, mercury, and particulate emissions.

As worldwide demand increases, new gas fields must be developed, many with high levels of CO_2. It is necessary to reduce CO_2 levels below 2 vol% from natural gas because it has no heating value and it causes corrosion in process equipment when in the presence of water (formation of carbonic acid). Amine absorption processes dominate the acid gas removal market, but membranes would be preferable in many cases if they can maintain good performance in the presence of aggressive feed streams. There are also significant economic advantages in building hybrid membrane/amine systems [5].

Hydrocarbon loss is a major cost to gas treatment plants, and it tends to be higher for membranes than for absorption processes. Glassy polymers such as polyimides tend to have good separation factors for CO_2 over hydrocarbons (principally methane, ethane, and propane in natural gas), but they cannot maintain this separation factor in feeds with high partial pressures of CO_2 and condensable (C_3+) hydrocarbons. These rigid polymers primarily rely on differences in penetrant diffusion coefficients as their separation mechanism. The CO_2 and heavy hydrocarbons tend to plasticize the membranes, a process in which the polymer chain segmental mobility is increased by the sorption of the plasticizing penetrants and the diffusion selectivity is reduced [6].

A recent field test showed that effective feed pretreatment is the most important factor for prolonging membrane life [7]. However, pretreatment costs can be very significant and periodically there are upset conditions where the pre-treatment systems fail and the membrane is exposed to liquid hydrocarbons and/or water. Water and hydrocarbon aerosols can get past coalescing filters and mist eliminators, consequently damaging the membranes. The development of more

solvent-resistant polymeric membranes would reduce the pre-treatment costs, reduce hydrocarbon loss to the permeate, extend the life of the membrane modules, and ultimately expand the market for membrane systems.

The development of plasticization-resistant copolyimide membranes is being investigated because there are 550 trillion SCF of natural gas in the lower 48 United States that cannot be processed due to high CO_2 content [8]. For a gas price of $3.00/MMBTU, this gas is worth ~ $1.3 trillion. In commercial applications of membrane-based CO_2/CH_4 separations, cellulose acetate polymers are most commonly used. A study of the separation of CO_2/CH_4 mixtures with cellulose acetate dense membranes showed significant plasticization at CO_2 partial pressure above 15 atm in the feed [3]. It has been shown that the membrane economics improve significantly as the permselectivity is increased [9], since hydrocarbon loss represents a significant operating cost. Moreover, significant capital costs are incurred for feed pre-treatment processes to prevent aromatic hydrocarbon exposure to the membranes, which has shown to be extremely detrimental to hollow fiber membranes in the field [7].

Membranes are economically and environmentally attractive alternatives to traditional CO_2 removal strategies such as amine absorption in many cases. They are portable and compact, making them valuable for offshore and remote-location gas processing. Membranes can also be combined with amine units for debottlenecking and process optimization. Typically the membrane unit would be used for the bulk separation, and the amine unit would remove the remaining CO_2 down to pipeline specifications [2] (< 2% CO_2 and < 4 ppm of H_2S [10]). Membranes can utilize the pressure driving force that is available at the wellhead to separate the CO_2 from the hydrocarbons, making the overall process quite efficient. It is energy-intensive to regenerate the amine solutions and there are environmental issues associated with spent amine disposal. In a membrane system the permeate may be re-injected into the gas reservoir, a potential strategy

for controlling emissions of greenhouse gases [11]. Operation at high permeate pressures is desirable from a CO_2 sequestration perspective, but it means that the average CO_2 concentration would be higher throughout the membrane, thus increasing the chances of plasticization. Moreover, as the CO_2 fraction in the feed increases, the membrane economics become more favorable, if the membrane performance remains stable. These two considerations underscore the importance of developing plasticization-resistant membranes.

1.3 POTENTIAL APPLICATIONS FOR ROBUST MEMBRANES

There are myriad applications for solvent-resistant polyimide membranes. For example, 1,3-butadiene is currently separated from mixed butenes and butanes by extractive distillation. Polyimide membranes have excellent separation factors for butadiene over butane (and presumably a good selectivity for butadiene over 1-butene, 2-butene and isobutene), but plasticization occurs at butadiene feed pressures above 0.5 atm at 50°C [12]. The development of robust membrane materials may allow these polyimides to maintain attractive separation properties at practically relevant feed pressures. Similar plasticization effects are seen for membrane separations of propylene/propane mixtures at 3 atm and 50°C [13].

Aromatic and aliphatic components in catalytically cracked naptha streams are also typically separated by extractive distillation. Pervaporation membranes offer a potentially simple, low-cost alternative or complementary separation technology to extractive distillation for these streams. Pervaporation would greatly benefit from the development of polymeric membranes that can withstand liquid organic feeds at temperatures of 120°C to 250°C [14]. Crosslinked polyimides have excellent thermal and chemical stability for these types of separations [15]. Fig. 1.1 shows a simple process flow diagram for the extractive

distillation process versus a membrane process. There may also be significant opportunity to build hybrid systems to debottleneck existing plants.

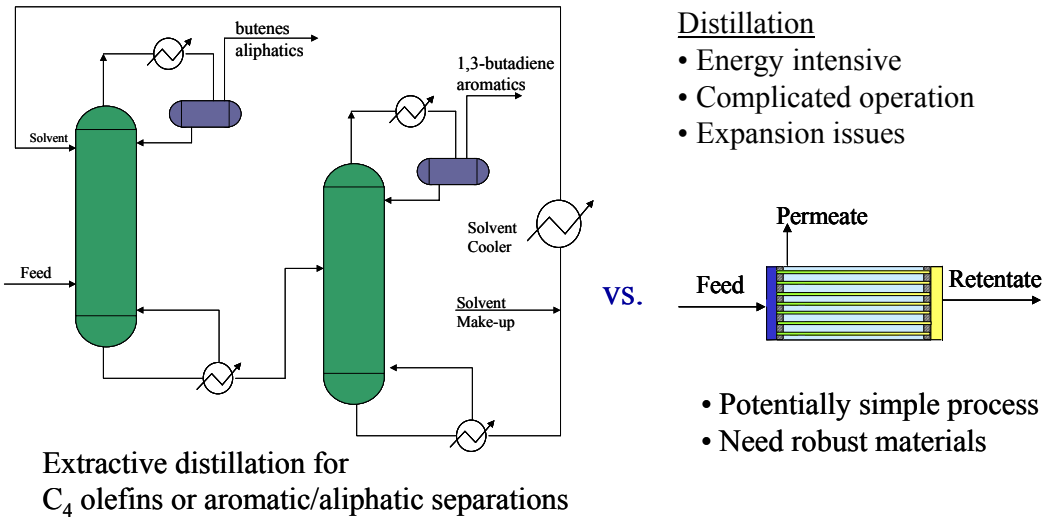

Figure 1.1: Comparison of extractive distillation and membrane processes

High-pressure CO_2 is also used in enhanced oil recovery applications, as shown in Fig. 1.2. The separation of hydrocarbons from the CO_2 is an extension of the natural gas purification that is the focus of this project. The harsh operating conditions involved require very robust membrane performance.

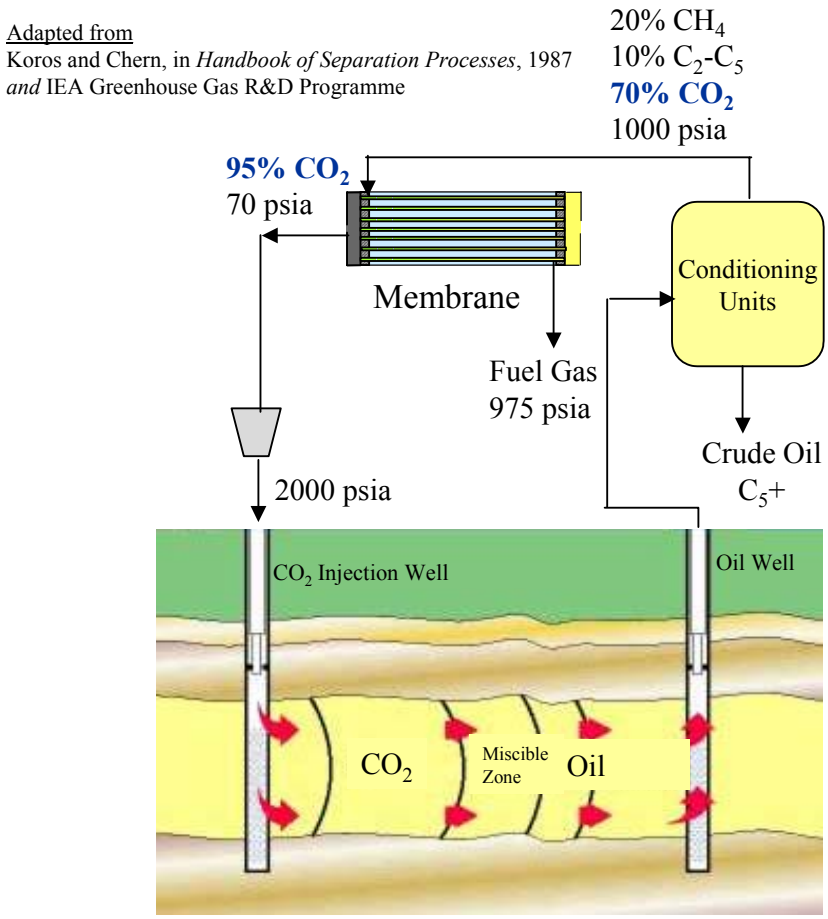

Figure 1.2: Membrane applications in CO_2 enhanced oil recovery

1.4 INDUSTRIAL GAS SEPARATION MEMBRANE PRODUCTION

Gas separation membranes are produced on an industrial scale by a phase inversion technique, in which hollow fibers are extruded from a spinnerette and then quenched in a water bath, as shown in Fig. 1.3 [16]. This process produces an asymmetric fiber with a dense skin on the outside that is responsible for the separation and a porous substructure that provides mechanical support. This morphology enables the packing of high surface area fiber bundles into small

volume modules. The thin skin allows for high gas throughput, since the flux is proportional to skin thickness for a given differential pressure driving force.

A particularly attractive process involves the formation of composite fibers through coextrusion of two polymers, one for the skin and one for the porous support [17]. The materials produced in our lab are relatively expensive compared to bulk commercial polymers such as polysulfone (Udel®), polyetherimide (Ultem®), and cellulose acetate. However, the composite morphology makes the costs reasonable, since the amount of polymer used for the skin is very small in comparison to that used for the support structure.

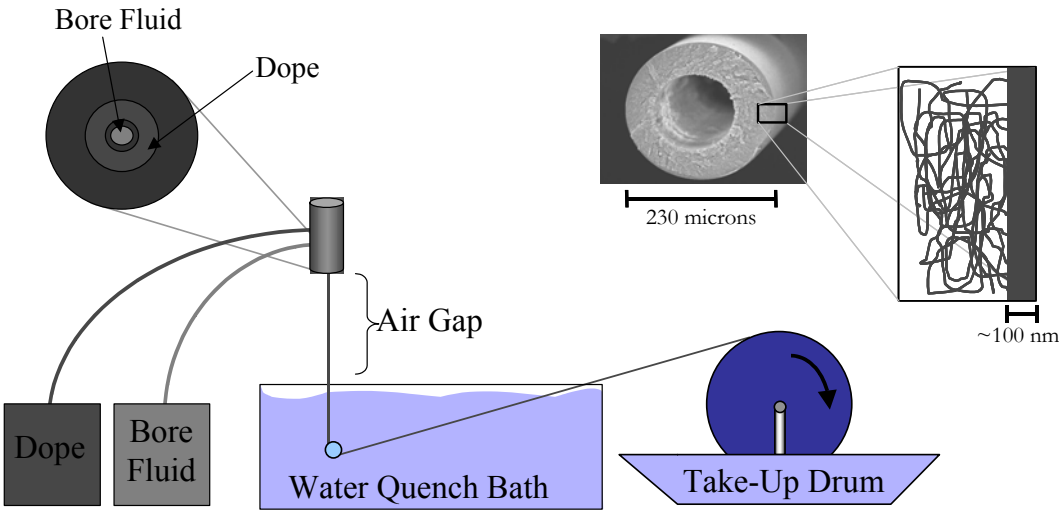

Figure 1.3: Formation of asymmetric hollow fiber membranes

1.5 MEMBRANE STABILIZATION STRATEGY

The goal of our work is to minimize plasticization-induced permselectivity losses by crosslinking high-performance polyimides within a framework that will likely fit into the existing industrial process for hollow fiber membranes. To make asymmetric hollow fibers from polyimides, these polymers need to be

soluble in common solvents such as 1-methyl-2-pyrrolidinone (NMP) and tetrahydrofuran (THF). Much research has been reported on polyimides derived from 4,4'-hexafluoroisopropylidene)diphthalic anhydride (6FDA), because they have excellent gas separation properties [18] and they are soluble in common solvents. There also have been reports of work directed toward spinning 6FDA-based polyimides into hollow fibers [19, 20]. The high solubility of these polymers is good from a processing standpoint, but it also means that they are particularly susceptible to plasticization, since plasticization involves significant swelling of the polymer matrix by the condensable components. The goal is to apply a post-treatment step involving thermal annealing and/or crosslinking that will stabilize the skin layer against plasticization. It has been shown that ultra-thin membranes (< 4 μm) tend to plasticize more easily thicker films [21], so the dense skin on the asymmetric fiber may be more sensitive and require more stabilization than the thick films (40-70 μm) studied in this project.

The work presented here has developed from the original work of Staudt-Bickel and Koros, who reported the synthesis of soluble polyimides that have a diamine monomer with a pendant carboxylic acid group which can be used to crosslink membranes via a post-treatment step (i.e., after membrane formation) [22]. These carboxylic acids were crosslinked with ethylene glycol and the monomer compositions were varied to tune the transport properties and the theoretical degree of crosslinking. Contrary to the conventional wisdom that crosslinking typically decreases the permeability [23], it was shown that the CO_2 permeability could be increased with crosslinking without sacrificing CO_2/CH_4 selectivity.

This project focuses on understanding how crosslinking stabilizes membranes against plasticization by probing the permeation, sorption, and swelling behavior. A simpler, more general crosslinking procedure has been developed that would be more easily implemented into the existing hollow fiber

production process than the original protocol. Techniques to quantify the crosslinking degree and to decouple the effects of thermal annealing and crosslinking (covalent and ionic) on long-term membrane stability have also been studied. The detailed research objectives are shown below.

1.6 RESEARCH OBJECTIVES

1. **Crosslink a polyimide with a variety of diol compounds to understand the effect of the diol structure on the membrane transport properties and the final degree of crosslinking**

The effects of crosslinking on the polymer chain packing and segmental mobility have a profound impact on the membrane transport properties. It is expected that the length and flexibility of the crosslinking agent affect the packing characteristics and the reactivity on the solid-state crosslinking reaction. With the new crosslinking protocol, the crosslinking reactions are broken up into two steps, monoesterification and transesterification (crosslinking) reactions, whereby the reaction yields can be analyzed at each step. The monoester conversion can be analyzed by ^{1}H-NMR and the crosslinked film can be analyzed with infrared spectroscopy (IR). The annealing temperature has a significant impact on the crosslinking conversion and the membrane transport properties. These effects are analyzed through permeation, sorption, fractional free volume, and X-ray diffraction characterization.

2. **Decouple effects of thermal annealing and covalent crosslinking on CO_2-induced plasticization by permeation and dilation measurements**

It has been shown that thermal annealing of aromatic polyimide films can have significant impacts on membrane stability against plasticization [24, 25] and on the CO_2/CH_4 selectivity [26]. These effects may be attributed to charge

transfer complexes between the electron donating diamine moiety and the electron accepting dianhydride fragment [27]. Incorporation 3,5-diaminobenzoic acid (DABA) into polyimides makes them more susceptible to stabilization by annealing. Therefore, it is of interest to measure the effects of annealing on the plasticization of the untreated and monoesterified (i.e., crosslinkable) membranes.

Simultaneous measurement of CO_2 sorption and dilation by *in-situ* spectroscopic ellipsometry [28] is a powerful technique to relate polymer structure to plasticization. Through our collaborative effort with Steve Sirard, Professor Peter Green, and Professor Keith Johnston, the effects of thermal annealing and chemical crosslinking can be decoupled to assess the effects on sorption, dilation, and diffusion as a function of CO_2 pressure and time. The non-Fickian relaxation-controlled plasticization can be analyzed to identify the key characteristics for stable membranes.

3. Investigate ionic crosslinking for plasticization resistance and membrane morphology

Polyimide ionomers are attractive materials because of their improved mechanical properties [29] and solvent resistance relative to the pure polyimides. Typically ions are added to the polyamic acid solution and the resulting film is cured at 300°C to finish the imidization [30, 31]. However, by copolymerizing DABA into a soluble polyimide, the carboxylic acid content can be tailored to see how the ion concentration (or crosslink density) affects the CO_2 plasticization.

Ionomers frequently contain ionic aggregates that arise from electrostatic interactions between ions [32]. The ion distribution can be probed directly by scanning transmission electron microscopy (STEM) [33, 34]. Dr. Andreas Taubert and Professor Karen Winey at the University of Pennsylvania have helped us analyze the ionomer morphologies with various ion contents through STEM, TEM, and small angle X-ray scattering (SAXS) analysis.

The carboxylic acid groups can be reacted with aluminum acetylacetonate [35, 36] at much lower temperatures (~ 130°C) than is typical for polyimide ionomers. The reaction conversion can be quantified by IR spectroscopy and the plasticization resistance is characterized by kinetic sorption and permeation at 40 atm feed pressure.

4. Measure the mixed gas separation properties of various membranes to evaluate effect of feed composition and pressure on CO_2/CH_4 separation factors

The permeation of gas mixtures through membranes is of great practical and fundamental interest. To assess the stability against plasticization, realistic, high-pressure separations are required. The CO_2/CH_4 separation factor can be affected by plasticization, non-ideal gas phase thermodynamics (affecting the driving forces for permeation), competitive sorption, and interacting flow processes (convective transport). The competitive sorption can be estimated through the Langmuir isotherm formalism, and for binary mixtures, the convective flow terms can be quantified from the model of Kamaruddin and Koros [37]. The separation of 50/50 CO_2/CH_4 mixtures up to 55 atm shows the effect of pressure on the CO_2/CH_4 separation factor and how these effects depend on the polymer structure.

It has been shown that small amounts of heavy hydrocarbons such as toluene can be detrimental to the polyimide membrane performance in natural gas separations [7, 38, 39]. Moreover, propane [13] and n-butane [12] can plasticize polyimide membranes at relatively low feed pressures. Therefore, the separation of more realistic natural gas mixtures is important to understand how various components can plasticize membranes and reduce the CO_2/CH_4 separation factor.

1.7 ORGANIZATION OF THE DISSERTATION

The dissertation contains eight chapters and two appendices. Chapter 2 gives background on membrane transport, sorption, diffusion, dilation, and plasticization. A short review of other stabilization approaches is also presented. In Chapter 3 the materials and experimental techniques are described. Chapter 4 discusses the effects of covalent crosslinking of various polyimides, along with quantification of the crosslink density by NMR and IR spectroscopy.

The effects of thermal annealing and covalent crosslinking on membrane stability are explored in Chapter 5. Spectroscopic ellipsometry was used to probe the sorption and dilation of various polyimides under high-pressure CO_2. These results are compared with the long-term kinetic permeation and sorption behavior to understand the relationship between plasticization and polymer structure.

The permeation and sorption behavior of two polyimide ionomers compared to the pure polyimides is explored in Chapter 6. Ion distributions in the polymer were imaged with STEM to understand how ion content is related to morphology and plasticization.

Chapter 7 describes CO_2/CH_4 separation properties for several mixtures, with and without hydrocarbons. The non-ideal transport effects were modeled by looking at competitive sorption, convective flow and non-ideal gas phase thermodynamics. Finally, in Chapter 8, conclusions are presented along with recommendations for future work.

REFERENCES

[1] Koros, W. J. and G. K. Fleming, Membrane-based gas separation, *J. Membr. Sci.*, **1993**, *83*, 1-80.

[2] Baker, R. W., Future directions of membrane gas separation technology, *Ind. Eng. Chem. Res.*, **2002**, *41*, 1393-1411.

[3] Houde, A. Y., B. Krishnakumar, S. G. Charati and S. A. Stern, Permeability of dense (homogeneous) cellulose acetate membranes to methane, carbon dioxide, and their mixtures at elevated pressures, *J. Appl. Polym. Sci.*, **1996**, *62*, 2181-2192.

[4] Energy Information Administration, *International Energy Outlook 2001*, DOE/EIA-0484, Washington, D.C. March 2001, p. 43.

[5] Bhide, B. D., A. Voskericyan and S. A. Stern, Hybrid processes for the removal of acid gases from natural gas, *J. Membr. Sci.*, **1998**, *140*, 27-49.

[6] Koros, W. J. and M. W. Hellums, Transport Properties, in *Encycl. Polym. Sci. Eng.*, **1990**, John Wiley and Sons, New York, *Suppl. Vol.*, pp. 724-802.

[7] Ratcliffe, C. T., A. Diaz, C. Nopasit, and G. Munoz, Application of membranes in CO_2 separation from natural gas: pilot plant tests on offshore platforms, presented at the Laurence Reid Gas Conditioning Conference, Norman, OK, Feb. 21-24, 1999.

[8] Meyer, H. S., Volume and distribution of subquality natural gas in the United States, Gas Research Institute, Chicago, IL, 2000.

[9] Bhide, B. D. and S. A. Stern, Membrane processes for the removal of acid gases from natural gas. II. effects of operating conditions, economic parameters, and membrane properties, *J. Membr. Sci.*, **1993**, *81*, 239-252.

[10] Spillman, R., Economics of gas separation membrane processes, in *Membrane Separations Technology. Principles and Applications*, Noble, R. D. and Stern, S. A.; Ed, Elsevier Science, Amsterdam, 1995, pp. 589-667.

[11] Parson, E. A. and D. W. Keith, Fossil fuels without CO_2 emissions, *Science*, **1998**, *282*, 1053-1054.

[12] Okamoto, K., K. Noborio, J. Hao, K. Tanaka and H. Kita, Permeation and separation properties of polyimide membranes to 1,3-butadiene and n-butane, *J. Membr. Sci.*, **1997**, *134*, 171-179.

[13] Tanaka, K., A. Taguchi, J. Hao, H. Kita and K. Okamoto, Permeation and separation properties of polyimide membranes to olefins and paraffins, *J. Membr. Sci.*, **1996**, *121*, 197-207.

[14] National Research Council, *Separations Technologies for the Industries of the Future*, National Academy Press, Washington D.C., 1998.

[15] Jizhong, R., C. Staudt-Bickel and R. N. Lichtenthaler, Separation of aromatics/aliphatics with crosslinked 6FDA-based copolyimides, *Sep. and Purif. Tech.*, **2001**, *22-23*, 31-43.

[16] Wallace, D. W., Crosslinked hollow fiber membranes:Implementation challenges and solutions for natural gas processing, presented at Separations Research Program Conference, Austin, TX, April 16, 2002.

[17] Ekiner, O. M., R. A. Hayes and P. Manos, Multicomponent gas separation membranes, U.S. Patent 5,085,676, E. I. du Pont de Nemours and Co., USA, 1992.

[18] Kim, T. H., W. J. Koros, G. R. Husk and K. C. O'Brien, Relationship between gas separation properties and chemical structure in a series of aromatic polyimdes, *J. Membr. Sci.*, **1988**, *37*, 45-62.

[19] Chung, T.-S., E. R. Kafchinski and R. Vora, Development of a defect-free 6FDA-durene asymmetric hollow fiber and its composite hollow fibers, *J. Membr. Sci.*, **1994**, *88*, 21-36.

[20] Kawakami, H., M. Mikawa and S. Nagaoka, Gas transport properties of asymmetric polyimide membrane with an ultrathin surface skin layer, *Macromolecules*, **1998**, *31*, 6636-6638.

[21] Wessling, M., M. L. Lopez and H. Strathmann, Accelerated plasticization of thin-film composite membranes used in gas separation, *Sep. and Purif. Tech.*, **2001**, *24*, 223-233.

[22] Staudt-Bickel, C. and W. J. Koros, Improvement of CO_2/CH_4 separation characteristics of polyimides by chemical crosslinking, *J. Membr. Sci.*, **1999**, *155*, 145-154.

[23] Bos, A., I. Punt, H. Strathmann and M. Wessling, Suppression of gas separation membrane plasticization by homogeneous polymer blending, *AIChE J.*, **2001**, *47*, 1088-1093.

[24] Bos, A., I. G. M. Punt, M. Wessling and H. Strathmann, Plasticization-resistant glassy polyimide membranes for CO_2/CH_4 separations, *Sep. and Purif. Tech.*, **1998**, *14*, 27-39.

[25] Krol, J. J., M. Boerrigter and G. H. Koops, Polyimide hollow fiber gas separation membranes: Preparation and the suppression of plasticization in propane/propylene environments, *J. Membr. Sci.*, **2001**, *184*, 275-286.

[26] Kawakami, H., M. Mikawa and S. Nagaoka, Gas transport properties in thermally cured aromatic polyimide membranes, *J. Membr. Sci.*, **1996**, *118*, 223-230.

[27] Salley, J. M. and C. W. Frank, Charge transfer in aromatic polyimides, in *Polyimides: Fundamentals and Applications*, Marcel Dekker, Inc., New York, 1996.

[28] Sirard, S. M., P. F. Green and K. P. Johnston, Spectroscopic ellipsometry investigation of the swelling of poly(dimethylsiloxane) thin films with high pressure carbon dioxide, *J. Phys. Chem. B*, **2001**, *105*, 766-772.

[29] St. Clair, A. K. and L. T. Taylor, A comparison of physical and mechanical properties of polyimide films containing different metal ions, *J. Appl. Polym. Sci.*, **1983**, *28*, 2393-2400.

[30] Thompson, D. W., M. L. Caplan and A. K. St. Clair, Reflective self-metalizing polyimide films, U. S. Patent 5,677,418, United States National Aeronautics and Space Administration, USA, 1997.

[31] Ono, K., M. Nishinaka and R. Akahori, Metal-containing polyamic acid compositions, polyimide films, their manufacture, polyimide moldings, and flexible printed circuit boards thereof, U.S. Patent 1,130,2375, Kanegafuchi Chemical Industry Co., Ltd., Japan, 1999.

[32] Eisenberg, A., B. Hird and R. B. Moore, A new multiplet-cluster model for the morphology of random ionomers, *Macromolecules*, **1990**, *23*, 4098-4107.

[33] Laurer, J. H. and K. I. Winey, Direct imaging of ionic aggregates in Zn-neutralized poly(ethylene-co-methacrylic acid) copolymers, *Macromolecules*, **1998**, *31*, 9106-9108.

[34] Winey, K. I., J. H. Laurer and B. P. Kirkmeyer, Ionic aggregates in partially Zn-neutralized poly(ethylene-ran-methacrylic acid) ionomers: shape, size, and size distribution, *Macromolecules*, **2000**, *33*, 507-513.

[35] Akkerman, J. M., A cross-linking mechanism of poly-acrylics with aluminum compounds, XVIIeme Congres Federation d'Associations de Techniciens des Industries des Peintures, Vernis, Emaux, et Encres d'Imprimerie de l'Europe Continentale (FATIPEC), Lugano, 1984.

[36] Matsui, S. and D. R. Paul, Pervaporation separation of aromatic/aliphatic hydrocarbons by crosslinked poly(methyl acrylate-co-acrylic acid) membranes, *J. Membr. Sci.*, **2002**, *195*, 229-245.

[37] Kamaruddin, H. D. and W. J. Koros, Some observations about the application of Fick's first law for membrane separation of multicomponent mixtures, *J. Membr. Sci.*, **1997**, *135*, 147-159.

[38] White, L. S., T. A. Blinka, H. A. Kloczewski and I.-f. Wang, Properties of a polyimide gas separation membrane in natural gas streams, *J. Membr. Sci.*, **1995**, *103*, 73-82.

[39] Al-Juaied, M., Characterization and analysis of asymmetric hollow fiber membranes for natural gas purification in the presence of heavy hydrocarbon, presented at Separations Research Program Conference, Austin, TX, April 16, 2002.

Chapter 2: Background and Theory

2.1 PURE GAS PERMEATION

Membrane material performance is characterized primarily in terms of penetrant transport properties, permeability and selectivity. Permeability is a measure of the membrane's intrinsic productivity and selectivity is a measure of the separation efficiency. For dense films with zero pressure on the downstream, the flux (n_A), normalized by the transmembrane partial pressure (Δp_A) and thickness (ℓ) is defined as the permeability ($\mathbf{P}_A$),

$$\mathbf{P}_A = n_A \frac{\ell}{\Delta p_A} \tag{2.1}$$

Permeability values are typically reported in Barrers $\left(1\,\text{Barrer} = 10^{-10}\,\frac{\text{cc(STP)}\cdot\text{cm}}{\text{cm}^2\cdot\text{cm Hg}\cdot\text{s}}\right)$.

The true thermodynamic driving force for membrane separations is the chemical potential gradient across the membrane, which may be significantly different from the partial pressure difference. This is particularly important in mixed gas permeation, as discussed in Chapter 7.

The *ideal* selectivity (i.e. pure gas feeds) between two gases A and B is defined as the ratio of their permeabilities,

$$\alpha_{AB} = \mathbf{P}_A / \mathbf{P}_B \tag{2.2}$$

According to the common solution-diffusion mechanism, the permeability can be written as the product of the diffusion coefficient, D, and the solubility coefficient, S,

$$\mathbf{P}_A = D_A S_A \tag{2.3}$$

From this relationship the *ideal* selectivity can be further expressed as,

$$\alpha_{AB} = \frac{D_A S_A}{D_B S_B} \tag{2.4}$$

For mixed gas feeds the separation factor can be calculated from,

$$\alpha_{AB} = \frac{\left(y_A / y_B\right)}{\left(x_A / x_B\right)} \tag{2.5}$$

where x_i is the mole fraction of component i on the upstream side and y_i is the mole fraction of component i on the downstream side, as measured by gas chromatography.

The solubility coefficient, S, is determined by the condensability of the penetrants, by the polymer-penetrant interactions and by the amount of free volume in the glassy polymer. The average diffusion coefficient, D, is a measure of the mobility of the penetrant between the upstream and downstream faces of the membrane. The diffusion coefficient depends on packing and motion of the polymer segments and on the size and shape of the penetrating molecules.

2.2 SORPTION

The solubility coefficient, S_A, for equilibrium gas sorption in glassy polymers is often described by the dual mode model [1],

$$S_A = \frac{C_A}{p_A} = k_{DA} + \frac{C'_{HA} b_A}{1 + b_A p_A} \tag{2.6}$$

where k_{DA} is the Henry's law constant, C'_{HA} is the Langmuir capacity constant, and b_A is the Langmuir affinity constant.

The Langmuir term represents molecules sorbed into the microvoids or free volume that exists due to the non-equilibrium structure of the glassy polymer. The Henry's law term describes molecules that dissolve into the normally well-packed regions of the polymer. At pressures where plasticization occurs in membrane separations, the sorption is dominated by the Henry's law mechanism.

The sorption of plasticizing penetrants in membranes can have significant effects on the diffusion coefficients of penetrants in the membrane, even when the sorption isotherm fits the Henry's law model. Therefore, it is difficult to tell anything about the plasticization of the membrane from sorption measurements. This is explored extensively in Chapters 4-6. A typical dual mode sorption isotherm for CO_2 in the polyimide 6FDA-DAM is shown in Fig. 2.1

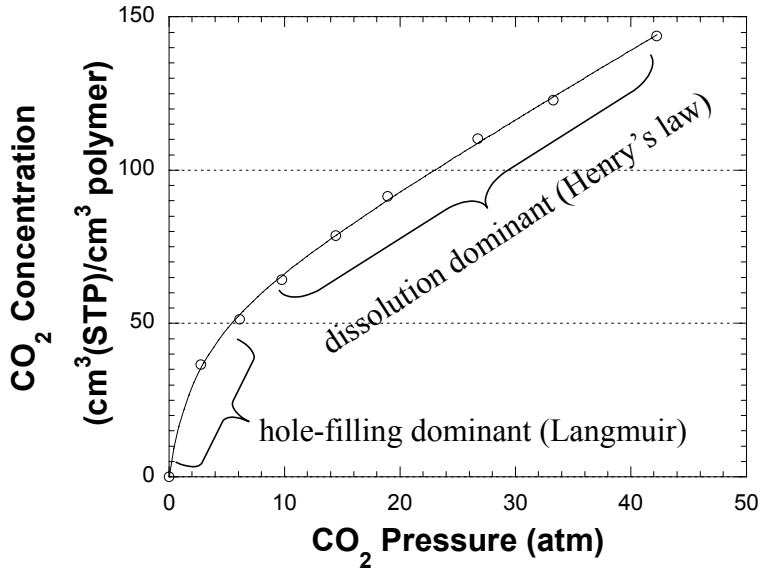

Figure 2.1: CO_2 sorption isotherm in 6FDA-DAM at 35°C

There are many other models used to describe gas sorption in glassy polymers. The non-equilibrium lattice fluid (NELF) model combines the Sanchez-Lacombe equation of state [2] with an additional term to account for the non-equilibrium nature of the glassy polymer [3]. This model requires PVT data and the dilation isotherm to predict the sorption and desorption isotherms. At low pressures the pure polymer density may be used to predict the sorption with no adjustable parameters. At high pressures where plasticization is important, the model does not offer significant advantage over the dual mode model.

The dual mode sorption model is the most commonly used model and it will be used throughout the remainder of this work since it has a complementary transport model that can be used to describe permeation through membranes. The effects of crosslinking on the CO_2 and CH_4 sorption can be interpreted by analyzing the dual mode parameters.

The kinetics of gas sorption into polymer films can be modeled by Fickian expressions [4],

$$\frac{M_t}{M_\infty} = 1 - \frac{8}{\pi^2}\sum_{n=0}^{\infty}\frac{1}{(2n+1)^2}\exp\left[-\frac{(2n+1)^2\pi^2 Dt}{4\ell^2}\right] \tag{2.7}$$

In this case, the polymer properties that govern diffusion are assumed to be unaffected by the sorbed penetrants. Sorption may also occur due to polymer chain relaxations facilitated by the diffusing penetrant molecules. The relaxation-controlled sorption and diffusion has been modeled empirically by applying a linear superposition of a relaxation function on the Fickian expression [5, 6]. This approach is phenomenological in nature, making it difficult to generalize for various polymer/penetrant systems at different temperatures, pressures etc.

2.3 DIFFUSION

The diffusion coefficient in polymers is given by [7],

$$D = \frac{1}{6} f\lambda^2 \tag{2.8}$$

where f is the frequency of diffusional jumps length λ in the polymer matrix limited by thermal motions of the polymer chain segments. In a permeation experiment, the diffusion coefficient in Eq. 2.3 reflects an average value across the membrane. Interpretation with regard to Eq. 2.8 must be considered in terms of average jump lengths and frequencies between the upstream and downstream conditions.

The flux across the membrane with some concentration gradient is given by Fick's law,

$$n_A = -D_A(C_A)\frac{\partial C_A}{\partial x} \tag{2.9}$$

The dual mode sorption and transport model has been successful at explaining the pressure dependence of the permeability, by assuming there are distinct diffusion coefficients for the Henry's law (D_D) and Langmuir populations (D_H) [8],

$$\mathbf{P}_A = k_{DA}D_{DA} + D_{HA}\frac{C'_{HA}b_A}{(1+b_A p_A)} \tag{2.10}$$

This dual mode transport model can be modified to model mixed gas permeabilities as shown in Chapter 7.

Similar in form to the Doolittle equation that describes the fluidity of simple hydrocarbon liquids [9], Cohen and Turnbull developed an expression for the diffusion coefficient of hard spheres in a glass [10],

$$D = A\exp\left(\frac{-\gamma v^*}{v_f}\right) \tag{2.11}$$

where A and γ are constants, v^* is the critical volume of gap opening to allow a diffusive jump, and v_f is the free volume in the glass. In Chapter 5 it is shown how the polymer free volume can be affected by CO_2 plasticization and how this affects the CO_2 diffusion coefficient.

2.4 DILATION BY SPECTROSCOPIC ELLIPSOMETRY

The dilation or swelling of a polymer film is an important measurement to understand how the sorbed volume of the dissolved penetrant changes as the polymer is plasticized by CO_2. Recently, Sirard et al. developed a technique to measure the swelling of thin polymer films in the presence of high-pressure CO_2 via spectroscopic ellipsometry [11].

Ellipsometry involves the reflection of polarized light off of a supported film and the substrate. The film thickness is calculated from the change in the polarization state of the light [12]. CO_2 sorption can be calculated from changes in the film refractive index from the Clausius-Mosotti equation [11, 13].

$$\frac{\langle n_j \rangle^2 - 1}{\langle n_j \rangle^2 + 2} = q_j \rho_j \tag{2.12}$$

where $<n_j>$ is the average index over a wavelength range from 410 to 750 nm, q is a constant, and ρ is the density. The mass concentration of CO_2 in the swollen film can be obtained from the following mixing rule [11, 13],

$$\frac{\langle n_j \rangle^2 - 1}{\langle n_j \rangle^2 + 2} = q_{CO_2} \rho_{CO_2} + q_{polymer} \rho_{polymer} \tag{2.13}$$

The polymer density can be obtained from the film swelling (h/h_0) and the pure polymer density (ρ_0).

$$\rho_{polymer} = \rho_0 \frac{h_0}{h} \tag{2.14}$$

The pure polymer density was measured in a density gradient column at 30°C and the pure polymer index of refraction was measured by ellipsometry at 1 atm in air at 35°C. The refractive index of sorbed CO_2 is assumed to be 1.23 [14] and its density is assumed to be 1.0 g/cm^3.

Solvent-induced glass transitions can be determined by the hysteresis of the swelling isotherm [15]. If there is no hysteresis (i.e., dilation and consolidation isotherms are conincident) then the polymer is rubbery, otherwise it is glassy (or simply in the "elastic" regime at low sorption levels, if it has not been plasticized at high pressures). This behavior is shown in Fig. 2.2, where CO_2 induces a glass transition ~ 60 atm at 35°C. This technique could be used for

a wide range of pressures and temperatures with different gases to better understand solvent-induced glass transitions.

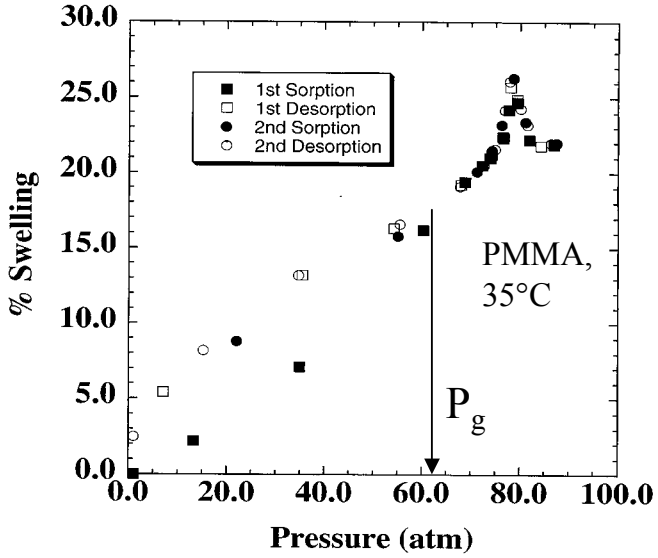

Figure 2.2: CO_2 swelling in PMMA by spectroscopic ellipsometry [15]

2.5 PLASTICIZATION

In glassy polymeric membrane applications, plasticization is generally defined to be an increase in the segmental motion of polymer chains, due to the presence of one or more sorbates, such that the permeability of both components increases and the selectivity decreases [16]. This increased mobility increases the frequency of gap openings and their average size (see Eq. 2.8). The loss in selectivity for CO_2/CH_4 [17] and propylene/propane separations [18] is mainly caused by a reduction in the diffusivity selectivity due to excessive segmental motion. In other words, the membrane is less able to discriminate between the subtle size and shape differences that control diffusion rates of various molecules in the glassy membrane.

In transport through membranes, the plasticization pressure is defined as the minimum in the permeation isotherm. A typical permeation isotherm is shown in Fig. 2.3. Below 15 atm the permeability decreases due to saturation of the Langmuir sites. Above 15 atm, the permeability increases as the polymer chain mobility increases due to plasticization by the dissolved CO_2. It's interesting that the equilibrium sorption isotherm retains its classical dual mode shape up to 40 atm (Fig. 2.1), but the CO_2 diffusion coefficient increases very significantly over this pressure range.

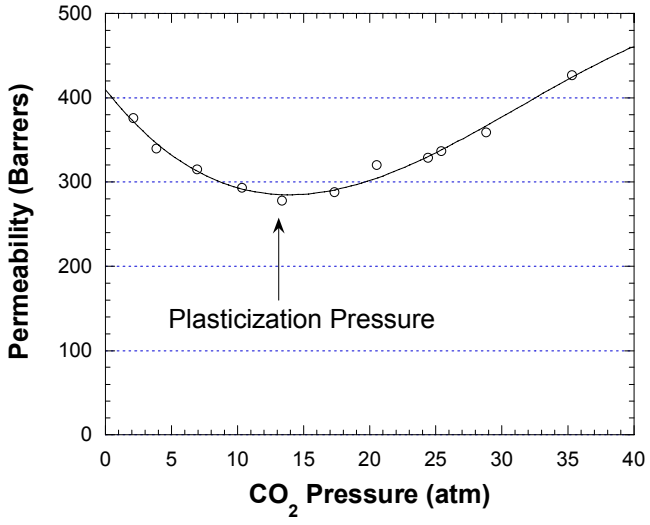

Figure 2.3: CO_2 permeation isotherm in 6FDA-DAM at 35°C

Dynamic mechanical spectra can be used to monitor the motion of specific groups on the polymer chains as a function of temperature [19]. These secondary relaxations are shifted to lower temperatures after conditioning with CO_2, implying that CO_2 enhances the segmental mobility. Main chain relaxations such as the glass transition are also significantly affected by sorption of CO_2. The glass transition temperature (T_g) of polyethersulfone is reduced by 105°C by

exposure to CO_2 at 35 atm [20] and the T_g of poly(phenylene oxide) is decreased by 226°C by exposure to CO_2 at 60 atm [21].

Sanders suggests that the movement of side groups on polymer chains may perturb the local packing of the polymer to an extent that allows easy passage of the small penetrant molecules [20]. Sorption of CO_2 can have a major impact on the bulk mechanical properties of the polymer (e.g. T_g, modulus etc.), but Sanders suggests that the motion of side groups governs the diffusion process. The increase in segmental mobility (local volume fluctuations as opposed to the long-range mobility that is characteristic of rubbery polymers) is due to the presence of condensable components such as CO_2 (confirmed by dynamic mechanical analysis and solid state NMR [22]). In a membrane process, this increased mobility results in a reduction in the diffusivity selectivity.

Various phenomenological models have been postulated to describe plasticization behavior. Stern and Saxena modified the dual mode transport model with a diffusion coefficient that is an exponential function of concentration to describe this plasticization behavior [23]. Later, Mauze and Stern modified the model to replace the total concentration by the so-called "dissolved" concentration, neglecting the concentration associated with Langmuir sorption mechanism, while maintaining the exponential diffusion expression [24].

A review of gas separation membrane plasticization was recently reported by Ismail and Lorna [25]. The end of this chapter gives a brief overview of some approaches for stabilizing membranes against plasticization, along with some practical constraints which limit the feasibility of many approaches.

This research project focuses on understanding how the polymer structure relates to the plasticization behavior. By measuring the sorption and permeation isotherms independently, the plasticization effects on sorption and diffusion can be decoupled. Moreover, by measuring the dilation isotherms, it can be shown

how sorption, diffusion, and swelling are all interconnected in a plasticized membrane.

In Chapter 5 it is shown that the diffusion coefficient can increase very significantly over very long time scales (i.e., weeks) for a plasticized membrane, and it is hypothesized that this diffusional behavior is related to the CO_2 concentration in the polymer and its partial molar volume. The long-term non-Fickian kinetics of these processes give insight into why plasticization leads to poor membrane performance and how it can be controlled through thermal annealing and/or chemical crosslinking.

Plasticization and aging of glassy polymers are inverse processes, both kinetic and rheological in nature. The viscoelastic response of the polymer matrix to the plasticizing penetrant depends on the pressure and temperature of the membrane operation. The non-Fickian CO_2-induced plasticization kinetics have been studied for permeation [26], sorption and dilation [6]. These processes have been described empirically because of the complex polymer chain relaxations that are a function of temperature, CO_2 concentration in the polymer, and the polymer mechanical properties. The goal of this work is to tune the polymer chain mobility through crosslinking and annealing such that the chain relaxations are constrained and the permeability of each component is stabilized and the membrane performance is predictable over practical operating periods.

2.6 REVIEW OF CROSSLINKING AND STABILIZATION APPROACHES

It has been shown by several investigations that crosslinking of polymeric gas separation membranes may be a useful method to improve the separation characteristics by decreasing plasticization at high CO_2 pressures. A short review of these approaches is presented below.

Heat treatment of membranes has been studied extensively on the commercial polyimide Matrimid®[27]. It has been shown that thermal annealing

of films at 350°C for 15-30 minutes significantly reduced CO_2 plasticization in pure gas and mixed gas permeation experiments. It was hypothesized that the heat treatment led to crosslinking, since the treated films were insoluble in strong solvents, and/or charge transfer complexes, since the samples were densified and darkly colored. However, the heat treatment significantly reduces the CO_2 permeability and the high temperatures that are required make this approach less desirable for large-scale membrane production.

Bos and co-workers have also blended Matrimid with polysulfone and the copolyimide P84 to improve membrane plasticization resistance [28]. The resulting membranes showed permeation and plasticization behavior that would be expected from the properties of the pure homopolymers. The plasticization resistance arises from the resistance of one of the components (P84 or PSF), but the resulting transport properties lie significantly below the state of the art performance for polymers [29]. It is not clear as to the time scales of the permeation measurements so the long-term stability needs to be addressed for these membranes.

Another approach to improving the resistance of polymeric membranes is the formation of semi-interpenetrating polymer networks, derived by heating a mixture of polyimides with monomers or oligomers containing reactive acetylene end groups. It has been shown, that the resistance to organic solvents is strongly improved by the formation of such polymer networks [30, 31]. Gas separation measurements at 10 atm feed pressure with membranes comprised of blends of polyetherimide and acetylene terminated monomers showed slightly lower CO_2/CH_4 selectivities than with the pure polyetherimide membrane [31]. Semi-interpenetrating networks derived from blends of Matrimid® and the acetylinic oligomers Thermid FA-700 also showed good plasticization resistance, but the permeability was reduced and high temperatures (265°C) were required for crosslinking [32].

Polyarylate or polyimide membranes with benzophenone moieties may be crosslinked by exposure to UV radiation. Depending on the time of irradiation a considerable improvement in the membrane selectivity can be reached [33-35], but the permeability is strongly reduced, presumably due to the densification and reduced mobility of the polymer after crosslinking. The plasticization resistance of these materials was not investigated. Commercially attractive processes also demand that reproducible separation characteristics and crosslinking degree can be guaranteed, which may be rather difficult with irradiation methods.

Polyimides can also be crosslinked by reaction with diamino compounds that open the imide ring [36]. This is an attractive approach because the reaction takes place at ambient temperatures. However, the CO_2 permeability was decreased very significantly, and the CO_2/N_2 selectivities were also decreased. Again, the plasticization behavior of these materials was not reported. Another approach for crosslinking membranes is the formation of hyper-branched polyimides by reaction of triamines with dianhydrides [37]. These materials can then be crosslinked during film formation by reaction with a variety of compounds. This novel approach led to an increase in the CO_2 permeability while maintaining the same ideal CO_2/N_2 selectivity, but the plasticization response was not reported.

Most of the preceding crosslinking methods involve procedures that would be difficult to apply in commercial membrane manufacturing processes. The work presented here mainly focuses on crosslinking membranes after film or fiber formation, via a post-treatment that could be added to the existing membrane production with small incremental costs. To maintain the hollow fiber morphology and to minimize production costs, mild processing temperatures are required (< 180°C preferably).

A new approach for synthesizing crosslinkable membrane materials has been demonstrated to be effective in the suppression of CO_2 plasticization [38].

This method is based on the idea that copolyimides with a specifiable number of functional groups (e.g. carboxylic acid) can be synthesized. The polymer properties can be tuned by the selection of monomers, while the crosslinking degree can be controlled by the carboxylic acid concentration and choice of crosslinking agent. Crosslinking as a post-treatment (i.e. after film or fiber formation) is possible by reacting the carboxylic acid groups with multi-functional alcohols. The advantage of this method is that the overall number of functional groups can be stoichiometrically controlled and, therefore, is reproducible. The crosslinking can be carried out as a post-treatment by applying moderate temperatures, so it appears to be a suitable process for the production of crosslinked hollow fibers.

REFERENCES

[1] Michaels, A. S., W. R. Vieth and J. A. Barrie, Solution of gases in polyethylene terephthalate, *J. Appl. Phys.*, **1963**, *34*, 1.

[2] Sanchez, I. C. and R. H. Lacombe, Statistical thermodynamics of polymer-solutions, *Macromolecules*, **1978**, *11*, 1145-1156.

[3] Doghieri, F. and G. C. Sarti, Nonequilibrium lattice fluids: a predictive model for the solubility in glassy polymers, *Macromolecules*, **1996**, *29*, 7885-7896.

[4] Hines, A. L. and R. N. Maddox, *Mass Transfer: Fundamentals and Applications*, Prentice Hall, Englewood Cliffs, NJ, 1985.

[5] Berens, A. R. and H. B. Hopfenberg, Diffusion and relaxation in glassy polymer powders: 2. separation of diffusion and relaxation parameters, *Polymer*, **1978**, *19*, 489-496.

[6] Wessling, M., I. Huisman, T. v. d. Boomgaard and C. A. Smolders, Dilation kinetics of glassy, aromatic polyimides induced by carbon dioxide sorption, *J. Polym. Sci.: Polym. Phys. Ed.*, **1995**, *33*, 1371-1384.

[7] Bueche, F., *Physical Properties of Polymers*, Interscience, Inc., New York, 1962.

[8] Koros, W. J., D. R. Paul and A. A. Rocha, Carbon dioxide sorption and transport in polycarbonate, *J. Polym. Sci., Polym. Phys. Ed.*, **1976**, *14*, 687.

[9] Doolittle, A. K., Newtonian flow. II. the dependence of the viscosity of liquids on free space, *J. Appl. Phys.*, **1951**, *22*, 1471-1475.

[10] Cohen, M. H. and D. Turnbull, Molecular transport in liquids and glasses, *J. Chem. Phys.*, **1959**, *31*, 1164-1169.

[11] Sirard, S. M., P. F. Green and K. P. Johnston, Spectroscopic ellipsometry investigation of the swelling of poly(dimethylsiloxane) thin films with high pressure carbon dioxide, *J. Phys. Chem. B*, **2001**, *105*, 766-772.

[12] Tompkins, H. G. and W. A. McGahan, *Spectroscopic Ellipsometry and Reflectometry*, John Wiley & Sons, Inc., New York, 1999.

[13] Bolton, B. A., S. Kint, G. F. Bailey and J. R. Scherer, Ethanol sorption and partial molar volume in cellulose acetate films, *J. Phys. Chem.*, **1986**, *90*, 1207-1211.

[14] Michels, A. and J. Hamers, The effect of pressure on the refractive index of carbon dioxide, *Physica*, **1937**, *4*, 995-1006.

[15] Sirard, S. M., K. J. Ziegler, I. C. Sanchez, P. F. Green and K. P. Johnston, Anomalous properties of poly(methyl methacrylate) thin films in supercritical carbon dioxide, *Macromolecules*, **2002**, *35*, 1928-1935.

[16] Koros, W. J. and M. W. Hellums, Transport properties, in *Encycl. Polym. Sci. Eng.*, **1990**, *Suppl. Vol.*, 724-802.

[17] Coleman, M. R. and W. J. Koros, Conditioning of fluorine containing polyimides. 1. effect of exposure to high pressure carbon dioxide on permeability, *Macromolecules*, **1997**, *30*, 6899-6905.

[18] Staudt-Bickel, C. and W. J. Koros, Olefin/paraffin gas separations with 6FDA-based polyimide membranes, *J. Membr. Sci.*, **2000**, *170*, 205-214.

[19] Fried, J. R., H. C. Liu and C. Zhang, Effect of sorbed carbon dioxide on the dynamic mechanical properties of glassy polymers, *J. Polym. Sci., Polym. Lett. Ed.* , **1989**, *27*, 385-392.

[20] Sanders, E. S., Penetrant-induced plasticization and gas permeation in glassy polymers, *J. Membr. Sci.*, **1988**, *37*, 63-80.

[21] Hachisuka, H., T. Sato, T. Imai, Y. Tsujita, A. Takizawa and T. Kinoshita, Glass transition temperature of glassy polymers plasticized by CO_2 gas, *Polym. J. (Tokyo)*, **1990**, *22*, 77-79.

[22] Sefcik, M. D. and J. Schaefer, Solid-state ^{13}C NMR evidence for gas-polymer interactions in the carbon dioxide-poly(vinyl chloride) system, *J. Polym. Sci.: Polym. Phys. Ed.*, **1983**, *21*, 1055-1062.

[23] Stern, S. A. and V. Saxena, Concentration-dependent transport of gases and vapors in glassy polymers, *J. Membr. Sci.*, **1980**, *7*, 47-59.

[24] Mauze, G. R. and S. A. Stern, The solution and transport of water vapor in polyacrylonitrile: A re-examination, *J. Membr. Sci.*, **1982**, *12*, 51-64.

[25] Ismail, A. F. and W. Lorna, Penetrant-induced plasticization phenomenon in glassy polymers for gas separation membrane, *Sep. and Purif. Tech.*, **2002**, *27*, 173-194.

[26] Wessling, M., S. Schoeman, T. v. d. Boomgaard and C. A. Smolders, Plasticization of gas separation membranes, *Gas Sep. and Purif.*, **1991**, *5*, 222-228.

[27] Bos, A., I. G. M. Punt, M. Wessling and H. Strathmann, Plasticization-resistant glassy polyimide membranes for CO_2/CH_4 separations, *Sep. and Purif. Tech.*, **1998**, *14*, 27-39.

[28] Bos, A., I. Punt, H. Strathmann and M. Wessling, Suppression of gas separation membrane plasticization by homogeneous polymer blending, *AIChE J.*, **2001**, *47*, 1088-1093.

[29] Robeson, L. M., Correlation of separation factor versus permeability for polymer membranes, *J. Membr. Sci.*, **1991**, *62*, 165-185.

[30] Rezac, M. E., E. T. Sorensen and H. W. Beckman, Transport properties of crosslinkable polyimide blends, *J. Membr. Sci.*, **1997**, *136*, 249-259.

[31] Rezac, M. E. and B. Schoberl, Transport and thermal properties of poly(ether imide)/acetylene-terminated blends, *J. Membr. Sci.*, **1999**, *156*, 211.

[32] Bos, A., I. G. M. Punt, M. Wessling and H. Strathmann, Suppression of CO_2-plasticization by semiinterpenetrating polymer network formation, *J. Polym. Sci., Polym. Phys. Ed.*, **1998**, *36*, 1547-1556.

[33] McCaig, M. S. and D. R. Paul, Effect of UV crosslinking and physical aging on the gas permeability of thin glassy polyarylate films, *Polymer*, **1999**, *40*, 7209-7225.

[34] Wright, C. T. and D. R. Paul, Gas sorption and transport in UV-irradiated polyarylate copolymers based on tetramethyl bisphenol-a and dihydroxybenzophenone, *J. Membr. Sci.*, **1997**, *124*, 161-174.

[35] Kita, H., T. Inada, K. Tanaka and K.-i. Okamoto, Effect of photocrosslinking on permeability and permselectivity of gases through benzophenone-containing polyimide, *J. Membr. Sci.*, **1994**, *87*, 139-147.

[36] Liu, Y., R. Wang and T.-S. Chung, Chemical cross-linking modification of polyimide membranes for gas separation, *J. Membr. Sci.*, **2001**, *189*, 231-239.

[37] Fang, J., H. Kita and K.-i. Okamoto, Gas permeation of hyperbranched polyimide membranes, *J. Membr. Sci.*, **2001**, *182*, 245-256.

[38] Staudt-Bickel, C. and W. J. Koros, Improvement of CO_2/CH_4 separation characteristics of polyimides by chemical crosslinking, *J. Membrane Sci.*, **1999**, *155*, 145-154.

Chapter 3: Materials and Experimental Procedures

3.1 INTRODUCTION

This chapter describes the polymer synthesis and crosslinking procedures. It also gives experimental details for casting films and preparing membranes for permeation and sorption measurements. Complementary measurements such as density, T_g, NMR and IR spectroscopy are also described. Measurement of thin film swelling and sorption made by in-situ spectroscopic ellipsometry are presented to establish the relationship between film swelling and plasticization. The ionomer membrane morphology has been characterized by scanning transmission electron microscopy (STEM), and X-ray energy dispersive spectroscopy (XEDS), and small angle X-ray scattering (SAXS). These characterization techniques provide insight into the relationship between polymer structure and plasticization, and provide guidance for a rational materials development strategy.

3.2 MATERIALS AND NOMENCLATURE

The monomers used in the polyimide synthesis are shown in Table 3.1.

Table 3.1: Monomer structures and suppliers

Name	*Structure*	*Supplier*
6FDA	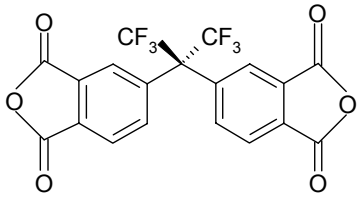 (4,4'-hexafluoroisopropylidene) diphthalic anhydride	Lancaster
6FpDA	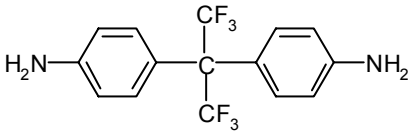 (4,4'-hexafluoroisopropylidene) dianiline	Aldrich
DAM	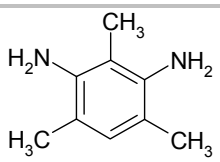 diaminomesitylene	Aldrich
DABA	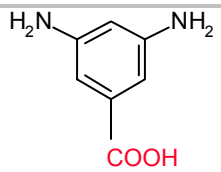 3,5-diaminobenzoic acid	Aldrich

The copolymers are named as 6FDA-DAM:DABA m:n or 6FDA-6FpDA:DABA m:n, where m:n is the diamine ratio in the copolymer. The structures of various copolymers are shown in Table 3.2

Table 3.2: Some representative polyimide structures

Name	***Structure***
6FDA-DAM:DABA m:n	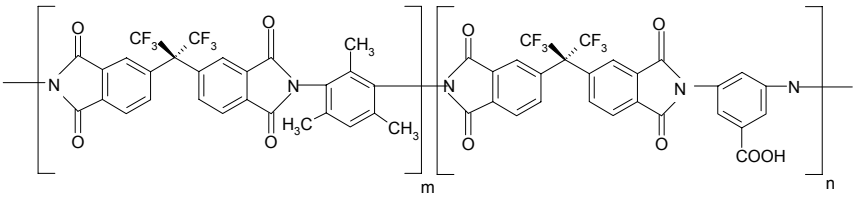
6FDA-6FpDA:DABA m:n	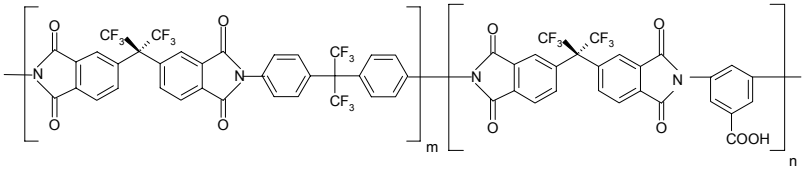

Covalent and ionic crosslinking agents are shown in Table 3.3.

Table 3.3: Covalent and ionic crosslinking and esterification agents

Name	*Structure*
Ethylene Glycol (EG)	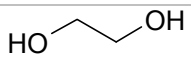
Butylene Glycol **(BG)**	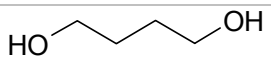
1,4-benzenedimethanol (BDM)	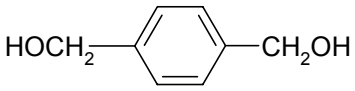
1,4-cyclohexanedimethanol (CHDM)	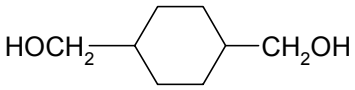
n-butanol	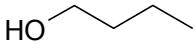
Aluminum acetylacetonate ($Al(AcAc)_3$)	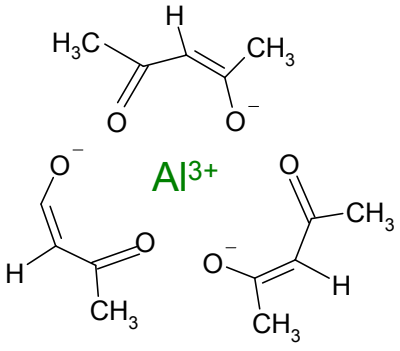

Gases were obtained from Air Liquide and used without further purification. Table 3.4 shows the gas purities and the typical concentrations of impurities.

Table 3.4: Gas purities for gases used in synthesis, permeation, and sorption

Gas	*Minimum Purity*	*Air Liquide Grade*	*Balance Composition (< x ppm)*
N_2	99.99	Industrial	Dew Point = –75°F; O_2 < 50.0, T.H.C.< 5.0
CO_2	99.99	Coleman Instrument (UHP)	H_2O < 5.0, O_2 < 10, CH_4 < 5.0, N_2 < 50
CH_4	99.0	CP	C_2H_6 < 1000, C_2H_4 < 1000, C_3H_8 < 200, C_3H_6 < 10.0, O_2 < 10, N_2 < 3000, CO < 5.0, CO_2 < 50.0, i-C_4 < 5.0, n-C_4 < 5.0
He	99.999	UHP	H_2O < 1.0, T.H.C.< 0.5, O_2 < 1.0, CO < 0.5, CO_2 < 0.5, H_2 < 1.0, Ar < 5.0
Air	N/A	Zero Grade	T.H.C.< 2

* T.H.C. ≡ total hydrocarbon content

3.3 POLYMER SYNTHESIS

The synthesis of soluble 6FDA-based polyimides is a two-step polycondensation reaction, as described previously [1]. First, an equimolar amount of dianhydrides and diamines is reacted in NMP (Aldrich, 99.5%) in a 100 mL three-neck flask with a Teflon stir bar at room temperature for ~ 18 h under a nitrogen purge (Air Liquide, industrial grade). The monomer concentration in the reaction solution was ~ 20% by volume. This concentration provides a good concentration to produce high molecular weight polymer. Equilibrium considerations favor higher concentrations, but the reaction kinetics become limited by the solution viscosity if the concentration is too high. The copolymers are expected to have random diamine sequence distributions due to the equilibrium nature of the reaction and from experimental studies [2]. The dianhydrides and diamines react to form a poly(amic acid) solution, which is then

converted to the polyimide by chemical imidization with equimolar amounts of acetic anhydride (AcAn) and triethylamine (TEA). The two reaction steps are shown in Fig. 3.1

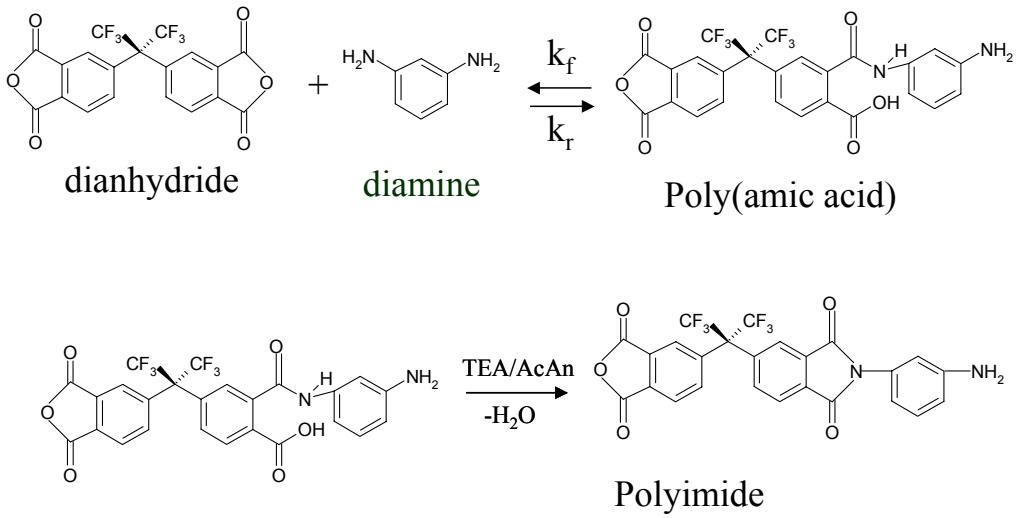

Figure 3.1: Reaction chemistry for polyimide synthesis

There is particular concern about keeping water out of the reaction solution. With this condensation polymerization, stoichiometry between the dianhydrides and diamines is essential for development of high molecular weight polymer. Water can hydrolyze the dianhydrides and alter the stoichiometry. Therefore, strict precautions were taken to minimize the amount of water in the reaction flask and to ensure monomer purity. Glassware was flamed with a propane torch before the monomers were added. The NMP and TEA were dried over 4A molecular sieves for at least 6 h. To ensure high purity of the monomers, the 6FDA, 6FpDA, and DAM were sublimed under vacuum at 3°C below their melting points. If not sufficiently pure from the supplier, DABA was recrystallized from water, according to the method in Appendix B. Diamines

were dissolved in NMP and then the dianhydrides were added to the reactor. An excess of dianhydrides in solution is to be avoided since this could irreversibly affect the equilibrium polymer molecular weight [3]. The NMP was added to the reactor via a transfer needle, to minimize water introduction.

After the poly(amic acid) solution became sufficiently viscous (after 18 h), NMP was added to make the polymer concentration ~ 12%. The reactor was fitted with a condenser and the polymer solution was heated to 50°C. Four times the stoichiometric amount of TEA and AcAn were mixed together in a dry vial and this mixture was added to the poly(amic acid) solution through a polyethylene syringe (slowly to prevent phase separation). The solution was then heated up to 105°C over a one-hour period and reacted at 105°C for another hour. The solution was then cooled to room temperature and poured into a 50/50 methanol/water mixture. The precipitated polymer was then filtered (P5 filter, Fisher) through a Buchner funnel, blended, and washed with methanol to remove any residual solvents. The polymer was dried overnight in the hood, and at 70°C for 12 h under vacuum and for 24 h at 130°C under vacuum.

3.4 FILM CASTING AND MASKING

Films for permeation and sorption were cast from ~ 2 wt% solutions in tetrahydrofuran (THF) or dichloromethane onto Teflon casting dishes inside a glove-bag. The casting dishes were machined from Teflon round-stock, with a diameter of 4 in. Particular care was taken to make sure the dish surface is smooth, to get an accurate thickness measurement. The polymer solutions are filtered through a 0.2 μm Teflon syringe filter (Cole Parmer), and the dishes were covered with a funnel for slow evaporation of the solvent. Additionally, ~ 25 mL of solvent was placed in a beaker in the glove-bag to saturate the atmosphere and slow the evaporation process and prevent phase separation. After three days, the

film was removed from the glove bag and dried under vacuum at a set temperature for 24 h. The annealing temperature is a variable that is very important in determining the membrane plasticization resistance and this is explored in detail in Chapters 4 and 5.

For permeation experiments, a piece of the film is placed between two pieces of aluminum tape (Avery Dennsion) with a hole in the center. The interface between the film and tape was coated with five-minute epoxy (Devcon®) and this is allowed to cure at room temperature for at least 6 h. The masked film is then scanned at 300 dpi resolution and the film area was measured with Scion Image® software. The membrane thickness was measured with a micrometer (Ames) multiple times over the film area to obtain an average, with a typical standard deviation less than 5% of the average. A schematic of the masked film and double o-ring cell is shown in Fig. 3.2

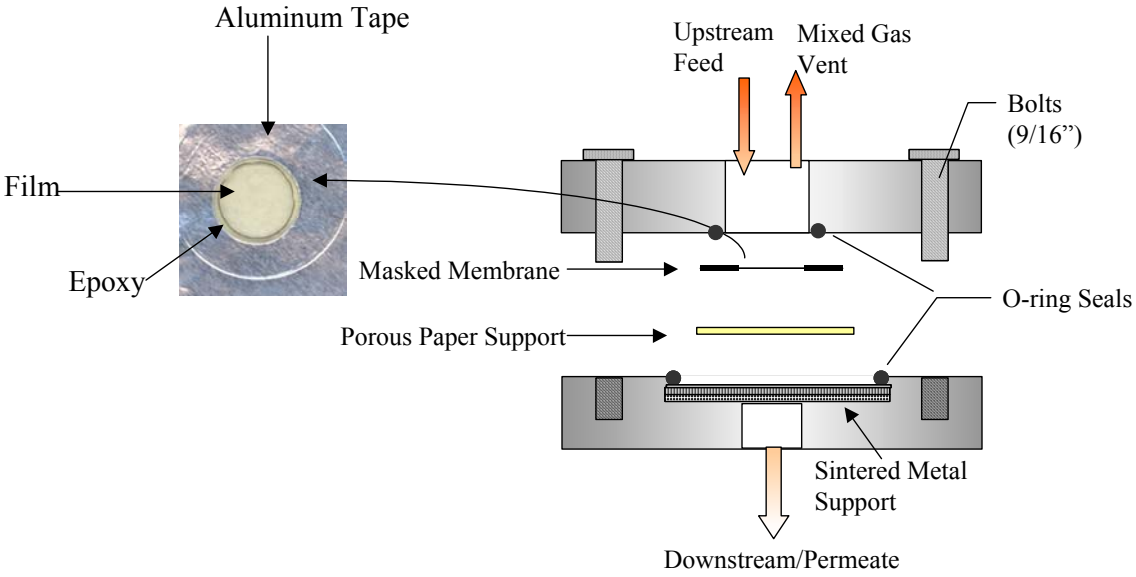

Figure 3.2: Permeation cell schematic

3.5 PERMEATION

To measure gas permeabilities, the masked membrane film is placed into a double O-ring cell and inserted into a pressure-rise permeation apparatus, as shown in Fig. 3.3.

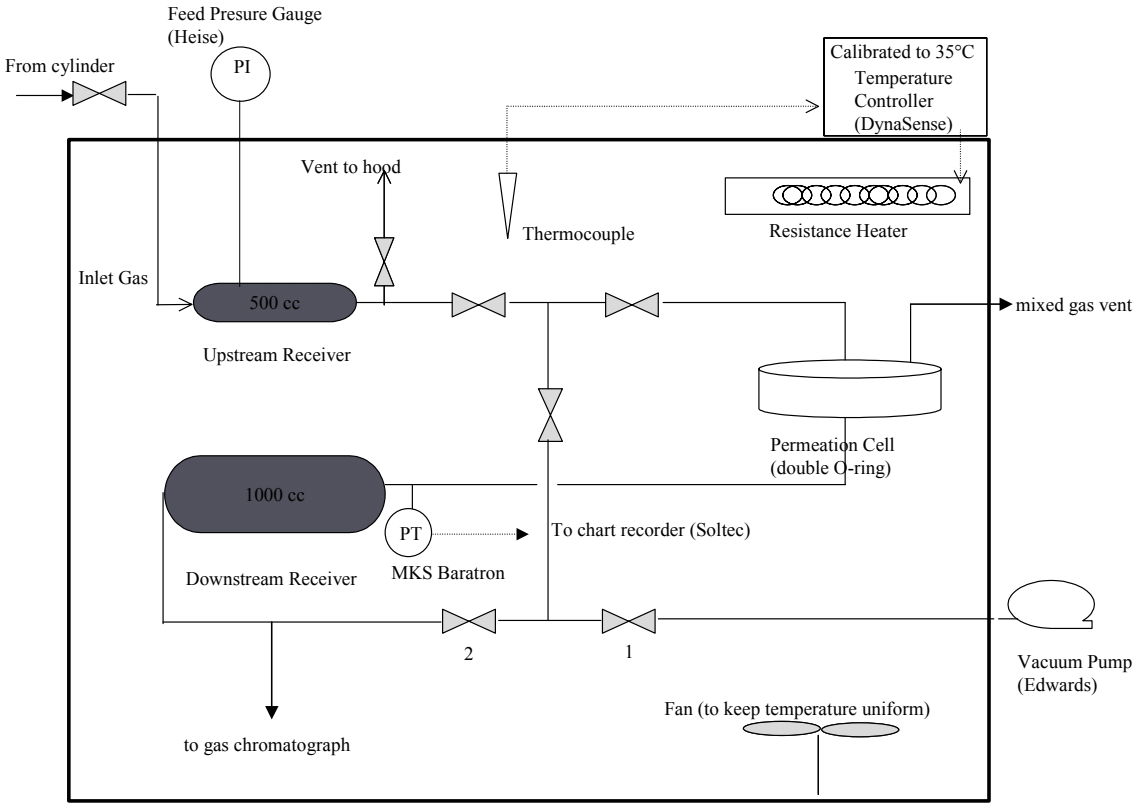

Figure 3.3: Pressure-rise permeation apparatus

The downstream volume was evacuated for 1 h and then for at least 12 h more after the upstream has been evacuated for 15 min. With zero pressure on the upstream, the leak rate was tested (before and after the CH_4 permeation, where the average was used). Typically the leak rate was less than 10% of the slowest gas flux at the lowest pressure at which it was measured. This leak rate was subtracted from the gas flux to calculate the permeability. The permeability of each gas was measured at a minimum of two pressures to ensure that there were no defects in the film. The downstream volume was calculated by the procedure shown in Appendix B.

For mixed gas permeation, the stage cut (permeate flow/feed flow) was kept below 1% by venting the upstream through a bubble flowmeter. This

prevents concentration polarization at the upstream face of the membrane to ensure a constant driving force across the film. The permeate composition was measured with an HP 5880A gas chromatograph, fitted with a Hayesep-R® (Supelco) packed column. The column temperature was kept between 80°C and 120°C and the TCD temperature was 200°C. Details of the mixed gas permeation system design have been previously reported [4]. Ultra high purity helium was used as the carrier gas and three replicates of the selectivity were taken to ensure the accuracy of the analysis at each pressure.

3.6 KINETIC PERMEATION AND PLASTICIZATION

Since plasticization of the rigid polyimides is a slow kinetic phenomenon, the plasticization pressure depends on the experimental time scales used to measure the permeation isotherm. The plasticization pressure for polyimides is typically greater than 10 atm, so above this pressure the membrane was exposed to the feed gas for 24 h before the permeability was measured. This ensures consistency in evaluating the shape of the permeation isotherm.

To quantify the time-dependent effects of plasticization as a function of the membrane morphology, the CO_2 feed pressure was increased to 40 atm over a four-hour period and the permeability is recorded over a period of 10 to 18 days. The relative permeability (P_t/P_0) is defined as the permeability at any time normalized by the permeability at time zero (i.e., after four hour period). The permeation lag time for these membranes was less than one hour, so the changes in the permeability are due to polymer chain relaxations and not to Fickian transient mass uptake to develop a steady-state concentration gradient.

3.7 SORPTION

The gas solubility in a polymer film can be determined from a pressure-decay sorption apparatus [5], as shown in Fig. 3.4. The cell and reservoir are

submerged in a temperature-controlled water bath to ensure isothermal operation. The technique is based on expanding gas from a reservoir into a cell, both with known volumes. The polymer sample (0.2-0.3 g) is placed in the cell and the amount of gas dissolved into the polymer is determined by mass balance between gas expansions. The sample was evacuated for 12 h prior to sorption measurements. The upstream tubing was evacuated for at least 15 minutes in between sorption intervals to ensure that the gas entering the cell is pure. The gas compressibility factors are calculated from the polynomial expressions given in Appendix A. The reservoir and cell volumes were determined by the procedure shown in Appendix B.

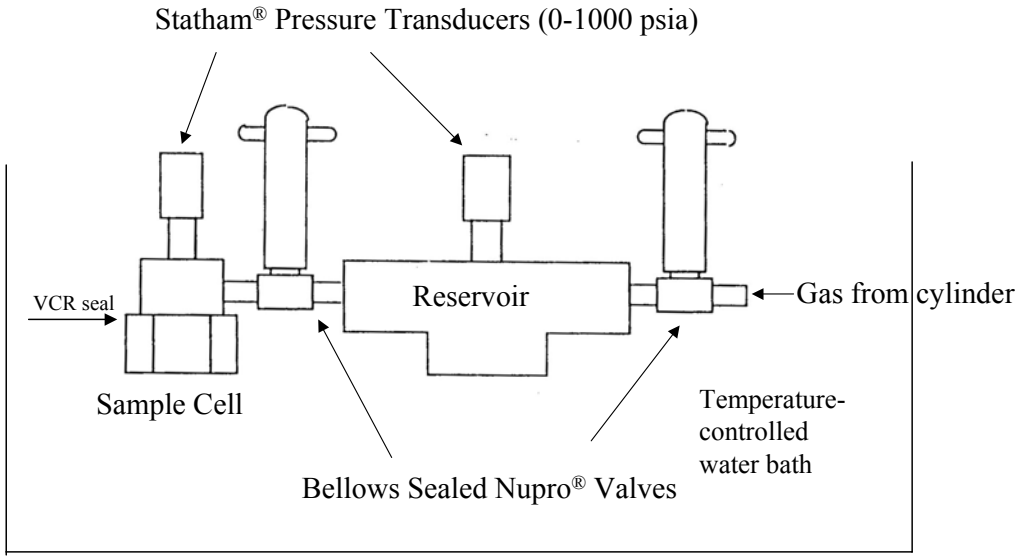

Figure 3.4: Pressure decay sorption apparatus

The pressure transducers are connected to a Keithley 2000 multimeter and this is connected to a data acquisition system with National Instruments LabVIEW® 6.0 software. This software is particularly valuable for determining when the system has reached equilibrium and describing the sorption kinetics. For a plasticized polymer, the approach to equilibrium may be very protracted.

Typically equilibrium was defined as a period of at least 12 h during which the cell pressure was constant, except at low pressures (< 15 atm) where this time to equilibrium may be shorter. Kinetic sorption experiments can be used to obtain penetrant diffusion coefficients (Eq. 2.7), but for the studies reported here, the purpose of the kinetic studies was to describe the long-term relaxation-induced sorption.

3.8 COVALENT CROSSLINKING

3.8.1 Post-Treatment

Proceeding from the work of Staudt-Bickel and Koros on covalently crosslinked polyimides [6], the DABA-containing copolyimide films were crosslinked with ethylene glycol under solid-state conditions via a post-treatment procedure. It is presumed that two steps are involved in the crosslinking reaction, as shown in Fig. 3.5. In the first step the carboxylic acid groups react with a large excess of ethylene glycol to form a monoesterified film. In the second step, the polymer chains are crosslinked by pulling vacuum on the film at elevated temperatures (e.g. 220°C) to set free the ethylene glycol from a transesterification reaction. Similar two-step reaction mechanisms are proposed in the synthesis of aromatic polyesters [7].

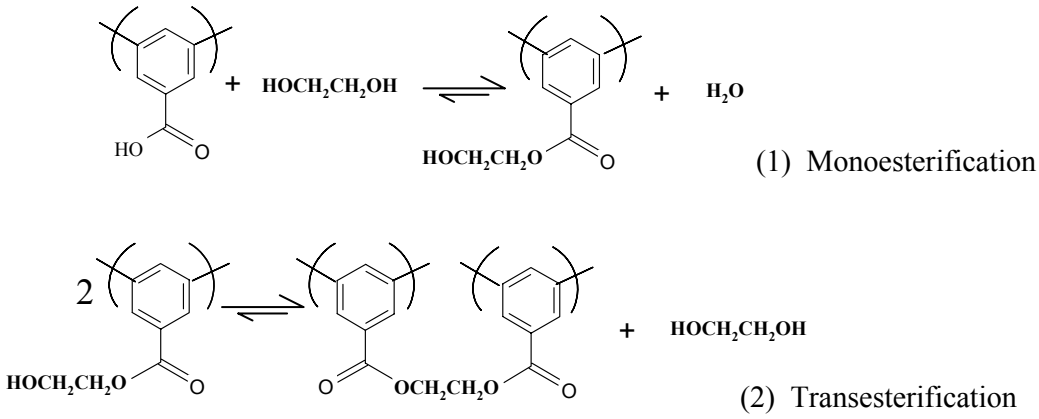

Figure 3.5: Covalent crosslinking reactions

Experimentally this process was performed by soaking film samples in ethylene glycol at 170°C for 12 h under N_2 purge at 11 psia. The vacuum line from the oven was fitted with a liquid N_2 trap to recover the vaporized ethylene glycol. After 12 h the film was removed from the pool of glycol and dried at 50°C while slowly pulling vacuum. The oven temperature was then slowly increased to 220°C to complete the crosslinking reaction and drying of the film over a 24-hour period. This protocol was developed to minimize defects formed during the removal of ethylene glycol from the film. To prove that the ethylene glycol caused only the desired crosslinking reaction, control tests were performed with 6FDA-6FpDA films, which contain no free carboxylic acid groups. Solubility and permeation tests confirmed the lack of chemical reaction with these films.

3.8.2 Monoester Formulation

The post-treatment approach produced membranes with good plasticization resistance, but the large uptake of ethylene glycol in the primary esterification reaction led to large swelling stresses and defects in the film during the removal of the glycol in the transesterification (crosslinking) reaction. When this procedure was applied to asymmetric hollow fibers, the fibers became brittle. The fibers have a delicate porous substructure and the large uptake of a viscous, high surface tension fluid is detrimental to this morphology. Therefore, a new crosslinking approach was developed to be more general (less reliant on the physical properties of the crosslinking agent) and to have better potential for production of crosslinked hollow fibers due to its more simple and mild processing steps.

The reaction is carried out at 140°C for 18 hrs in NMP with ~ 5 mg *p*-toluenesulfonic acid per gram of polymer for catalysis. The reaction flask and polymer were dried under vacuum for 12 h at 100°C to remove water from the system. The reaction flask was fitted with a condenser and a continuous nitrogen purge. The esterification reaction is acid catalyzed [8] and it has been shown that *p*-toluenesulfonic acid speeds up the esterification reaction kinetics [9].

After completion of the monoesterification reaction, the polymer solution was cooled to room temperature and the polymer was precipitated in methanol, blended, washed with methanol, and dried at 70°C for 24 h under vacuum. The temperature was kept low to prevent crosslinking of the polymer particles. The polymer was then cast into a film from THF and the films were dried at elevated temperatures (> 200°C) under vacuum to activate the crosslinking reaction.

In the monoesterification step, the equilibrium may be pushed to the formation of the ester by adding a large excess of diol compound (40-70 times the stoichiometric amount) to the polymer solution. In the transesterification step, the

equilibrium was pushed to the formation of crosslinks by pulling vacuum and removing the volatile diol from the film.

3.9 IONIC CROSSLINKING

Ionically crosslinked copolyimides derived from DABA-containing structures can be obtained by coordinating a multivalent cation with the carboxylate anion. A 20% excess of the stoichiometric amount of aluminum acetylacetonate, $Al(AcAc)_3$, was added to the casting solution (THF). The films were dried at 130°C under full vacuum for 24 h to complete the crosslinking. The advantage for this method is that during the crosslinking reaction the volatile acetylacetone is set free. Thereby, the equilibrium of the crosslinking reaction can be shifted towards the crosslinked structure at elevated temperatures, as illustrated in Fig. 3.6.

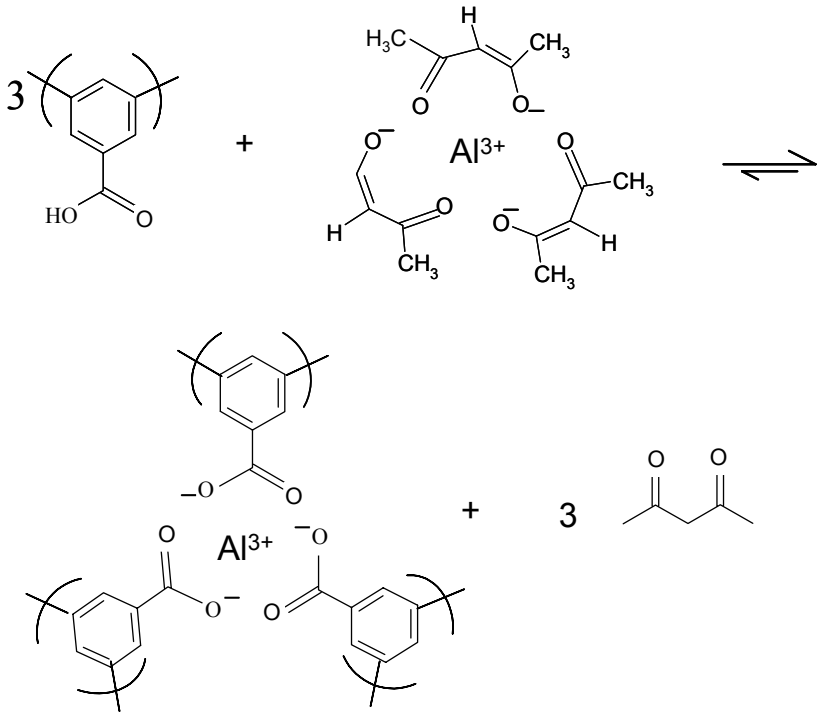

Figure 3.6: Ionic crosslinking reaction

3.10 SPECTROSCOPY

3.10.1 NMR Spectroscopy

The copolymer compositions and esterification conversions were measured with a Bruker AC250 ^{1}H NMR operating at 250 MHz with DMSO-d_6 as the solvent. The polymer sample (~ 0.030 g) was dried under vacuum for 12 h at 70°C. Introduction of water into the sample was minimized to suppress the water peak at 3.3 ppm and to more clearly resolve the protons of interest. The chemical shifts were referenced to the solvent pentet centered at 2.49 ppm.

Sixteen scans were obtained and a Fourier transform was applied to these data. Calculation of the yield of the esterification reactions is discussed in Chapter 4.

3.10.2 Infrared (IR) Spectroscopy

The principles of IR spectroscopy [10] and detailed analysis of functional group absorptions [11] have been discussed extensively in the literature. The polyimide IR spectra were obtained with a Nicolet Magnum 550 IR spectrometer with a N_2 purge. Samples for IR were prepared by making a 10-12 wt% polymer solution in acetone or 4-methyl-2-pentanone (Aldrich, 99+%) and placing ~ 0.5 mL of the solution on a silicon wafer, then spin-coating at 3000 RPM for 15 seconds (Photo Resist spinner by Headway Research). These films were dried under the same conditions as those of the free-standing films.

The silicon wafers have an aluminum backing so the spectrometer can be operating in the reflectance mode. Thin films are advantageous since the peaks are clearly resolved and sufficient transmittance through the films. Moreover, any adsorbed water is quickly removed from the films by the dry N_2 purge.

3.10.3 Spectroscopic Ellipsometry [12]

Ellipsometry is used to measure supported-film thicknesses from approximately 10 and 1000 nm. By reflecting polarized light off the film surface and the substrate and measuring the change in the polarization state of the light, the film thickness and refractive index can be measured independently [13]. Recently, Sirard et al developed a technique to measure polymer film swelling in the presence of high pressure CO_2 [14]. A schematic of the *in-situ* spectroscopic ellipsometer apparatus is shown in Fig. 3.7

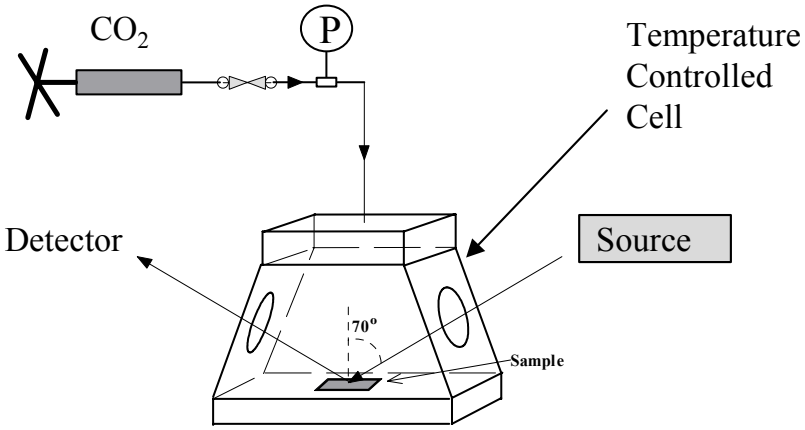

Figure 3.7: In-situ spectroscopic ellipsometer (adapted from [14])

Silicon (100) wafers (Wafer World) were cut into 1 cm x 1 cm squares. The wafers were cleaned [15] by initially soaking in a 50/50 (w/w) hydrochloric acid (EM Science)/methanol (EM Science) solution for 30 min. The wafers were then rinsed with excess deionized water (NANOpure II, Barnstead) and then dried with nitrogen gas (Matheson Gas Products, >99.999%). The wafers were then soaked in 95% sulfuric acid (Mallinckrodt) for 30 min and subsequently rinsed with deionized water and dried with nitrogen gas. The native oxide thickness was measured for each wafer with spectroscopic ellipsometry (J.A. Woollam) prior to coating. The native oxide was between 1.5 and 2.0 nm for all of the samples.

To prepare the supported thin films, the polyimide was initially dissolved in 2-methyl-4-pentanone (Aldrich, 99+ %). The solution was then spin-coated onto the silicon wafers by using a photoresist spinner (Headway Research, Inc.). The concentration of the solution was adjusted in order to achieve films of the desired thickness at a spin rate of 3000 rpm. The thin films were heat treated under vacuum at their respective temperatures for 24 h.

A M-44 spectroscopic ellipsometer set up in the rotating analyzer configuration was used for all of the experiments. The angle of incidence for all measurements was 70^o from the vertical. The experiments were performed in a specially designed high-pressure ellipsometry cell. The details of the cell design can be found elsewhere [14, 16].

After loading the samples in the high-pressure cell, CO_2 (Air Products, >99.9999%) was charged to the cell using a manual pressure generator (High-Pressure Equipment Co.). Pressure was controlled with a strain gauge pressure transducer (Sensotec). The cell was heated using four cartridge heaters (Omega) that were inserted in the top of the cell. The cell was allowed to reach thermal equilibrium for 30 minutes before samples were taken. Measurements were made approximately every 15 minutes between pressure increments.

The thickness and refractive index of the swollen films were extracted from the ellipsometer data by assuming a 4-layer optical model. The 4-layer optical model consists of a CO_2 atmosphere layer, a swollen polymer layer, a SiO_2 native oxide layer, and a silicon substrate layer. Literature values were used for the refractive index of the CO_2 atmosphere [17], the SiO_2 native oxide [18], and the silicon substrate [19]. The fitting parameters for the swelling experiments were the thickness and refractive index of the swollen polymer film, the angle of incidence, and the offset in the ellipsometric delta parameter due to window birefringence. The refractive index of the swollen polymer film was modeled using a Cauchy dispersion relationship $n(\lambda) = A + \frac{B}{\lambda^2} + ...$ [13].

3.10.4 Electron Microscopy and X-ray spectroscopy [20]

These techniques were used to analyze ionomer morphologies and ion distribution. General transmission electron microscopy (TEM) background is

given by Williams and Carter [21] and the scanning TEM (STEM) technique is described by Keyse et al. [22].

The ionomers were stored under vacuum at room temperature at all times except for sample preparation purposes. Thin sections were prepared as follows: polystyrene (PS, M_w ~ 250,000 g/mol, Aldrich) was molded into ~ 300 μm thick films. A small piece of the polyimide film was cut and deposited between two PS layers. The PS/sample/PS stack was compression molded for 5 minutes at ~ 1000 psi and ~ 107ºC. The sample embedded between the PS layers still had its original shape and sharp edges, indicating that no mixing between PS and ionomer occurred. Thin sections with nominal section thickness of 75 nm were microtomed at room temperature with a diamond knife, floated in deionized water and collected on Mo support grids.

Both transmission electron microscopy (TEM) and STEM experiments were performed on a JEOL 2010F field emission electron microscope operated at 200 kV and equipped with a Princeton Gamma Tech (PGT) X-ray energy dispersive spectrometer, a Gatan bright field (BF), and a JEOL annular dark field (ADF) detector. For STEM experiments, a 50 μm condenser aperture, an ADF collection angle of ~ 40 mrad, and a 0.5 nm probe was used. The sample was maintained at a vacuum of ~ 2 x 10^{-5} Pa during all microscopy experiments. STEM magnifications ranged from 30,000 to 600,000X and the image acquisition time was 21 seconds. The samples looked identical before and after STEM image acquisition, showing that the rastering electron beam does not measurably alter the microstructure of the material, even though some carbon contamination was observed. TEM experiments were made in the same microscope at 200 kV with a 150 μm condenser aperture, a 30 μm objective aperture, and a 20 μm diffraction aperture. TEM negatives were digitalized with an Agfa Duoscan T2500 at 2000 dpi. Image analysis was performed with Adobe Photoshop 5.0® using standard

procedures, including background correction, gray level adjustments, and contrast enhancement.

X-ray Energy Dispersive Spectroscopy (XEDS) experiments were performed in the JEOL 2010F in STEM mode with a probe size of 1 nm to increase the signal to noise ratio. Overall spectra were acquired by rastering the electron beam over the sample in imaging mode for 5 minutes. Spot spectra were acquired by placing a stationary probe on the point of interest and collecting a spectrum for 100 s. Data analysis was performed with the IMIX software from PGT using the "qualitative" acquisition mode: after background subtraction, the individual *K* lines of C, O, N, F, and Al from the sample and the Mo *M* lines from the grid were deconvoluted using IMIX routines and the integrated counts were recorded. Occasionally, Si *K* lines from the detector were also observed.

3.11 SMALL ANGLE X-RAY SCATTERING [20]

Small Angle X-ray Scattering (SAXS) is a technique used to describe interparticle spacing and has been used to describe the morphology of ionomers [23, 24]. General background on X-ray principles is given by Guinier [25].

All SAXS experiments were made on all films in a q range from ~ 0.25 to 5.5 nm^{-1}, where q is the scattering vector. In order to obtain reasonable scattering intensities, multiple polymer layers were assembled so that the total sample thickness was ~ 1 mm. SAXS experiments were done on a previously described [26] Multiple Angle X-Ray Scattering (MAXS) apparatus using $CuK_{\alpha 1}$ radiation (λ = 1.5408 Å) and a Bruker HiStar multiwire detector that provided highly sensitive area detection with very low dark current. An integral vacuum was maintained between the generator and the detector, to reduce both attenuation and small-angle scattering by air and windows.

3.12 WIDE ANGLE X-RAY DIFFRACTION

Wide angle X-ray diffraction patterns of polyimide films were obtained with a Philips APD 3520 diffractometer, Cu K_α source (λ = 1.54Å). The apparatus scanned over the range 5-70°, with a dwell time of 3 s and a step size of 0.5°. The d-spacing was calculated from Bragg's equation $n\lambda = 2d\sin\vartheta$, where n = 1. The average d-spacing is determined from a polynomial curve of the data in the region of the main peak.

3.13 GLASS TRANSITION TEMPERATURE

Dynamic scanning calorimetry thermograms were measured on a Perkin-Elmer DSC 7 with a heating rate of 20°C/min under an N_2 purge. The T_g was determined from the second heating run (after sample was heated above T_g and cooled to room temperature), to eliminate artifacts of the polymer thermal history.

3.14 POLYMER DENSITY

Polymer film densities at 30°C were measured with a Techne DC-01 density gradient column filled with aqueous $Ca(NO_3)_2$ solutions. A linear calibration curve (density versus position) was established by placing glass beads of known density into the column. The beads and samples reached their equilibrium positions after a 24 h period. Each film density was measured at least twice.

3.15 GEL FRACTIONS

The gel fractions were determined by soaking the polymer films in THF for five days at 25°C. The gelled films were dried under vacuum for 24 h and weighed to determine the fraction of the original film that does not dissolve after crosslinking and/or heat treatment.

3.16 REPRODUCIBILTY AND ERROR ANALYSIS

From a previously published propagation of error analysis [27], the estimated uncertainty in the permeability measurements is ~ 7% and in the selectivity ~ 3%. Most pure gas permeation experiments were replicated to ensure their validity. The uncertainty in the sorption measurements is estimated to be ~ 0.5% [28]. Sorption isotherms were replicated for several films and showed good reproducibility. Due to the time-consuming nature of the measurements, extensive replication was not possible. Details of the number of permeation and sorption measurements for each polymer film (i.e., composition and thermal treatment) can be found in Appendix C.

REFERENCES

[1] Husk, G. R., P. E. Cassidy and K. L. Gebert, Synthesis and characterization of a series of polyimides derived from 6FDA, *Macromolecules*, **1988**, *21*, 1234-1238.

[2] Bessenov, M. I. and V. A. Zubkov, *Polyamic Acids and Polyimides: Synthesis, Transformations, and Structure*, CRC Press, Boca Raton, 1993.

[3] Takekoshi, T., Synthesis of polyimides, in *Polyimides: Fundamentals and Applications*, Marcel Dekker, Inc., New York, 1996.

[4] O'Brien, K. C., W. J. Koros, T. A. Barbari and E. S. Sanders, A new technique for the measurement of multicomponent gas transport through polymeric films, *J. Membr. Sci.*, **1986**, *29*, 229-238.

[5] Koros, W. J. and D. R. Paul, Design considerations for measurement of gas sorption in polymers by pressure decay, *J. Polym. Sci., Polym, Phys. Ed.*, **1976**, *14*, 1903-1907.

[6] Staudt-Bickel, C. and W. J. Koros, Improvement of CO_2/CH_4 separation characteristics of polyimides by chemical crosslinking, *J. Membr. Sci.*, **1999**, *155*, 145-154.

[7] Kang, C.-K., Modeling of solid-state polymerization of poly(ethylene terephthalate), *J. Appl. Polym. Sci.*, **1998**, *68*, 837-846.

[8] Loudon, G. M., *Organic Chemistry*, Benjamin/Cummings, Menlo Park, CA, 1988.

[9] Kuo, C.-T. and S.-A. Chen, Kinetics of polyesterification: Adipic acid with ethylene glycol, 1,4-butanediol and 1,6-hexanediol., *J. Polym. Sci.: Polym. Chem. Ed.*, **1989**, *27*, 2793-2803.

[10] Conley, R. T., *Infrared Spectroscopy*, Allyn and Bacon, Inc., Boston, 1972.

[11] Silverstein, R. M. and F. X. Webster, *Spectrometric Identification of Organic Compounds, 6th Ed.*, John Wiley and Sons, Inc., New York, 1997.

[12] This work was performed by Steve Sirard at the University of Texas at Austin.

[13] Tompkins, H. G. and W. A. McGahan, *Spectroscopic Ellipsometry and Reflectometry*, John Wiley & Sons, Inc., New York, 1999.

[14] Sirard, S. M., P. F. Green and K. P. Johnston, Spectroscopic ellipsometry investigation of the swelling of poly(dimethylsiloxane) thin films with high pressure carbon dioxide, *J. Phys. Chem. B*, **2001**, *105*, 766-772.

[15] Cras, J. J., C. A. Rowe-Taitt, D. A. Nivens and F. S. Ligler, Comparison of chemical cleaning methods of glass in preparation for silanization, *Biosensors & Bioelectronics*, **1999**, *14*, 683-688.

[16] Sirard, S. M., K. J. Ziegler, I. C. Sanchez, P. F. Green and K. P. Johnston, Anomalous properties of poly(methyl methacrylate) thin films in supercritical carbon dioxide, *Macromolecules*, **2002**, *35*, 1928-1935.

[17] Obriot, J., J. Ge, T. K. Bose and J. M. St-Arnaud, Determination of the density from simultaneous measurements of the refractive index and the dielectric constant of gaseous CH_4, SF_6, CO_2, *Fluid Phase Equilibria*, **1993**, *86*, 315-350.

[18] Philipp, H. R., Silicon dioxide (SiO_2)(glass), in *Handbook of Optical Constants of Solids*, Harcourt Brace Jovanovich, Orlando, 1985.

[19] Jellison, G. E., *Optical Materials*, **1992**, *1*, 41.

[20] This work was performed by Dr. Andreas Taubert at the University of Pennsylvania.

[21] Williams, D. B. and C. E. Carter, *Transmission Electron Microscopy-A Textbook for Materials Science*, Plenum Press, New York, 1996.

[22] Keyse, R. J., P. Goodhew and G. W. Lorimer (Ed.), *Introduction to Scanning Transmission Electron Microscopy*, Springer-Verlag, New York, 1998.

[23] Yarusso, D. J. and S. L. Cooper, Microstructure of ionomers - interpretation of small-angle X-ray scattering data, *Macromolecules*, **1983**, *16*, 1871-1880.

[24] Yarusso, D. J. and S. L. Cooper, Analysis of SAXS data from ionomer systems, *Polymer*, **1985**, *26*, 371-378.

[25] Guinier, A., *X-ray Diffraction in Crystals, Imperfect Crystals, and Amorphous Bodies*, W. H. Freeman, San Francisco,1963.

[26] Taubert, A. and K. I. Winey, Imaging and x-ray microanalysis of a poly(ethylene-ran-methacrylic acid) ionomer melt neutralized with sodium, *Macromolecules*, **2002**, *35*, 7419-7426.

[27] Vu, D. Q., Formation and characterization of asymmetric carbon molecular sieve and mixed matrix membranes for natural gas purification, Ph.D. Dissertation, The University of Texas at Austin, 2001.

[28] Punsalan, D. T., A sorption and dilation investigation of amorphous glassy polymers and physical aging, Ph.D. Dissertation, The University of Texas at Austin, 2001.

Chapter 4: Covalent Crosslinking: Effects on Membrane Transport

This chapter focuses on covalent crosslinking of 6FDA-6FpDA:DABA and 6FDA-DAM:DABA copolymers. The 6FpDA-based polymers have lower permeability, lower sorption, and higher CO_2/CH_4 selectivities than the DAM-based copolymers. These copolymers combined with various crosslinking treatments allow for the tailoring of the membrane transport properties over a wide range of values.

4.1 CO_2 AND CH_4 PERMEATION RESULTS

4.1.1 6FpDA:DABA Copolymers

The 6FDA-6FpDA:DABA 2:1 membranes were crosslinked with ethylene glycol via the traditional post-treatment protocol, as described in Chapter 3. The effects of crosslinking on the pure gas CO_2 permeation properties are shown in Fig. 4.1.

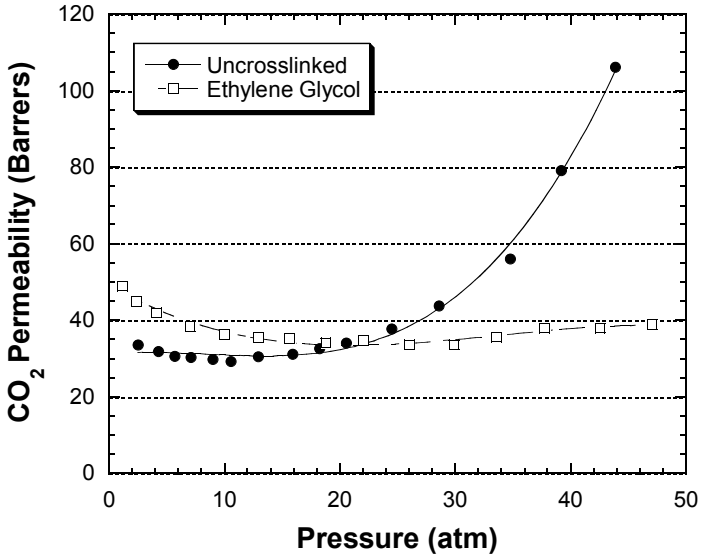

Figure 4.1: CO_2 permeation isotherms for 6FDA-6FpDA:DABA 2:1 membranes at 35°C

The uncrosslinked material plasticizes significantly above 20 atm, whereas the crosslinked membrane is relatively stable for feed pressures up to 50 atm. Crosslinking this polymer with ethylene glycol increases the permeability, with a small sacrifice in the ideal CO_2/CH_4 selectivity, as shown in Table 4.1. The ideal selectivities are measured at 10 atm, where the polymers are not plasticized by CO_2. This is a higher pressure than for much of the membrane data in the literature, and it provides a more conservative measurement of the selectivity since dual mode effects are more prevalent at lower pressures, thus inflating the CO_2 permeability more than that of CH_4. In mixed gas separations (described in Chapter 7), the selectivity is slightly higher for the crosslinked sample. The increase in permeability is contrary to the common perception that crosslinking generally decreases the permeability [1].

Table 4.1: 6FDA-6FpDA:DABA membrane properties at 35°C and 10 atm

Polymer	Crosslink Agent	CO_2 Permeability (Barrers)	CO_2/CH_4 Ideal Selectivity
6FDA-6FpDA [2]	None	63	36
6FDA-6FpDA:DABA 2:1	None	29	45
2:1	Ethylene Glycol	36	42
1:2	None	17	50
6FDA-DABA* [3]	None	3.4	63

* Feed pressure of 2 atm

The untreated membranes show the typical copolymer behavior, where increasing DABA fractions decrease the permeability and increase the selectivity, reflecting the characteristic permeability/selectivity trade-off [4, 5]. The $-CF_3$ groups on the 6FpDA moiety disrupt chain packing and give the membranes high permeabilities.

4.1.2 Control Experiments

In order to confirm that the covalent crosslinking approach is necessary to stabilize the membranes against plasticization, several control experiments were performed. It has been shown that heat treatments of polyimides are effective for reducing membrane plasticization [6, 7]. Polyimides are known to form charge transfer complexes when heated [8, 9], so it is necessary to decouple the physical and chemical changes to the polymer due to the heat treatment that accompanies the crosslinking reaction. Fig. 4.2 shows the CO_2 permeation isotherms for the uncrosslinked polymers 6FDA-6FpDA and 6FDA-6FpDA: DABA 2:1 with various treatments. All films were dried for 24 h at 220°C.

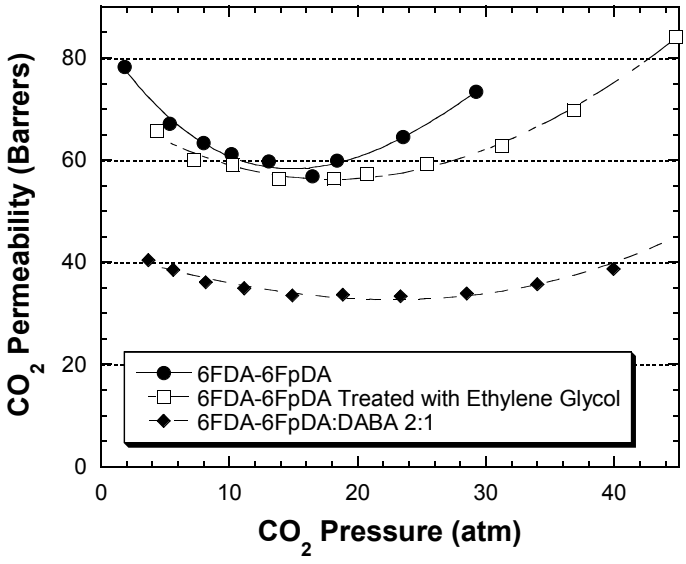

Figure 4.2: Control experiments for CO_2 plasticization

The heat treatment for the 2:1 polymer leads to an increase in the plasticization pressure (the minimum in the isotherm), but it is not as stable as the covalently crosslinked membrane. The decoupling of physical and chemical changes to the polymer structure as a function of the thermal treatment is discussed in Chapter 5.

The ethylene glycol post-treatment had no effect on the plasticization resistance or the CO_2 permeability of 6FDA-6FpDA, verifying that there is no reaction without the carboxylic acid from the DABA group. Only the 2:1 films treated with ethylene glycol were insoluble in THF, whereas the others remained completely soluble, whether treated with glycol or not.

4.1.3 DAM:DABA Copolymers

With the monoester crosslinking protocol (described in Section 3.8.2) it is much easier to crosslink membranes than with the traditional post-treatment. It eliminates the large swelling stresses and defects that arise during the crosslinking

step. Moreover, the procedure is much more general (i.e., less dependent on the physical properties of the diol), and can be easily scaled up. By breaking up the reaction into two steps, the reaction yields at each step can be analyzed by spectroscopic methods. In this chapter, the effects of the monoesterified polymer structure (different esterification treatments and different thermal annealing temperatures) on the membrane properties are investigated.

The copolyimide 6FDA-DAM:DABA 2:1 was chosen for several reasons. For CO_2/CH_4 separations, its transport properties lie near the state-of-the-art performance limit for solution-processable polymers [4]. It has very high CO_2 sorption and is subject to plasticization at relatively low feed pressures (~ 15 atm) if it is annealed at low temperatures (< 150°C). The glass transition temperature of 365°C is well above the annealing temperatures, but there is still sufficient mobility to carry out the transesterification crosslinking reaction. However, the yield of this solid-state reaction is highly dependent on the diol structure. This polymer is also susceptible to stabilization against plasticization with high-temperature thermal annealing. In Chapter 5 the effects of physical annealing and chemical crosslinking are decoupled to develop a criterion for stability in high-pressure separations.

The effects of esterification and crosslinking on the transport properties are expected to be i.) polymer packing changes from pendant ester groups ii.) decreased chain mobility from crosslinking iii.) changes in penetrant solubility arising from chemical and physical changes to the polymer. These effects can be isolated through different thermal treatments and esterification reactions.

The 2:1 membranes were crosslinked with ethylene glycol (EG), butylene glycol (BG), and 1,4-cyclohexanedimethanol (CHDM), all dried at 220°C for 24 h (Fig 4.3). Again the crosslinked membranes are more stable than the uncrosslinked. The plasticization of the films crosslinked with EG and CHDM is a likely result of the incomplete esterification in the monoester step as discussed

in Section 4.5.1 and the steric hindrance to crosslinking in the solid state. This monoesterification step could be optimized for these diols to increase the crosslink density.

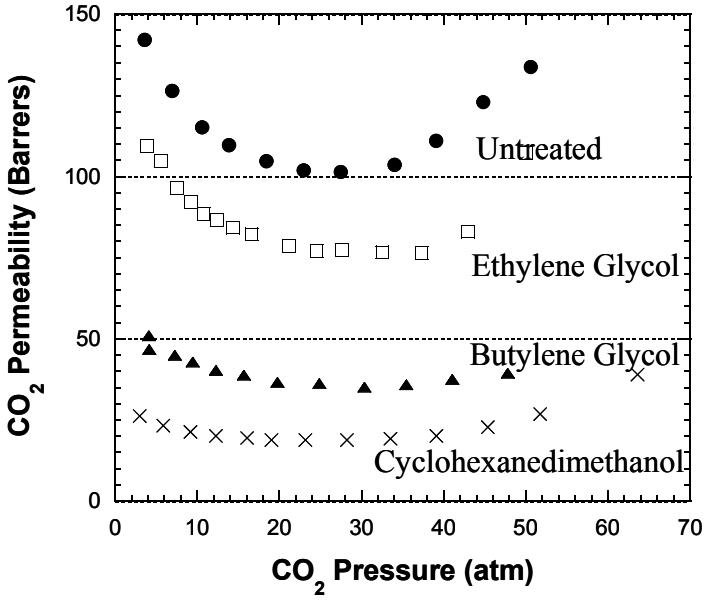

Figure 4.3: CO_2 permeation isotherms for 6FDA-DAM:DABA 2:1 membranes crosslinked with EG, BG, and CHDM

The benzenedimethanol (BDM) monoester membrane was treated at 295°C in order to obtain a film that was insoluble in THF. This was necessary because of the low monoester conversion in solution and subsequent low reactivity in the solid-state. The film was more brightly colored than the untreated film dried under the same conditions, presumably due to absorption of light in the visible region from the aromatic crosslinking agent. However, even without any esterification treatment, the 2:1 film becomes insoluble in THF after a 295°C treatment for reasons discussed in Chapter 5. Nevertheless, even a small amount of crosslinking with BDM causes an increase in the permeability (Fig. 4.4), likely because of the rigid nature of the aromatic crosslinking agent that disrupts the polymer chain packing. This annealing temperature is likely to be too

high for the commercial production of asymmetric hollow fiber membranes, but it does lead to very stable membranes, as described in Chapter 5.

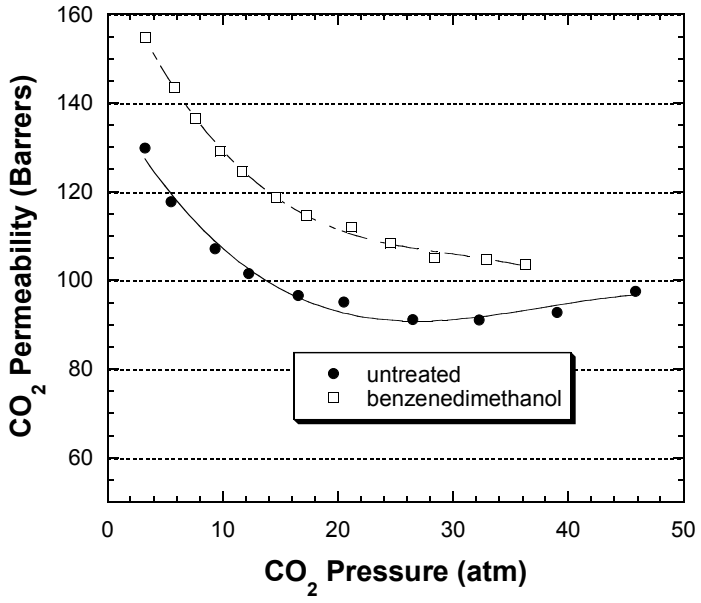

Figure 4.4: CO_2 permeation isotherms for 6FDA-DAM:DABA 2:1 membranes untreated and crosslinked with 1,4-benzenedimethanol at 295°C for 24 h.

The thermal treatment clearly has a simultaneous effect on the crosslink density and the CO_2 permeability. Fig. 4.5 shows these effects for the esterification agents described above. Section 5.3 shows CO_2 permeation isotherms for the untreated and CHDM monoester membranes.

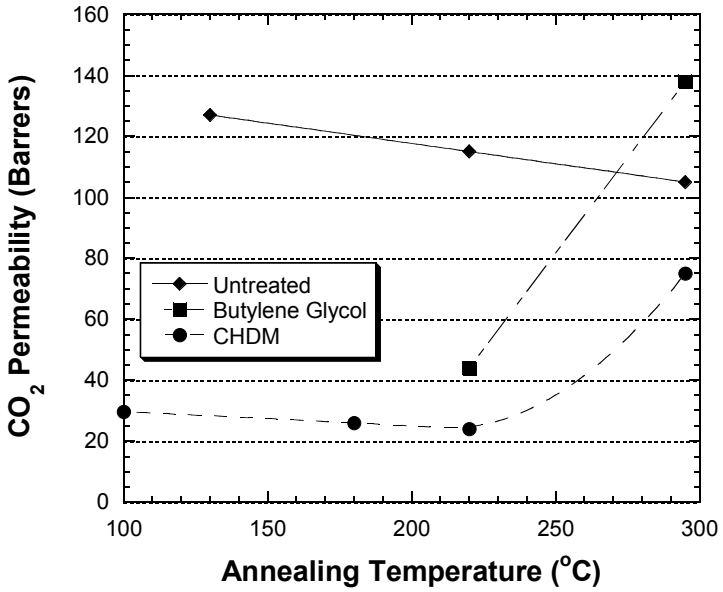

Figure 4.5: Effect of thermal treatment and esterification on 6FDA-DAM:DABA 2:1 CO_2 permeability at 10 atm and 35°C

The data in Fig 4.5 show that the thermal treatment can significantly affect the permeability. The crosslink density for the films crosslinked with CHDM and BG increases at higher temperatures (as confirmed by IR spectroscopy) and so does the permeability, again contrary to the conventional view that crosslinking tends to decrease the permeability. Without any crosslinking, high-temperature annealing tends to decrease the permeability due to physical aging. However, for the crosslinked membranes, it appears that the packing disruption introduced by insertion of the crosslinking molecules between the polymer chains tends to increase the permeability. The increase in free volume may also arise from the elimination of pendant diol groups as the transesterification reaction proceeds. This somewhat counter-intuitive result provides a way to tune the free volume distribution and to stabilize membranes against plasticization.

The various esterification and thermal treatments have a significant impact on the CO_2 permeabilities, but the CO_2/CH_4 selectivity is also a critical factor in analyzing the membrane performance. Table 4.2 shows the CO_2 permeabilities and ideal selectivities at 10 atm feed pressure for the 6FDA-DAM:DABA polymers.

Table 4.2: 6FDA-DAM:DABA membrane properties at 35°C and 10 atm.

Polymer	**Crosslink Agent**	**CO_2 Permeability (Barrers)**	**CO_2/CH_4 Ideal Selectivity**
6FDA-DAM	None	290	21
6FDA-DAM:DABA 2:1	None	127	29
2:1	Ethylene Glycol	90	30
2:1	Butylene Glycol	44	34
2:1	1,4-cyclohexanedimethanol	21	30
1:2	None	29	45
6FDA-DABA* [3]	None	3.4	63

* Feed pressure of 2 atm

Similar to the 6FpDA:DABA membranes, the untreated DAM:DABA membranes show the typical copolymer behavior. As more DABA is incorporated into the backbone, both permeabilities decrease, but the CO_2/CH_4 selectivity increases. The permeability/selectivity trade-off for various esterification treatments of the 2:1 do not follow a simple relationship, as has been discussed empirically [4] and fundamentally [5]. The complex morphology of the crosslinked membranes is dependent on the crosslinking agent length and flexibility. These characteristics affect its reactivity in the solid state and the polymer packing characteristics (free volume distribution etc.).

4.2 CO_2 SORPTION

4.2.1 Films Annealed at 220°C

Figures 4.6 and 4.7 show the CO_2 sorption isotherms for the 6FDA-6FpDA:DABA 2:1 and 6FDA-DAM:DABA 2:1 polymers, respectively.

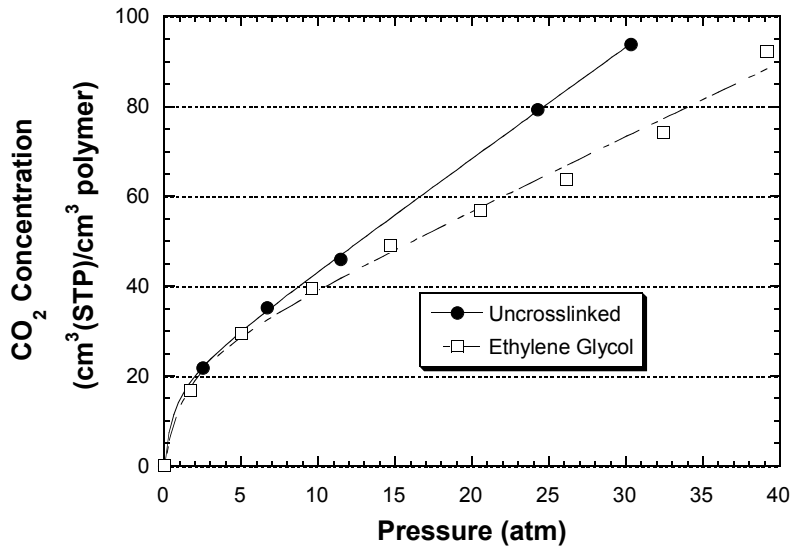

Figure 4.6: CO_2 sorption isotherms for 6FDA-6FpDA:DABA 2:1 membranes crosslinked with ethylene glycol

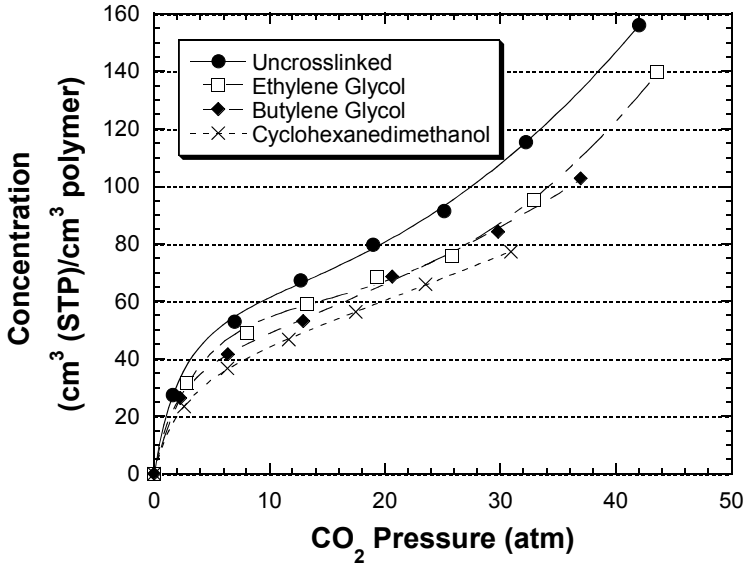

Figure 4.7: CO_2 sorption isotherms for 6FDA-DAM:DABA 2:1 membranes crosslinked with various diols

It has been suggested that plasticization occurs for a variety of glassy polymers when the CO_2 concentration reaches a threshold value of ~ 37 ± 7 cm^3(STP)/cm^3 polymer at 25°C [10], but it appears that a more complex criterion applies, at least at 35ºC. The polymers studied by Bos et al. were not crosslinked and, except for the two polyimides, all had glass transition temperatures below 225°C. The use of rigid, packing disrupted polymers leads to high Langmuir sorption capacities (e.g. 6FDA-6FpDA and 6FDA-DAM), allowing CO_2 sorption levels to reach 100 cm^3(STP)/cm^3 polymer before the onset of plasticization in pure gas CO_2 permeation. The CO_2 sorption levels are strongly dependent on the segmental packing, and the plasticization resistance is related to the segmental mobility, not just to a simple concentration threshold. It is hypothesized that both

intra-chain and inter-chain rigidity are necessary to preserve diffusion selectivity for feeds with high CO_2 partial pressures.

Interestingly, the sorption isotherms for the covalently crosslinked polymers tend to show an upturn at pressures above 25 atm, whereas the permeation isotherms remain flat. This is contrary to the conventional wisdom that the permeation isotherm will reach its minimum value at lower pressures than that of the sorption coefficient isotherm (S=C/p). This unusual behavior has been observed for many polyimides in our laboratory.

The CO_2 sorption isotherms can be fit to the dual mode model for pressures below 25 atm where the model fits adequately to measure the effect of crosslinking on the sorption via the hole-filling and dissolution mechanisms. The parameters are summarized in Table 4.3.

Table 4.3: CO_2 sorption dual mode parameters at 35°C

Polymer	Crosslink Agent	k_D (cm^3(STP)/cm^3 polymer atm)	C_H' (cm^3(STP)/cm^3 polymer)	b (1/atm)
6FDA-6FpDA [11]	None	1.93	31.3	0.673
6FDA-6FpDA:DABA 2:1	None	2.47	19.7	1.66
6FDA-6FpDA:DABA 2:1	EG	1.62	25.7	0.790
6FDA-DAM	None	2.18	55.0	0.42
6FDA-DAM:DABA 2:1	None	1.73	51.3	0.58
6FDA-DAM:DABA 2:1	BG	1.66	36.0	0.78
6FDA-DAM:DABA 2:1	EG	1.05	53.5	0.41
6FDA-DAM:DABA 2:1	CHDM	1.36	37.0	0.58

Covalent crosslinking tends to decrease the Henry's law coefficient, k_D, and made all films insoluble in THF.

4.2.2 Films annealed at 100°C and 295°C

The data in Fig. 4.6 and 4.7 suggest that crosslinking decreases the CO_2 sorption. However, the esterification treatments simultaneously change the polymer composition, confounding the true cause of the reduced sorption. By annealing monoester films at various temperatures, the effect of crosslink density on the sorption isotherms can be quantified. When the films are annealed at 100°C, there is essentially no crosslinking. When the films are annealed at 295°C, there is significant crosslinking.

Fig. 4.8 and 4.9 show the effect of the annealing temperature on the CO_2 sorption isotherms for the 6FDA-DAM:DABA 2:1 BG and CHDM monoesters.

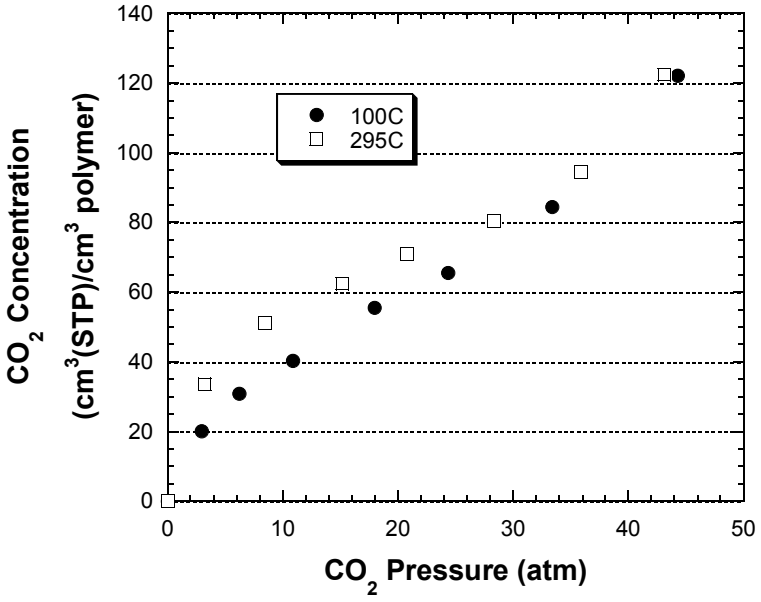

Figure 4.8: Effect of annealing temperature for 6FDA-DAM:DABA 2:1 BG monoester

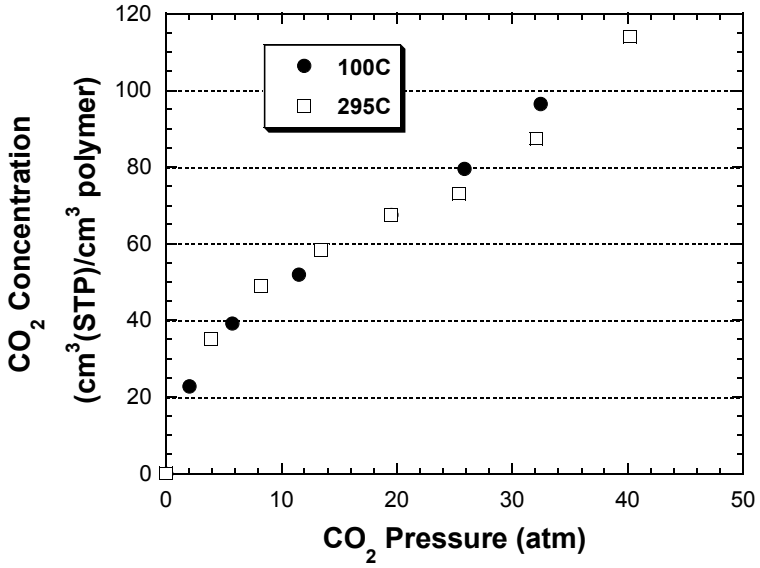

Figure 4.9: Effect of annealing temperature for 6FDA-DAM:DABA 2:1 CHDM monoester

Table 4.4: CO_2 sorption dual mode parameters at 35°C for 6FDA-DAM:DABA 2:1 monoester films annealed at 100°C and 295°C

Polymer	**Crosslink Agent**	**k_D (cm^3(STP)/cm^3 polymer atm)**	**C_H' (cm^3(STP)/cm^3 polymer)**	**b (1/atm)**
BG	100	1.81	24.5	0.54
BG	295	1.35	46.8	0.55
CHDM	100	1.82	31.1	0.51
CHDM	295	0.814	59.9	0.29

From the data in Fig. 4.6 and 4.7 it appears that covalent crosslinking decreases the CO_2 sorption, especially at high pressures. This is reflected in the lower Henry's law coefficient (k_D) values for the crosslinked films. However, the data in Fig 4.8 and 4.9 show that for a given starting monoester polymer, films that are annealed at higher temperatures and have more crosslinking have *higher* sorption. Upon inspection of the dual mode parameters in Table 4.4, it's clear that greater crosslinking levels lead to an increase in the Langmuir capacity constant (C_H') and a decrease in the k_D values. This is supported by the permeation data in Fig. 4.5 where the CO_2 permeability is increased with the higher crosslinking density from annealing at 295°C. This change in the free volume is also apparent from the wide angle X-ray diffraction patterns of the CHDM monoester, treated at 100°C and 295°C. The average d-spacing of an amorphous polymer reflects the average interchain spacing [12] and this is correlated with the gas permeability for polyimides [13]. Annealing the CHDM monoester at 295°C increases the average d-spacing to 5.53Å from 5.28 Å for the film annealed at 100°C, as shown in Fig. 4.10.

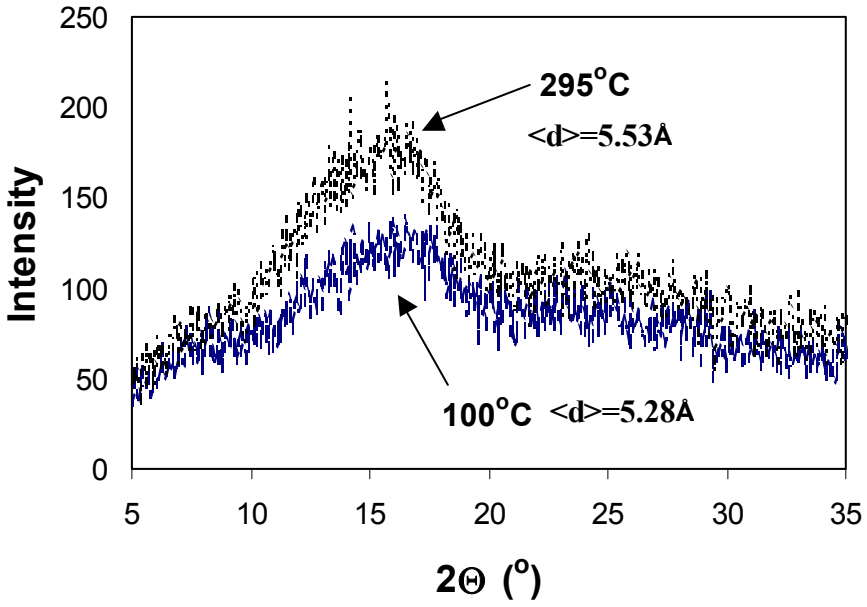

Figure 4.10: Wide angle X-ray diffraction pattern for 6FDA-DAM:DABA 2:1 CHDM monoester dried at 100°C and 295°C

4.3 CH_4 SORPTION

Much of this project focuses on how polymer structure relates to CO_2 plasticization, but the CH_4 sorption provides an important contrast because it does not plasticize the polymer significantly. In this sense it interacts less with the polymer. However, crosslinking still shows a significant impact on the CH_4 sorption, as shown in Fig. 4.11 and 4.12.

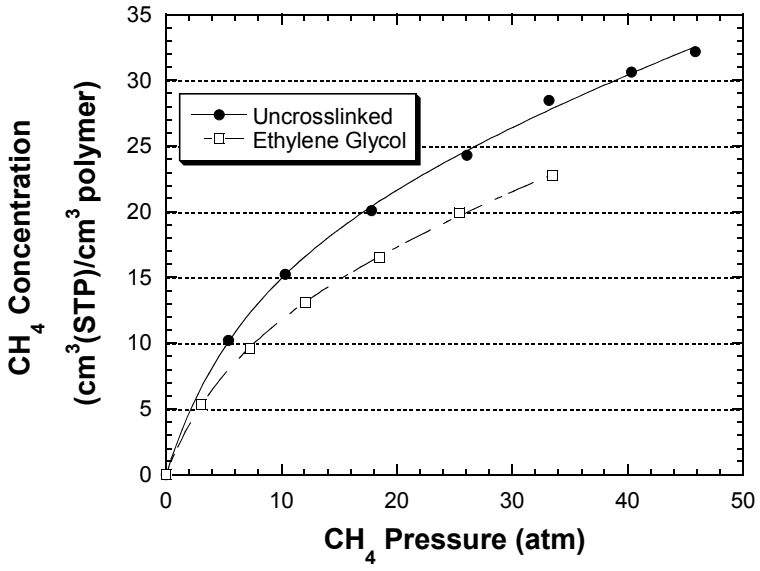

Figure 4.11: CH_4 sorption isotherms for 6FDA-6FpDA:DABA 2:1 membranes crosslinked with ethylene glycol

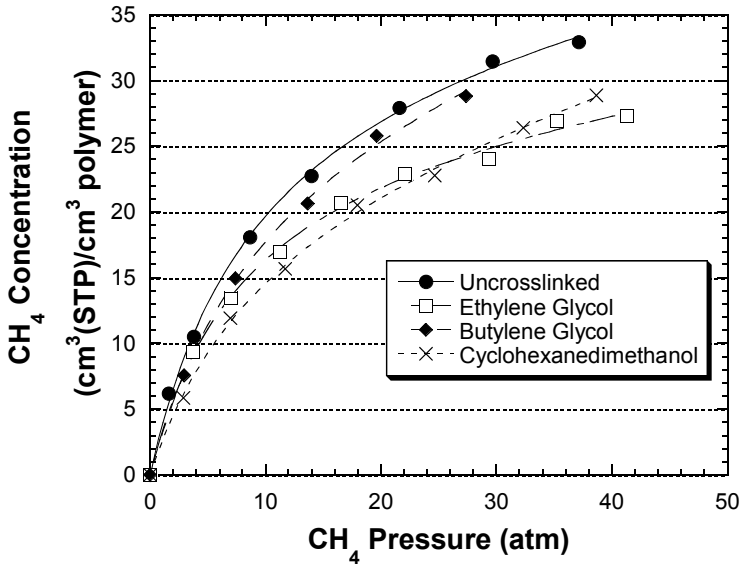

Figure 4.12: CH_4 sorption isotherms for 6FDA-DAM:DABA 2:1 membranes crosslinked with ethylene glycol, butylene glycol, and cyclohexanedimethanol

The dual mode sorption parameters are summarized in Table 4.5.

Table 4.5: CH_4 sorption dual mode parameters at 35°C

Polymer	**Crosslink Agent**	**k_D (cm^3(STP)/cm^3 polymer atm)**	**C_H' (cm^3(STP)/cm^3 polymer)**	**b (1/atm)**
6FDA-6FpDA [11]	None	0.211	28.7	0.0754
6FDA-6FpDA:DABA 2:1	None	0.290	23.2	0.108
6FDA-6FpDA:DABA 2:1	EG	0.303	15.8	0.124
6FDA-DAM	None	0.226	35.6	0.111
6FDA-DAM:DABA 2:1	None	0.137	35.3	0.108
6FDA-DAM:DABA 2:1	EG	0.107	27.7	0.124
6FDA-DAM:DABA 2:1	BG	0.258	30.2	0.101
6FDA-DAM:DABA 2:1	CHDM	0.244	24.3	0.0994

The effect of crosslinking on the CH_4 sorption is not as clear as that for CO_2. The Langmuir capacity constant is decreased with crosslinking, which is not always the case for CO_2. The Henry's law sorption is typically not decreased with crosslinking as it is for CO_2.

In pure gas experiments, the solubility selectivity above 5 atm is ~ 3. In mixed gas systems, the solubility selectivity is typically higher due to a higher Langmuir affinity constant for CO_2 over CH_4 [14]. However, changes in the polymer structure (monomer and crosslinking selection) affect the diffusion selectivity much more than the solubility selectivity. To understand the effects on the diffusion coefficients, the effects of polymer structure on the density and corresponding fractional free volume can be analyzed.

4.4 GLASS TRANSITION, DENSITY, AND FREE VOLUME

For rubbery polymers, crosslinking typically increases the T_g of polymers [15]. However, covalent crosslinking of the copolyimides has a negligible impact on the glass transition temperature. It also appears that the T_g does not scale with the crosslink density because the more reactive BG crosslinked films are presumably much more highly crosslinked than the EG film, yet they show very similar T_g's. This is again contrary to conventional wisdom for more flexible polymer backbones [15]. The effect of crosslinking on the copolyimide T_g's is shown in Table 4.6.

Table 4.6: Effect of crosslinking on T_g

Polymer	**Crosslinking Agent**	**Thermal Treatment (°C)**	**Tg (°C)**
6FDA-6FpDA:DABA 2:1	None	220	313
"	EG	220	323
6FDA-DAM:DABA 2:1	None	220	358
"	EG	295	364
"	BG	220	363
	BG	295	350
"	BDM	295	356

The effects of copolymer composition on the DAM:DABA and 6FpDA:DABA glass transition temperatures are shown in Fig. 4.13, and they show the typical copolymer behavior.

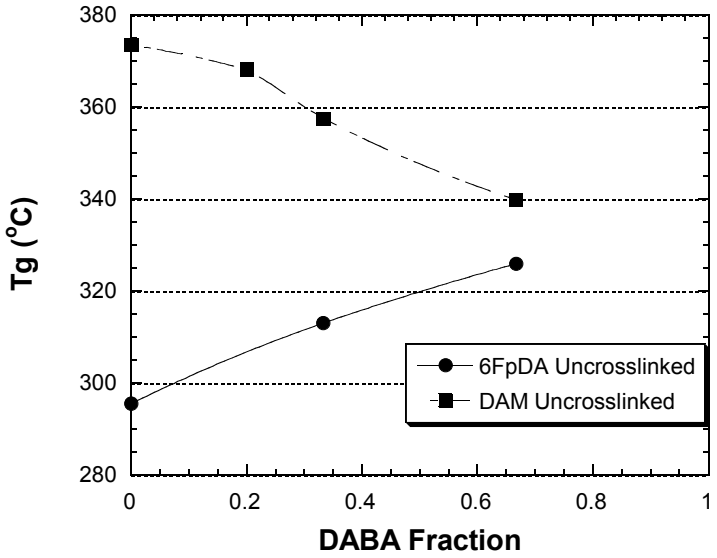

Figure 4.13: T_g as a function of copolymer composition

The effects of crosslinking on the film density and fractional free volume are shown in Table 4.7 along with characteristic CO_2 permeabilities and diffusion coefficients at 10 atm feed pressure. There is not a simple correlation between free volume and the permeability. Similar observations have been noted by others for the 6FDA-based family of polyimides [16]. The permeability coefficients may be related to the free volume distribution as well as the absolute amount of fractional free volume. Unfortunately, characterization of the distribution of free volume is complicated by the formation of the rigid crosslinked network structure. Currently, in fact, it is not possible to deconvolute the relative contributions of absolute free volume and distribution of free volume on separation performance in the crosslinked samples. Techniques such as positron annihilation lifetime spectroscopy (PALS) have shown good correlation with the CO_2 diffusion coefficient in polyimides [17] and may be promising for the crosslinked

polyimides as well. It would be of great interest to see how crosslinking changes the free volume distribution via *in-situ* PALS in the presence of both plasticizing and non-interacting penetrants [18, 19].

Table 4.7: Polymer properties for 6FDA-DAM:DABA 2:1 with various chemical treatments

Crosslinking Agent	Thermal Treatment (°C)	Density (g/cm^3)	Fractional Free Volume	CO_2 Permeability * (Barrers)	CO_2 Diffusion Coefficient * (10^{-8} cm^2/s)
None	220	1.404	0.149	127	15.8
EG	220	1.404	0.149	90	12.7
BG	220	1.411	0.139	46	8.2
BDM	295	1.409	0.145	130	15.8

* permeability and diffusion coefficients measured at 10 atm feed pressure

4.5 SPECTROSCOPY

4.5.1 NMR

The reaction conversion in the monoesterification step may be quantified by ^{1}H NMR. The methylene proton nearest the ester bond ("c" in Fig 4.14) appears at ~ 4.2 ppm in the spectra, and this does not overlap with any other peaks from the polymer or solvent (DMSO-d_6). The conversion of carboxylic acids to esters may be calculated by taking the ratio of the area of this methylene peak with that of the aromatic protons, compared with the theoretical ratios at complete conversion from the known copolymer composition. The aromatic proton from the DAM moiety (at 7.3 ppm) is clearly resolved, so the internal consistency of the conversion calculation can be checked by the inclusion and exclusion of this peak from the areas of the aromatic protons. A representative NMR spectrum of a

monoester is shown in Fig. 4.14, where the conversion is essentially 100% for the 2:1 polymer esterified with butylene glycol. The conversion for this particular polymer may also be calculated from the peaks arising from the "a" and "b" in the butylene glycol moiety, as shown in Fig. 4.14.

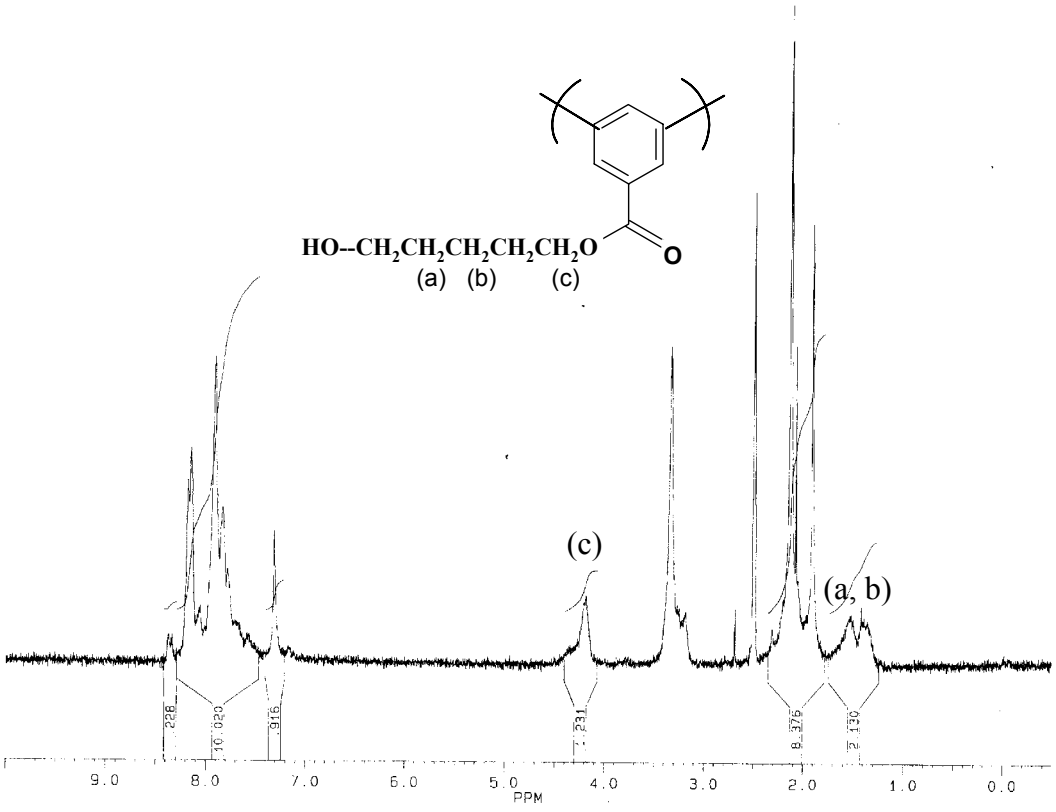

Figure 4.14: NMR spectrum of 6FDA-DAM:DABA 2:1 butylene glycol monoester

The monoesterification reaction in NMP gives the reactants good mobility for reaction, and the large excess of glycol (40-70 times the stoichiometric amount) should clearly favor the formation of the ester product and prevent crosslinking in solution. However, alcohols can form complexes with NMP and

this may affect their reactivity in solution [20]. The aromatic ring in 1,4-benzenedimethanol is electron withdrawing and it shows the lowest conversion, due to its poor nucleophilicity. A summary of the monoester conversions is shown in Table 4.8.

Table 4.8: Monoester Conversions for 6FDA-DAM:DABA 2:1

Crosslinking Agent	Conversion (%)
Ethylene Glycol	37
Butylene Glycol	100
1,4-cyclohexanedimethanol	50
1,4-benzenedimethanol	16

The monoesterification reaction is carried out at lower temperatures and with much lower acid concentrations than is typically used for esterification reactions with diols. An extensive review of esterification reactions by Fradet and Marechal showed that most lightly catalyzed esterifications of aromatic carboxylic acids have been carried out at temperatures above 180°C [21]. To obtain higher conversions, the monoester reaction could be carried out at higher temperatures, in a different solvent, at higher concentrations, or the water could be distilled from the solvent during the reaction.

To obtain high crosslinking conversions, it is necessary to have at least 50% conversion for the monoester reaction, since this could still lead to the theoretical 100% conversion in the solid-state crosslinking reaction.

4.5.2 IR Spectroscopy

When the monoester film is dried under vacuum at elevated temperatures, a transesterification (i.e., crosslinking) reaction is activated. In the glassy solid-state, the reactant mobility is much lower, and the equilibrium can only be pushed

toward the formation of crosslinks by removing the volatile glycol from the film. The crosslinking degree is therefore limited by the intrinsic reactivity of the alcohol group and its mobility in the solid-state to attack the ester carbon atom. This is in contrast to the solid-state polymerizations of poly(ethylene terepthalate) and poly(butylene terepthalate) where the reaction temperature occurs well above the glass transition temperature and there is much greater reactant mobility [22].

The solid-state crosslinking reaction can be monitored by IR spectroscopy. Fig. 4.15 shows the chemical modifications to the polymer by the monoesterification and transesterification reactions for the 2:1 polymer. The IR technique is only semi-quantitative in determining the crosslinking degree, because the OH group can be involved in hydrogen bonding, thus complicating the quantitative analysis. The O—H stretching absorption from the carboxylic acid in the DABA moiety is a broad peak in the region 3000-3600 cm^{-1}, agreeing well with the literature values [23]. The crosslinking conversion can be observed by the diminishing peaks at 3300 cm^{-1} and 2950 cm^{-1} with the crosslinking reaction. The peak at 2900 cm^{-1} is likely the aliphatic C—H stretch from the pendant butylene glycol molecules [23]. The peak centered at 3300 cm^{-1} is most likely the O—H stretch from the BG group. The density of these groups is decreased as the transesterification crosslinking reaction proceeds.

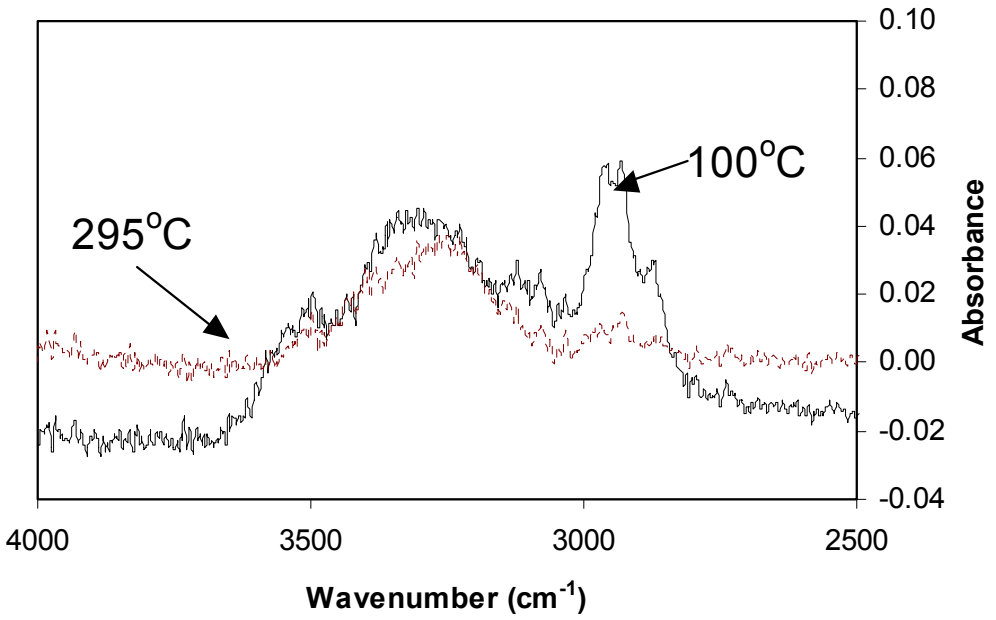

Figure 4.15: IR spectra showing the effect of annealing temperature on the 6FDA-DAM:DABA 2:1 butylene glycol monoester

4.5 CONCLUSIONS

Two covalent crosslinking protocols have been investigated to crosslink the 6FDA-6FpDA:DABA 2:1 and 6FDA-DAM:DABA 2:1 copolymers. The monoester approach offers significant advantages over the traditional post-treatment, in that it can be easily scaled up, is less dependent on the physical properties of the diol crosslinking agent, the esterification reaction yields can be characterized spectroscopically, and it is much more likely to be implemented in the commercial production of asymmetric hollow fiber membranes. The solid-state crosslinking reaction takes place well below the glass transition temperature of these copolymers, and no additives are required to activate the reaction.

The crosslinking agent and the annealing temperature have a huge impact on the membrane transport properties for a given copolymer. With high annealing temperatures, for the monoester there is an increase in the free volume either due to disruption of polymer chain packing by the insertion of the crosslinking molecules between the chains or from the creation of free volume by removal of the pendant diol groups. This change in the free volume is supported by sorption and wide angle X-ray measurements. When the CO_2 sorption is analyzed within the dual mode framework, higher annealing temperatures for the monoester lowers the Henry's law coefficient, k_D, and increases the Langmuir capacity constant, C_H'. The total sorption is not necessarily decreased by crosslinking, but the esterification treatments generally decrease the sorption. The change in the mode of sorption appears to be critical in determining the polymer swelling, which is explored in Chapter 5.

REFERENCES

[1] Bos, A., I. Punt, H. Strathmann and M. Wessling, Suppression of gas separation membrane plasticization by homogeneous polymer blending, *AIChE J.*, **2001**, *47*, 1088-1093.

[2] Coleman, M. R. and W. J. Koros, Conditioning of fluorine containing polyimides. 1. effect of exposure to high pressure carbon dioxide on permeability, *Macromolecules*, **1997**, *30*, 6899-6905.

[3] Hirayama, Y., T. Yoshinaga, S. Nakanishi and Y. Kusuki, Relation between gas permeabilities and structure of polyimides, in *Polymer Membranes for Gas and Vapor Separations*, American Chemical Society Symposium Series, 733, 1999, pp. 194-214.

[4] Robeson, L. M., Correlation of separation factor versus permeability for polymer membranes, *J. Membr. Sci.*, **1991**, *62*, 165-185.

[5] Freeman, B. D., Basis of permeability/selectivity tradeoff relations in polymeric gas separation membranes, *Macromolecules*, **1999**, *32*, 375-380.

[6] Bos, A., I. G. M. Punt, M. Wessling and H. Strathmann, Plasticization-resistant glassy polyimide membranes for CO_2/CH_4 separations, *Sep. and Purif. Tech.*, **1998**, *14*, 27-39.

[7] Krol, J. J., M. Boerrigter and G. H. Koops, Polyimide hollow fiber gas separation membranes: Preparation and the suppression of plasticization in propane/propylene environments, *J. Membr. Sci.*, **2001**, *184*, 275-286.

[8] Salley, J. M. and C. W. Frank, Charge transfer in aromatic polyimides, in *Polyimides: Fundamentals and Applications*, Marcel Dekker, Inc., New York, 1996.

[9] Kawakami, H., M. Mikawa and S. Nagaoka, Gas transport properties in thermally cured aromatic polyimide membranes, *J. Membr. Sci.*, **1996**, *118*, 223-230.

[10] Bos, A., I. G. M. Punt, M. Wessling and H. Strathmann, CO_2-induced plasticization phenomena in glassy polymers, *J. Membr. Sci.*, **1999**, *155*, 67-78.

[11] Coleman, M. R., Isomers of fluorine-containing polyimides for gas separation membranes (glassy polymers), Ph.D. Dissertation, The University of Texas at Austin, 1992.

[12] Schwartz, L. H. and H. B. Cohen, *Diffraction from Materials*, Academic Press, New York, 1977.

[13] Kim, T. H., W. J. Koros, G. R. Husk and K. C. O'Brien, Relationship between gas separation properties and chemical structure in a series of aromatic polyimides, *J. Membr. Sci.*, **1988**, *37*, 45-62.

[14] Sanders, E. S. and W. J. Koros, Sorption of carbon dioxide, ethylene, nitrous oxide and their binary mixtures in poly(methyl methacrylate), *J. Polym. Sci., Polym. Phys. Ed.*, **1986**, *24*, 175-188.

[15] Nielsen, L. E., Crosslinking - effect on physical properties of polymers, *J. Macromol. Sci., Rev. Macromol. Chem.*, **1969**, *3*, 69-103.

[16] Singla, S., H. W. Beckman and M. E. Rezac, Localized chain mobility and gas transport properties of thermoplastic aromatic polymers, *J. Membr. Sci.*, **2002**, *208*, .257-267.

[17] Nagel, C., K. Guenther-Schade, D. Fritsch, T. Strunskus and F. Faupel, Free volume and transport properties in highly selective polymer membranes, *Macromolecules*, **2002**, *35*, 2071-2077.

[18] Hong, X., Y. C. Jean, H. J. Yang, S. S. Jordan and W. J. Koros, Free-volume hole properties of gas-exposed polycarbonate studied by positron annihilation lifetime spectroscopy, *Macromolecules*, **1996**, *29*, 7859-7864.

[19] Yuan, J. P., H. Cao, E. W. Hellmuth and Y. C. Jean, Subnanometer hole properties of CO_2-exposed polysulfone studied by positron annihilation lifetime spectroscopy, *J. Polym. Sci. Polym. Phys. Ed.*, **1998**, *36*, 3049-3056.

[20] Hong, P. D., C. M. Chou and C. H. He, Solvent effects on aggregation behavior of polyvinyl alcohol solutions, *Polymer*, **2001**, *42*, 6105-6112.

[21] Fradet, A. and E. Marechal, Kinetics and mechanisms of polyesterifications. I. Reactions of diols with diacids, *Adv. Polym. Sci.*, **1982**, *43*, 51-142.

[22] Schultz, J. M., S. Fakirov, *Solid State Behavior of Linear Polyesters and Polyamides*, Prentice Hall, Englewood Cliffs, NJ, 1990.

[23] Silverstein, R. M. and F. X. Webster, *Spectrometric Identification of Organic Compounds, 6th Ed.*, John Wiley and Sons, Inc., New York, 1997.

Chapter 5: Effects of Thermal Annealing and Covalent Crosslinking on CO_2-induced Plasticization: Coupling of Sorption, Swelling, and Diffusion

5.1 INTRODUCTION

Recently, compressed CO_2 has emerged as an alternative solvent because it is non-toxic, non-flammable, inexpensive, and has easily tunable solvent properties near the critical point. However, the high pressures required in supercritical applications and the expensive nature of most CO_2 surfactants and stabilizers make high-pressure CO_2 separations attractive for avoiding high raw materials and recompression costs. Membranes have potential for these types of separations [1], but an understanding of the CO_2/polymer interactions is necessary to develop next-generation materials. It has been demonstrated that CO_2 is very effective at swelling and plasticizing polymers and this property has been used advantageously in the impregnation, extraction, and foaming of polymer films [2, 3]. However, swelling and plasticization are detrimental to membrane performance. Thus, designing effective membranes for high-pressure CO_2 separations presents a difficult challenge.

Many polyimides are not soluble in common solvents such as 1-methyl-2-pyrolidinone (NMP) and tetrahydrofuran (THF), so they must be cast as a polyamic acid and then thermally imidized at 300°C. However, in many applications it is desirable to work with soluble polyimides, so they can easily be cast into films or spun into asymmetric hollow fibers without the aggressive thermal cure. Polyimides derived from 6FDA tend to have excellent transport properties and processing characteristics, but they are highly susceptible to plasticization. The two most common approaches for stabilizing these materials have been crosslinking [4, 5] and/or thermal treatments [6, 7]. In order to

establish a stability criterion, it is necessary to decouple the physical annealing and chemical crosslinking that occur simultaneously during the thermal treatment.

The effect of crosslinking on the sorption and dilation of CO_2 in rubbery polymers may be estimated through the Flory-Rhener model, but no similar model exists for crosslinking of glassy polymers. In this chapter we probe the effect of the polymer chain rigidity on the CO_2 sorption, permeability, and the polymer dilation to understand how the polymer properties are affected by sorbed CO_2 and the implications this has for membrane separations, particularly in the long-term stability.

It has been shown for some 6FDA-based polyimides that the polymer dilation kinetics can be very protracted at CO_2 pressures above 20 atm, as the polymer chains relax under the plasticizing effect of the sorbed CO_2 [8, 9].

The use of *in-situ* spectroscopic ellipsometry is a powerful tool for analyzing thin film sorption and dilation, since thin films can sorb differently [10] and plasticize at lower pressures [11] than thick films. Complications in the analysis of sorption in glassy polymers by simple interferometric techniques have been reported [12] due to the difficulties in independently decoupling the thickness and refractive index from the optical data. In contrast, ellipsometry can independently determine the thickness and refractive index of a thin film, allowing for reasonably accurate estimates of sorption levels in rigid glassy polymers. In addition, a CO_2-induced T_g (or P_g) may also be determined from the hysteresis behavior of the sorption and desorption curves [13].

The main objective of this chapter is to understand how the sorption, dilation, and diffusion processes are coupled in a plasticized gas separation membrane, and how the polymer structure may be modified by thermal annealing and chemical crosslinking to control the diffusion coefficient in the presence of high CO_2 concentrations. A clear relationship between the relaxation-controlled

sorption, permeation, and dilation has yet to be described either empirically or theoretically.

Spectroscopic ellipsometry is used to measure the dilation and estimate the CO_2 sorption in very high T_g (~ 360°C) polyimide thin films with various heat treatments and covalent crosslinking. Sorption measurements on bulk free-standing films by the pressure-decay method are compared with the ellipsometric measurements for the supported thin films. Plasticization of the polymer in permeation experiments is correlated to the polymer swelling, to explain why these polyimides plasticize and why covalent crosslinking and thermal annealing are effective approaches for stabilizing these membranes.

5.2 POLYMER FILM SOLUBILITY AS A FUNCTION OF THERMAL AND CHEMICAL TREATMENTS

Thermal treatments of polyimide films can change their solubility properties significantly [14]. Table 5.1 shows how the solubility of the polymers studied here change with annealing temperature. For annealing at 295°C, the 6FDA-DAM:DABA 2:1 film becomes lightly colored and insoluble, whereas the 6FDA-DAM remains completely soluble and colorless. Changes in film color with annealing are typically attributed to the formation of charge transfer complexes (CTC), between the electron-donating diamine fragments and the electron-accepting imide fragments [15].

Table 5.1: Polyimide solubility for various thermal and chemical treatments

Polymer	**Esterification**	**Thermal Treatment (°C)**	**Solubility in NMP at 120°C after 5 days**
6FDA-DAM	None	295	Soluble
6FDA-DAM:DABA 2:1	None	220	Soluble
6FDA-DAM:DABA 2:1	None	295	Gelled

It appears that the changes in solubility are associated with the presence of the DABA moiety. Infrared spectroscopy was used to see if the thermal annealing results in crosslinking (chemical via anhydride formation, opening of the imide ring to form crosslinks, or physical from dimerization of the carboxylic acid groups of the DABA moieties. No visible changes to the spectra, as shown in Fig. 5.1.

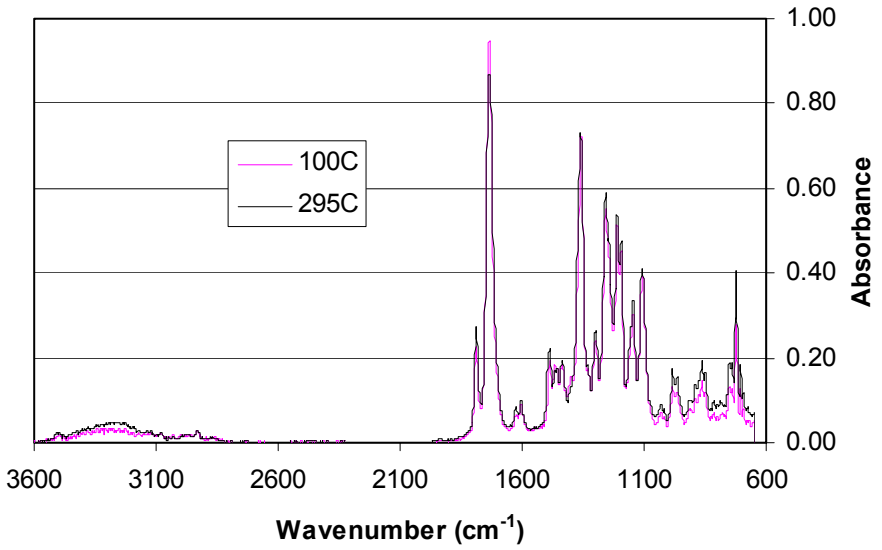

Figure 5.1: IR spectra for 6FDA-DAM:DABA 2:1 annealed at 100ºC and 295ºC for 24 h

It is known that polyimide solubility is related to the electron delocalization, which is affected by the packing density (steric effects) and the presence of electron-withdrawing groups [16]. Typically in the solid-state, intermolecular CTC dominates over intramolecular CTC via π-bonding overlap between donor and acceptor moieties. The heat treatment at 295°C makes the normally soluble 2:1 polyimide insoluble, possibly due to CTC or physical or chemical crosslinking. Some control experiments are recommended in Section 8.2.3 to further understand the structural factors which lead to this stabilization with heat treatments.

5.3 PERMEATION ISOTHERMS FOR BULK FREE-STANDING FILMS

In this chapter, it is shown how the polymer free volume can be affected by CO_2 plasticization and how the CO_2 diffusion coefficient increases as a result. Heat treatment of aromatic polyimides is an effective approach for reducing CO_2

plasticization in high-pressure membrane separations. The polyimides tend to become more darkly colored with thermal treatments, presumably showing the formation of charge transfer complexes and physical aging [7]. Fig. 5.2 and 5.3 show the effect of heat treatments and covalent crosslinking of the 6FDA-DAM:DABA 2:1 polyimide on the CO_2 permeation isotherms.

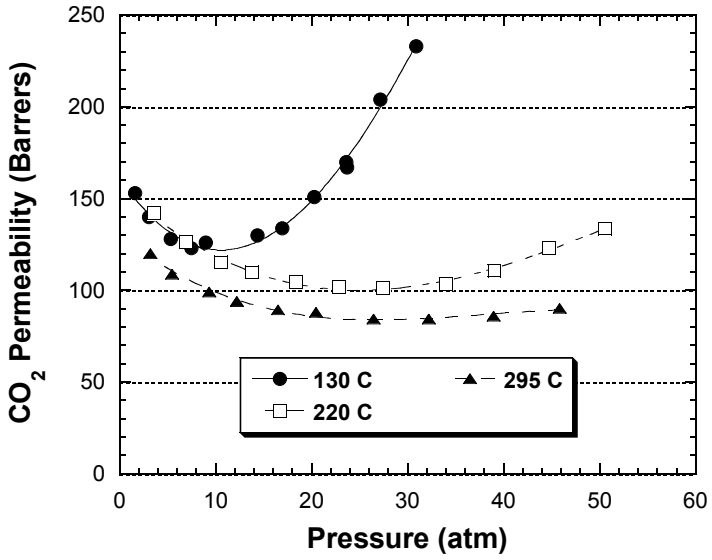

Figure 5.2: CO_2 permeation isotherms at 35°C for untreated 2:1 films annealed at 130°C, 220°C, 295°C

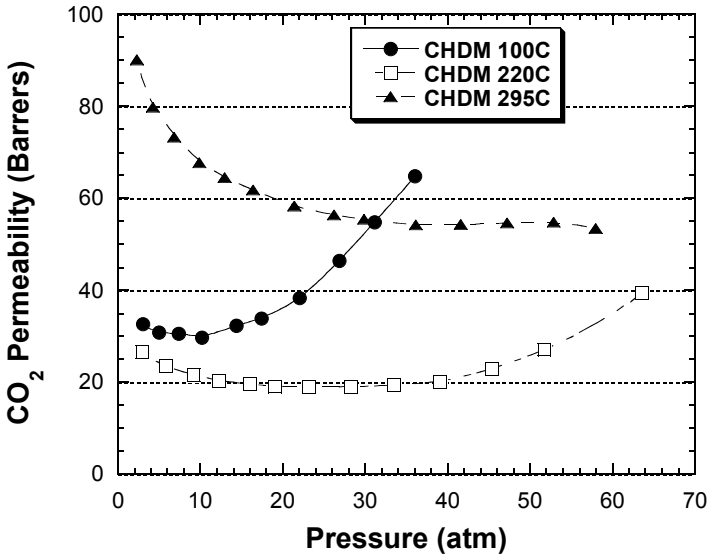

Figure 5.3: CO_2 permeation isotherms at 35°C for 2:1 CHDM monoester films annealed at 100°C, 220°C, 295°C

The permeation isotherms show that increased annealing temperature gives the membranes better resistance to CO_2 plasticization. For the untreated polymer, the increased annealing temperatures decrease the CO_2 permeability. However, for the CHDM monoester, the permeability goes through a minimum with respect to the annealing temperature, as shown in Fig. 4.5. The film treated at 295°C shows much more "dual mode" character for pressures below 20 atm (i.e., decreasing permeability with increasing pressure), which supports the hypothesis that the free volume has been increased by insertion of the bulky crosslinking agent between the polymer chains. The CHDM film annealed at 295°C shows the best plasticization resistance, but the untreated film at 295°C is very stable as well.

5.4 SORPTION ISOTHERMS

5.4.1 Pressure-decay technique

The CO_2 sorption isotherms in Figure 5.4 show that thermal annealing of the 6FDA-DAM:DABA 2:1 films with free carboxylic acid groups (i.e. untreated) tends to decrease the CO_2 sorption, especially at high pressures. Surprisingly, the sorption curves for the 220°C and 295°C treatments are not too different, despite the fact that the solubility of these films in organic solvents (THF, NMP etc.) is *very* different (Table 5.1).

Crosslinking with CHDM does not necessarily *decrease* the sorption, but it appears to change the *mechanism* of the sorption, in contrast to the untreated polymers. The dual mode sorption parameters for CO_2 are shown in Table 5.2.

For the untreated films, higher temperature thermal annealing decreases the Langmuir capacity constant, C_H', which is consistent with an accelerated physical aging process, where the free volume decreases by a diffusive mechanism [17]. The Henry's law sorption coefficient, k_D, is also significantly reduced with heat treatment, reflecting the lower sorption at high pressures, where plasticization effects are observed. It appears that the high temperature annealing increases the cohesive energy density of the polymer, thus lowering the energetic gain for sorbing CO_2 molecules by the dissolution mechanism.

The CHDM monoesters show different sorption behavior with respect to the annealing temperature. Similar to the untreated polymer, the Henry's law sorption coefficient, k_D, is also significantly reduced with heat treatment, but it has a greater temperature dependence. However, the Langmuir capacity constant, C_H', increases with increased annealing temperatures. This is consistent with the permeation results in Fig. 5.3, where the annealing at 295ºC increases the permeability (from increased free volume) and it shows greater so-called "dual mode" behavior at low pressures.

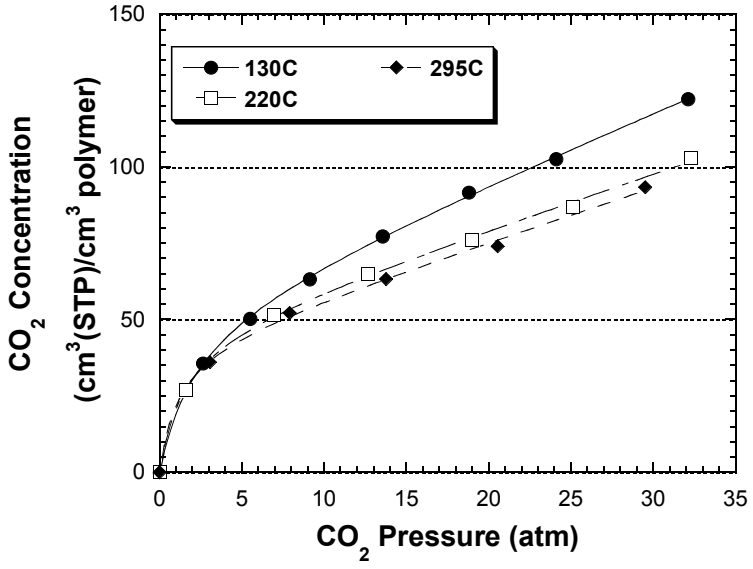

Figure 5.4: CO_2 Sorption isotherms at 35°C for 2:1 untreated bulk films annealed at 130°C, 220°C, 295°C

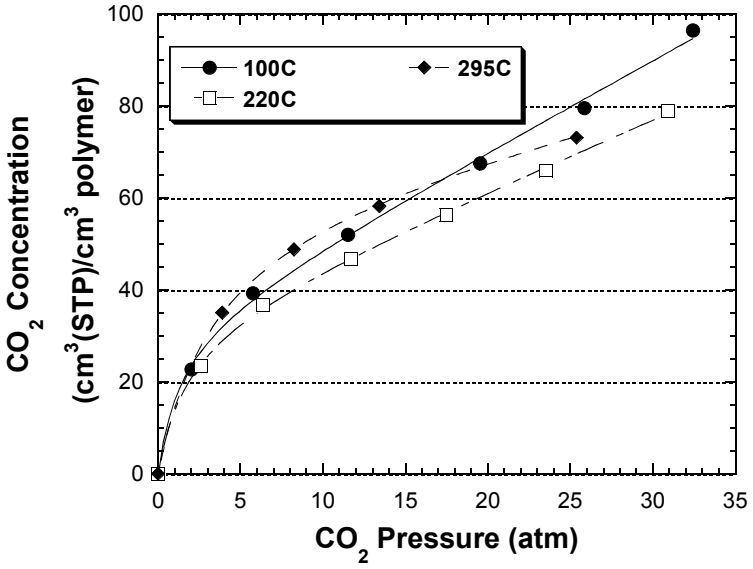

Figure 5.5: CO_2 Sorption isotherms at 35°C for 2:1 CHDM monoester bulk films annealed at 100°C, 220°C, 295°C

Table 5.2: CO_2 dual mode sorption parameters from pressure decay measurements at 35ºC

Thermal Treatment (°C)	k_D (cm^3(STP)/ cm^3 polymer atm)	C_H' (cm^3(STP)/ cm^3 polymer)	b (1/atm)
130 Untreated	2.23	54.2	0.45
220 Untreated	1.77	46.6	0.69
295 Untreated	1.74	42.4	0.90
100 CHDM	1.82	31.1	0.51
220 CHDM	1.36	37.0	0.58
295 CHDM	0.814	59.9	0.29

5.4.2 CO_2 Sorption from Refractive Index for Supported Thin Films

The solubility of gases in polymers can be measured by the pressure-decay method or by gravimetric means. The sorption can also be calculated from the refractive index of the solvent-laden polymer. A major advantage of using spectroscopic ellipsometry is that both dilation and sorption can be measured simultaneously and studies of the kinetics of each process are possible.

The refractive index of the film as a function of pressure is shown in Fig. 5.6. At low pressures, the refractive index increases as the microvoids are filled with CO_2 and the polymer densifies. Once these voids are saturated, the index decreases as the polymer becomes less dense with the increased dissolution of CO_2 into the polyimide. The sharp drop in the index around 75 atm likely arises in part to excess CO_2 sorbed onto/into the polymer due to compressibility effects, as was observed for PMMA [13]. At 35°C, this critical sorption of CO_2 should only occur over a small pressure range.

After exposure to high-pressure CO_2 (100 atm), the film contracts as the CO_2 pressure is decreased, but not to its pre-conditioned state. The result of this partial relaxation of the polymer chains (i.e., excess free volume) is a lower refractive index, as shown in Figure 5.6. This hysteresis behavior is discussed in further detail after analysis of the sorption isotherms.

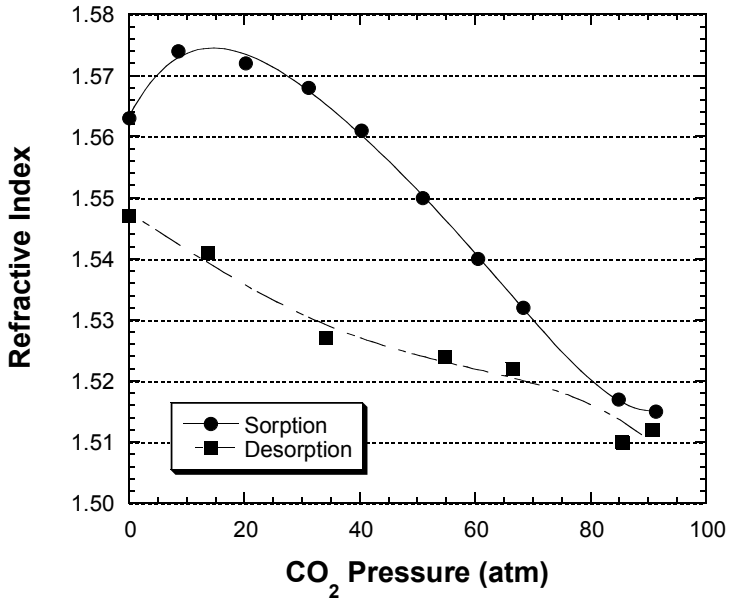

Figure 5.6: CO_2 refractive index isotherms at 35°C for 2:1 untreated bulk films annealed at 220°C

The procedure for calculating CO_2 mass fractions from the Clausius-Mosotti equation is described in Chapter 3. The CO_2 density and refractive index in the polymer were assumed to be 1.0 g/cm^3 and 1.233, respectively [18]. The density and refractive index of CO_2 are linearly correlated, in the pressures studied here [18]. The densities of the pure polymers were 1.4 g/cm^3, as measured in a density gradient column filled with aqueous calcium nitrate solutions. The refractive index was measured with spectroscopic ellipsometry for

each unconditioned sample at 1 atm (in air). Fig. 5.7 shows a comparison of the two sorption measurements for the untreated 2:1 films treated at 220°C.

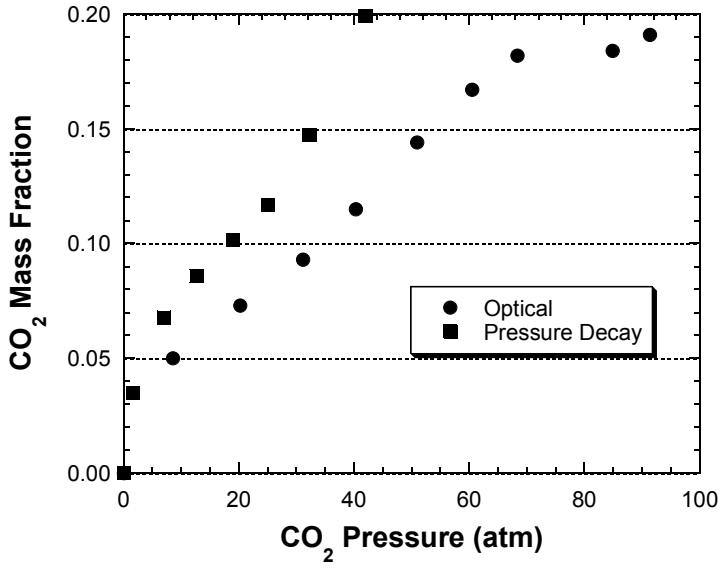

Figure 5.7: CO_2 sorption isotherms at 35°C for 2:1 untreated bulk films annealed at 220°C

The dual mode parameters, excluding the Langmuir affinity constant, *b*, are shown in Table 5.3. It was not possible to fit this parameter because too few data points were collected in the low-pressure region. For these calculations, the value of *b* was assumed to be the same as that for the bulk film measurements.

Table 5.3: CO_2 dual mode sorption parameters ellipsometer measurements

Thermal Treatment (°C)	**k_D (cm^3(STP)/ cm^3 polymer atm)**	**C_H' (cm^3(STP)/ cm^3 polymer)**
130 Untreated	2.06	15.9
220 Untreated	1.80	20.0
295 Untreated	1.13	21.0
100 CHDM	1.73	14.4
220 CHDM	1.49	10.5
295 CHDM	1.02	25.1

The sorption in the thin films calculated from the refractive index measurements is consistently lower than the sorption in thick films as measured by pressure decay. The sorption via Henry's law mechanism agrees reasonably well between the pressure-decay and ellipsometric techniques, and it shows consistent trends with respect to annealing temperatures. The offset primarily reflects differences in the Langmuir sorption capacity. The amount of free volume in a glassy polymer is dependent on the polymer structure and the thermal history. Aging effects in glassy polymers are more significant in thin films, as it is envisioned that the film densifies by a mechanism of diffusion of free volume to the free surface of the film. The characteristic path length for this diffusion determines the amount of aging at a given time [17]. The films used for the ellipsometry experiments were approximately 120 nm thick, whereas the films used for the pressure decay sorption were approximately 50,000 nm thick. The characteristic aging time scales as the film thickness squared, so there will be significant differences in the aging of the two films. Thus, one should expect

lower C_H's for the thin films relative to the thicker bulk films. In general, both techniques give consistent trends regarding the effect of heat treatment and chemical crosslinking on the sorption of CO_2 in the membranes.

5.5 DILATION OF SUPPORTED THIN FILMS

The dilation of glassy polymers is complicated by the different sorption mechanisms of hole-filling and dissolution (i.e., dual mode sorption). Various theoretical studies have been reported [19, 20] along with experimental characterization by dilatometry [21] and optical interferometry [12, 22]. Optical interferometry gives the product of the film thickness and the refractive index, thus requiring a known relationship between refractive index and thickness. Ellipsometry offers the advantage that thickness and refractive index are determined independently [23, 24].

The sorption and desorption dilation isotherms are shown in Figure 5.8 and 5.9 for the untreated and monoester films, respectively. It is clear that increasing heat treatment (Figure 5.8) leads to lower dilation at pressures below 80 atm, but above this pressure the swelling is very similar for all three films. The dilation becomes less sensitive to pressure above 80 atm because the CO_2 activity does not change appreciably with increasing pressure (P^{sat} = 78.7 atm at 35°C). For the desorption isotherms, large hysteresis is shown, reflecting the slow chain relaxations that are characteristic of glassy polymers. All of the polyimides studied here have T_g's of approximately 360°C, and since there is hysteresis in the sorption/desorption curves, this indicates that the CO_2 has not induced a glass transition, as was seen for PMMA previously [13], even though the CO_2 sorption is roughly twice as high as that of PMMA.

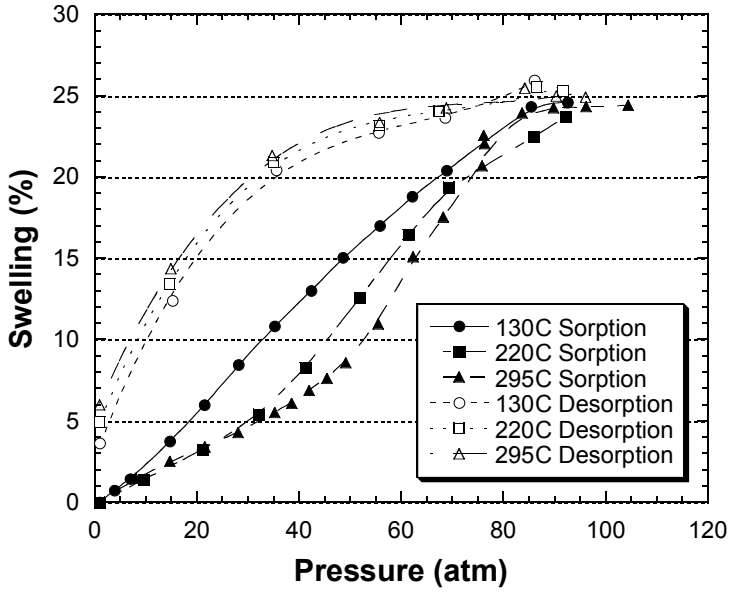

Figure 5.8: CO_2 swelling isotherms at 35°C for 2:1 untreated bulk films annealed at 130°C, 220°C, 295°C

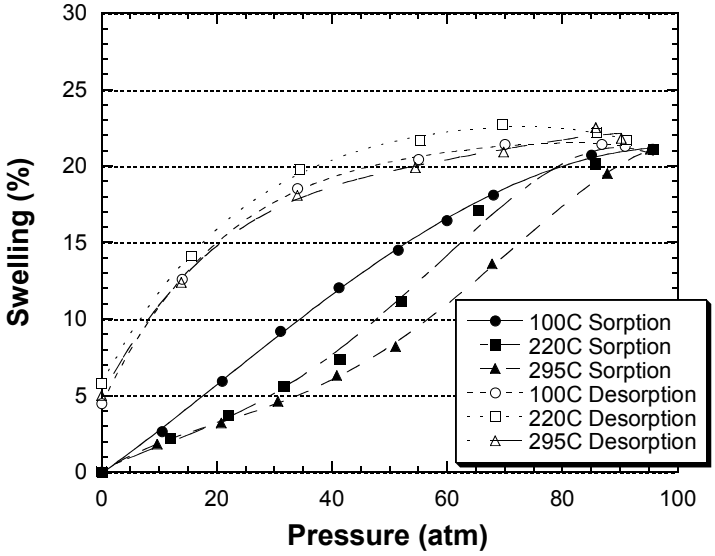

Figure 5.9: CO_2 swelling isotherms at 35°C for 2:1 CHDM monoester bulk films annealed at 100°C, 220°C, 295°C

In the study of high-pressure CO_2 sorption and dilation in PMMA, several researchers have assumed that an inflection point (i.e., upturn) in the swelling isotherm corresponded to the isothermal glass transition [25, 26]. However, it's clear from Figure 5.8 (as evidence by hysteresis) that there can be an inflection in the swelling isotherm without a glass transition. Moreover, for the uncrosslinked films treated at 130°C and 220°C, the pressures at which the inflection occurs (and the curves diverge from each other, 11 atm and 32 atm, respectively) corresponds to the respective plasticization pressures in the permeation isotherms (Fig. 5.2). Similar relationships are seen for the CHDM monoester films (Fig. 5.3). This increase in the permeability is a result of an increase in the diffusion coefficient, since the sorption isotherms do not show an upturn at these pressures. This increase in the diffusion coefficient is a result of the increase in the polymer chain segmental mobility and concomitant increase in free volume.

At 90 atm, the three untreated samples all have similar swelling, indicating that CO_2 may disrupt the physical interactions (e.g. charge transfer complexes) promoted by thermal annealing. CO_2 can act as a Lewis acid and have favorable interactions with the polar polyimide [27]. The desorption curves for the three annealed samples are also quite similar, though the higher the treatment temperature, the greater the hysteresis.

5.6 KINETICS OF PLASTICIZATION

5.6.1 Permeation

Plasticization is characterized by polymer chain relaxations that tend to reduce the separation efficiency for glassy polymeric membranes and cause unpredictable long-term performance. Fig. 5.10 and 5.11 show the effect of thermal annealing and crosslinking on the kinetic permeation at 40 atm feed pressure. The relative permeability (P_t/P_0) is defined as the ratio of the

permeability at any time to that at time zero (i.e., after four hour period, over which the feed pressure is increased to 40 atm). For the films treated at 100°C and 130°C, the initial permeability was chosen as the permeability measured at 8 atm feed pressure, since the films show significant increases in the permeability even within the four-hour time it takes to increase the pressure to 40 atm.

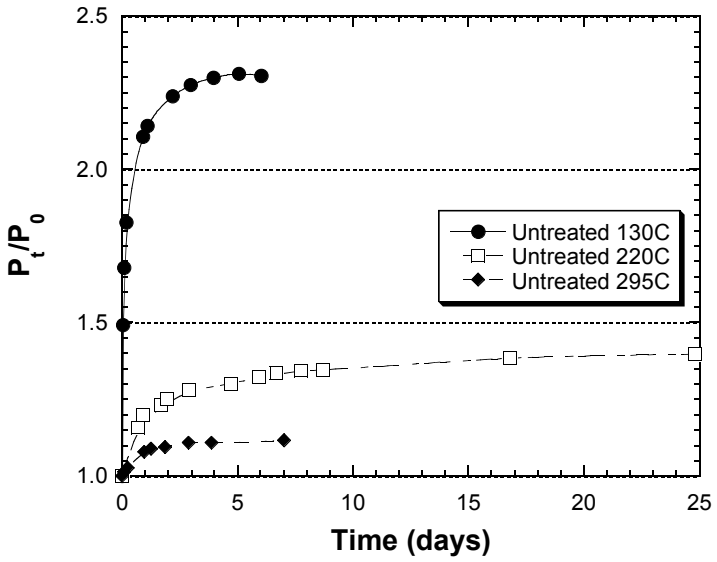

Figure 5.10: CO_2 kinetic permeability at 35°C and 40 atm for 2:1 untreated films annealed at 130°C, 220°C, and 295°C

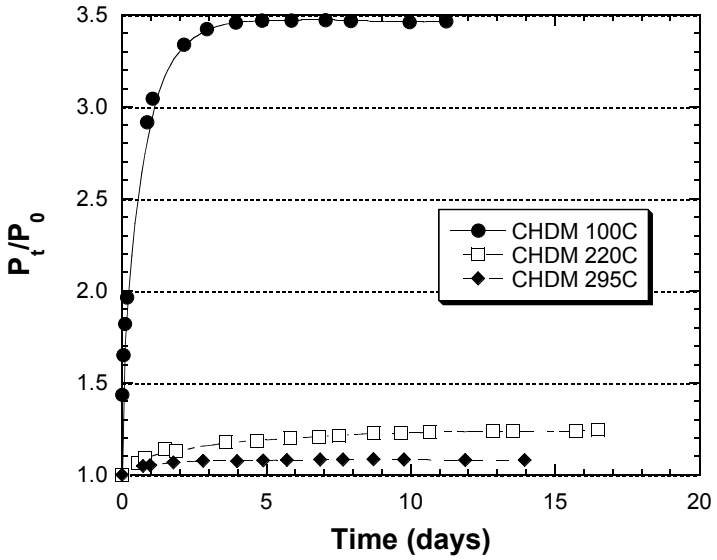

Figure 5.11: CO_2 kinetic permeability at 35°C and 40 atm for 2:1 CHDM monoester films annealed at 100°C, 220°C and 295°C

For both the untreated and CHDM membranes, higher annealing temperatures lead to much better stability. At the low temperature treatments, both membranes are very unstable. With a 220°C treatment the untreated film is completely soluble in THF and it shows a much more significant increase in the CO_2 permeability over time than does the insoluble, crosslinked membrane. For a 295°C treatment, both films are insoluble and show good stability against CO_2 plasticization.

5.6.2 Sorption

Kinetic sorption experiments by the pressure decay method show some deviations from Fickian uptake at 40 atm CO_2 pressure for these polymers. At higher pressures, the time taken to reach equilibrium for the thick films can be quite protracted, but the amount of excess gas sorbed as a result of these

relaxations is small in comparison to the corresponding non-Fickian swelling and permeability increases.

Figure 5.12 shows the kinetic sorption for the CHDM monoester annealed at 100°C and 295°C. The annealing temperature does not have a huge impact on the equilibrium CO_2 concentrations or the kinetic path taken to reach these equilibrium values. This is quite different from the permeation and swelling behavior, where the films annealed at higher temperatures have much more stable CO_2 permeabilities and do not swell as much. In Section 5.6.3, a correlation between the long-term swelling and the long-term permeability is shown (for a given annealing temperature). Since the long-term sorption does not depend much on the annealing temperature for the CHDM monoester, it appears that the increases in CO_2 permeability are caused by increases in the film swelling from the polymer chain relaxations facilitated by the sorbed CO_2.

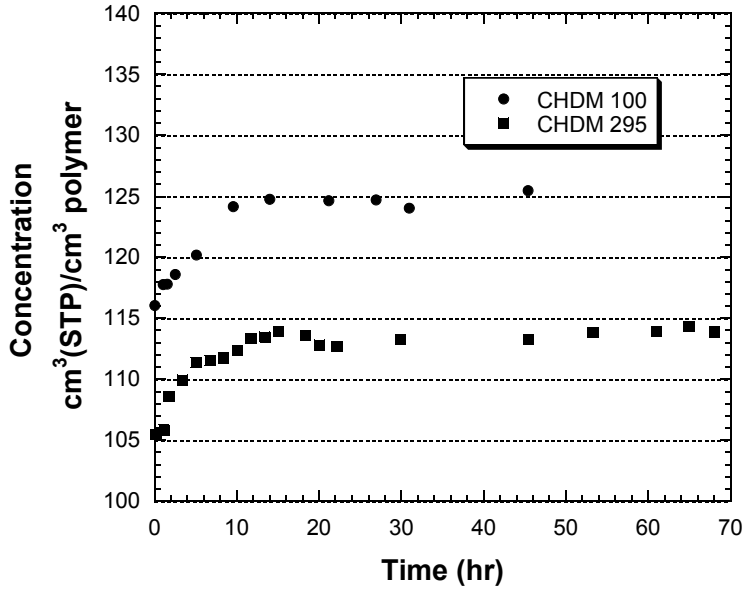

Figure 5.12: CO_2 kinetic sorption by pressure decay at 35°C and 40 atm for 2:1 CHDM monoester films annealed at 100°C and 295°C

5.6.3 Swelling

The kinetic dilation experiments in Fig. 5.13 show that the films continue to swell over long times, even in the absence of significant sorption due to polymer chain relaxations. This swelling reflects an increase in the polymer free volume as the chains rearrange themselves due to the increased mobility facilitated by the CO_2 molecules. This underscores the importance of experimental time scales in assessing polymer properties under conditions of plasticization.

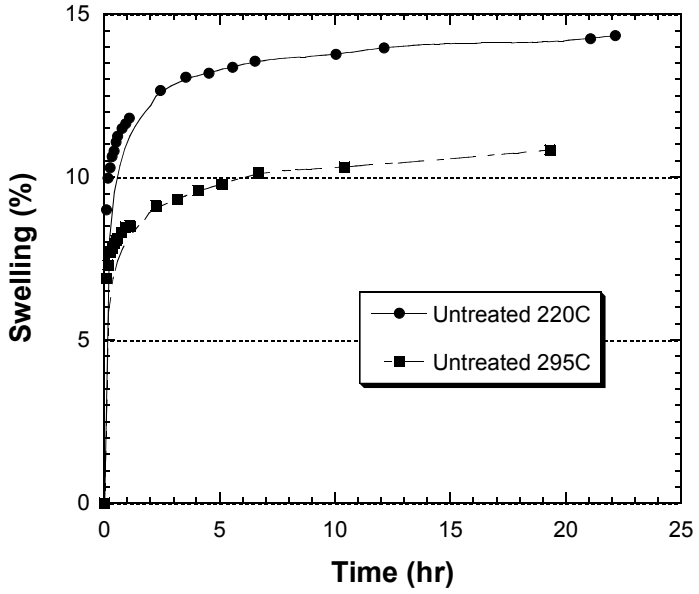

Figure 5.13: CO_2 kinetic swelling at 35°C and 40 atm for 2:1 untreated films annealed at 220°C and 295°C

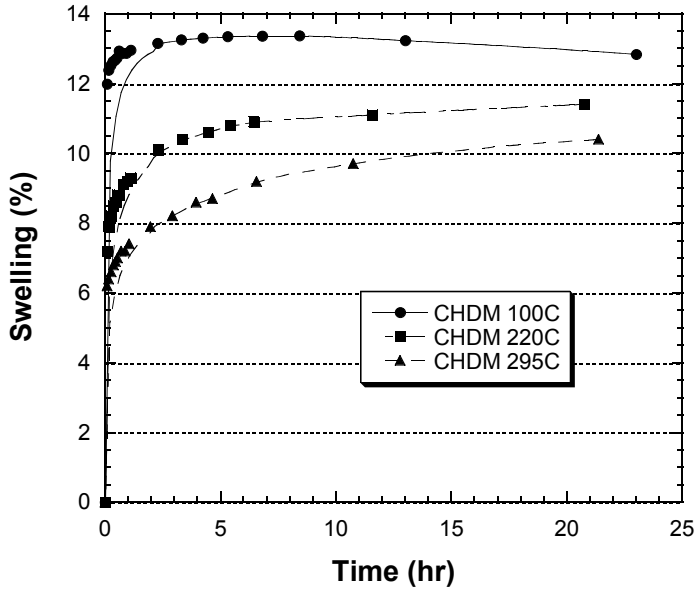

Figure 5.14: CO_2 kinetic swelling at 35°C and 40 atm for 2:1 CHDM monoester films annealed at 100°C, 220°C, 295°C

It is difficult to compare the absolute time scales of the kinetic permeation, sorption, and swelling because in the swelling experiments the films are very thin and supported on a substrate. In the permeation experiment, there is a concentration gradient across the film so the plasticization effects (e.g, polymer relaxations, changes in free volume) are likely to be different than if the pressure is isotropic. Nevertheless, there are some important observations regarding the coupling of permeation and swelling, namely the asymptotic limits of swelling and permeation, along with the kinetics of approaching this asymptote.

Increased annealing temperatures for both the untreated and CHDM films lead to better stability, both in permeation and swelling. There is a direct correlation between the asymptotic values of permeability and swelling with respect to annealing temperature for both polymers. Moreover, the kinetic trajectory at which the swelling approaches this asymptotic value is related to the polymer's resistance to plasticization. The films annealed at 130°C and 100°C are much less resistant to plasticization because they do not have crosslinks or charge transfer complexes acting to retard swelling. Therefore they reach their pseudo steady-state values very quickly. This is directly analogous to the permeability behavior shown in Fig. 5.10 and 5.11, where the membranes annealed at low temperatures become unstable very quickly *and* the amplitude of this instability is great. Thermal annealing and/or crosslinking is effective in suppressing these instabilities, which leads to more robust membrane performance in the presence of aggressive feed streams.

5.7 EFFECT OF CROSSLINKING: GLASSY VERSUS RUBBERY POLYMERS

Since the polyimides are extremely rigid, any restricted mobility from crosslinking has a much greater effect on the effect of CO_2 facilitated segmental motion than simple heat treatments where there are only physical interactions. These effects are similar to those seen in ionomers, where the rigidifying effects

of ionic clusters increases as the T_g of the matrix polymer increases [29]. For rubbery polymers such as poly(dimethylsiloxane), the effect of crosslinking on CO_2 swelling can be modeled with the Flory-Rhener expression [30]

$$\ln a = \ln \Phi_2 + (1-\Phi_2) + \chi(1-\Phi_2)^2 + V_2\left(\frac{\upsilon_e}{V_o}\right)\left[(1-\Phi_2)^{1/3} - \left(\frac{1-\Phi_2}{2}\right)\right] \qquad (5.1)$$

where a is the penetrant activity in the vapor phase, Φ_2 is the volume fraction of penetrant in the polymer, χ is the Flory-Huggins polymer-penetrant interaction parameter, V_2 is the penetrant molar volume, and ν_e/V_0 is the crosslink density in the pure polymer (moles/cm^3).

The maximum degree of crosslinking (ν_e/V_0) in the polyimide is 3.9×10^{-4} mole/cm^3. Fig. 5.15 shows the effect of crosslinking on CO_2 swelling in PDMS, versus the experimental data of Fleming [28] where $\nu_e/V_0 = 1.24 \times 10^{-4}$. The effect of crosslinking is estimated from Eq. 5.1, where χ is a function of pressure [31] and $V_2 = 46$ cm^3/mole [28]. There is a negligible effect of crosslinking on the sorption and swelling of CO_2 in PDMS, whereas the effect on both parameters is significant for the polyimides, as shown in Figure 5.4 and 5.8.

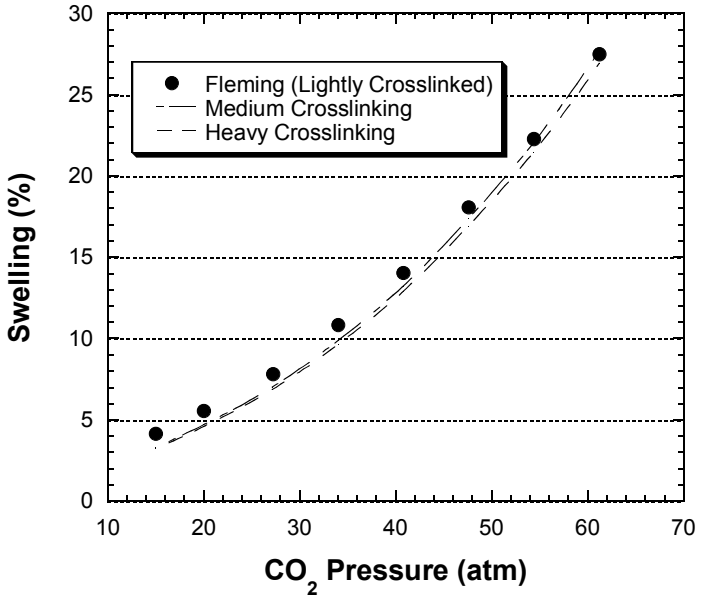

Figure 5.15: Effect of crosslinking on CO_2 dilation at various pressures with rubbery PDMS (crosslinking densities: $\nu_e/V_0 = 1.2 \times 10^{-4}$, 4.8×10^{-4}, 1.4×10^{-3} mole/cm^3)High-pressure CO_2 permeation through lightly crosslinked PDMS has also shown plasticization effects [32]. However, the magnitude of this permeation plasticization is fairly small and arises partially from an upturn in the CO_2 sorption isotherm ~ 27 atm. As opposed to the significant changes in the diffusion coefficient for the rigid polyimide glasses, the pressure dependence of the permeability represents a balance between hydrostatic compressive forces that decrease free volume and plasticizing effects that increase free volume. Plasticization effects on the CO_2 permeability in glassy polymers are much greater because the diffusion coefficient is very sensitive to changes in the segmental mobility, whereas a rubbery polymer behaves more like a viscous liquid and has great mobility even in the absence of CO_2. As a result, the moderate increase in free volume has a smaller impact on the large amount of free volume present in the rubbery materials.

5.8 CONCLUSIONS

The CO_2-induced plasticization of 6FDA-DAM:DABA 2:1 polyimide films at 35°C was characterized by comparing the swelling, sorption, and permeation responses to thermal annealing and covalent crosslinking. The *in-situ* spectroscopic ellipsometry technique is effective at simultaneously measuring sorption and swelling in thin (~ 120 nm) films. Hysteresis in the swelling isotherm indicated that no glass transition was induced by exposure to high-pressure CO_2 (~ 80 atm), since hysteresis is not seen with rubbery polymers.

Increased annealing temperatures resulted in better permeation plasticization resistance for the untreated films, but solid-state covalent crosslinking with 1,4-cyclohexanedimethanol at 220°C was more effective at suppressing plasticization than simple thermal treatments. With annealing at 295°C the untreated films become insoluble in NMP whereas the films treated at 220°C remain completely soluble. For the untreated membranes, the CO_2 permeability decreases with increased annealing temperatures. However, the CO_2 permeability increases as the polymer becomes more highly crosslinked, due to the packing disruption introduced by the crosslinking agents between the polymer chains.

Non-Fickian dilation and permeation kinetics were much more protracted than the sorption kinetics. The shapes of the kinetic curves for permeation ($\boldsymbol{P_t/P_0}$) and dilation are similar, and their offsets from the initial values are correlated. These results indicate that free volume increases over long times in a plasticized membrane (i.e., dilation in the absence of sorption). The swelling characterizes the plasticization behavior, since it describes the effect of the sorbed CO_2 on the polymer properties (e.g. free volume or segmental mobility) that control the CO_2 diffusion through the polymer. A correlation was observed between the plasticization pressure in permeation experiments with that of an inflection point

in the dilation isotherm, suggesting that the increase in polymer free volume causes the increase in the CO_2 diffusion coefficient.

REFERENCES

[1] Ohya, H., T. Higashijima, Y. Tsuchiya, H. Tokunaga and Y. Negishi, Separation of supercritical carbon dioxide and isooctane mixtures with an asymmetric polyimide membrane, *J. Membr. Sci.*, **1993**, *84*, 185-189.

[2] Goel, S. K. and E. J. Beckman, Nucleation and growth in microcellular materials: Supercritical CO_2 as foaming agent, *AIChE J.*, **1995**, *41*, 357-367.

[3] Kazarian, S. G., Applications of FTIR spectroscopy to supercritical fluid drying, extraction, and impregnation, *Appl. Spec. Rev.*, **1997**, *32*, 301-348.

[4] Bos, A., I. G. M. Punt, M. Wessling and H. Strathmann, Suppression of CO_2-plasticization by semiinterpenetrating polymer network formation, *J. Polym. Sci., Polym. Phys. Ed.*, **1998**, *36*, 1547-1556.

[5] Staudt-Bickel, C. and W. J. Koros, Improvement of CO_2/CH_4 separation characteristics of polyimides by chemical crosslinking, *J. Membr. Sci.*, **1999**, *155*, 145-154.

[6] Krol, J. J., M. Boerrigter and G. H. Koops, Polyimide hollow fiber gas separation membranes: Preparation and the suppression of plasticization in propane/propylene environments, *J. Membr. Sci.*, **2001**, *184*, 275-286.

[7] Bos, A., I. G. M. Punt, M. Wessling and H. Strathmann, Plasticization-resistant glassy polyimide membranes for CO_2/CH_4 separations, *Sep. and Purif. Tech.*, **1998**, *14*, 27-39.

[8] Wessling, M., I. Huisman, T. v. d. Boomgaard and C. A. Smolders, Dilation kinetics of glassy, aromatic polyimides induced by carbon dioxide sorption, *J. Polym. Sci.: Polym. Phys. Ed.*, **1995**, *33*, 1371-1384.

[9] Bohning, M. and J. Springer, Sorptive dilation and relaxational processes in glassy polymer gas systems – I. poly(sulfone) and poly(ether sulfone), *Polymer*, **1998**, *39*, 5183-5195.

[10] Sirard, S. M., P. F. Green and K. P. Johnston, Spectroscopic ellipsometry investigation of the swelling of poly(dimethylsiloxane) thin films with high pressure carbon dioxide, *J. Phys. Chem. B*, **2001**, *105*, 766-772.

[11] Wessling, M., M. L. Lopez and H. Strathmann, Accelerated plasticization of thin-film composite membranes used in gas separation, *Sep. and Purif. Tech.*, **2001**, *24*, 223-233.

[12] Fleming, G. K. and W. J. Koros, Comments on measurement of gas-induced polymer dilation by different optical methods, *J. Polym. Sci.: Polym. Phys. Ed.*, **1987**, *25*, 2033-2038.

[13] Sirard, S. M., K. J. Ziegler, I. C. Sanchez, P. F. Green and K. P. Johnston, Anomalous properties of poly(methyl methacrylate) thin films in supercritical carbon dioxide, *Macromolecules*, **2002**, *35*, 1928-1935.

[14] Zhou, H., J. Liu, Z. Qian, S. Zhang and S. Yang, Soluble fluorinated polyimides derived from 1,4-(4'-aminophenoxy)-2-(3'-trifluoro methylphenyl)benzene and aromatic dianhydrides, *J. Polym. Sci., Part A: Polym. Chem.*, **2001**, *39*, 2404-2413.

[15] Salley, J. M., C. W. Frank, T. Miwa and R. Roginski, Charge transfer in polyimides, *Adv. Polyimide Sci. Technol., Proc. Int. Conf. Polyimides, 4th*, **1993**, 441-450.

[16] Hayes, R. A., Highly soluble clear polyimides, U.S. Patent 4,912,197, E.I. Du Pont de Nemours and Co., 1990.

[17] McCaig, M. S., D. R. Paul and J. W. Barlow, Effect of film thickness on the changes in gas permeability of a glassy polyarylate due to physical aging part II. mathematical model, *Polymer*, **2000**, *41*, 639-648.

[18] Lewis, J. E., R. Biswas, A. G. Robinson and M. Maroncelli, Local density augmentation in supercritical solvents: electronic shifts of anthracene derivatives, *J. Phys. Chem. B*, **2001**, *105*, 3306-3318.

[19] Vrentas, J. S. and C. M. Vrentas, Sorption in glassy polymers, *Macromolecules*, **1991**, *24*, 2404-2412.

[20] Wissinger, R. G. and M. E. Paulaitis, Molecular thermodynamic model for sorption and swelling in glassy polymer-carbon dioxide systems at elevated pressures, *Ind. Eng. Chem. Res.*, **1991**, *30*, 842-851.

[21] Fleming, G. K. and W. J. Koros, Dilation of substituted polycarbonates caused by high-pressure carbon dioxide sorption, *J. Polym. Sci., Part B: Polym. Phys.*, **1990**, *28*, 1137-1152.

[22] Sefcik, M. D., Dilation of polycarbonate by carbon dioxide, *J. Polym. Sci., Polym. Phys. Ed.*, **1986**, *24*, 935-956.

[23] Azzam, R. M. A. and N. M. Bashara, *Ellipsometry and Polarized Light*, North-Holland Publishing Co., Elsevier, 1977.

[24] Tompkins, H. G. and W. A. McGahan, *Spectroscopic Ellipsometry and Reflectometry*, John Wiley & Sons, Inc., New York, 1999.

[25] Wissinger, R. G. and M. E. Paulaitis, Swelling and sorption in polymer-CO_2 mixtures at elevated pressures, *J. Polym. Sci., Polym. Phys. Ed.*, **1987**, *25*, 2497-2510.

[26] Kamiya, Y., K. Mizoguchi, K. Terada, Y. Fujiwara and J. S. Wang, CO_2 sorption and dilation of poly(methyl methacrylate), *Macromolecules*, **1998**, *31*, 472-478.

[27] Kazarian, S. G., M. F. Vincent, F. V. Bright, C. L. Liotta and C. A. Eckert, Specific intermolecular interaction of carbon dioxide with polymers, *J. Am. Chem. Soc.*, **1996**, *118*, 1729-1736.

[28] Fleming, G. K. and W. J. Koros, Dilation of polymers by sorption of carbon dioxide at elevated pressures. 1. Silicone rubber and unconditioned polycarbonate, *Macromolecules*, **1986**, *19*, 2285-2291.

[29] Eisenberg, A., B. Hird and R. B. Moore, A new multiplet-cluster model for the morphology of random ionomers, *Macromolecules*, **1990**, *23*, 4098-4107.

[30] Flory, P. J., *Principles of Polymer Chemistry*, Cornell University Press, Ithaca, 1992.

[31] Shim, J. J. and K. P. Johnston, Adjustable solute distribution between polymers and supercritical fluids, *AIChE J.*, **1989**, *35*, 1097-1106.

[32] Jordan, S. M. and W. J. Koros, Permeability of pure and mixed gases in silicone rubber at elevated pressures, *J. Polym. Sci.: Polym. Phys. Ed.*, **1990**, *28*, 795-809.

Chapter 6: Novel Polyimide Ionomers: CO_2 Plasticization, Morphology, and Ion Distribution

6.1 INTRODUCTION

Polyimides have a broad range of applications from microelectronics to gas separation membranes. Many polyimides are insoluble in common solvents such as N-methyl-2-pyrrolidinone (NMP) and tetrahydrofuran (THF). Therefore, films or coatings are cast from the polyamic acid. This precursor polymer is then thermally imidized near 300°C. However, the (4,4'-hexafluoroisopropylidene) diphthalic anhydride (6FDA) based polyimides tend to be soluble in common solvents due to the fluorine groups on the dianhydride moiety. As a result, these polyimides are attractive for applications such as the production of asymmetric hollow fiber gas separation membranes where high-temperature thermal treatments are problematic.

Various researchers have added metal salts and organometallic compounds to polyimides to improve their properties. Typically, the metal compound is added to a solution of the polyamic acid and this mixture is cast into a film. As the film is thermally cured at high temperatures, the metal ions react with the carboxylic acid groups of the polyamic acid. These ionomer structures are often complicated due to the competition of ring closure (i.e., conversion of polyamic acid to the polyimide) with acid group neutralization by the metal cations. Gel-formation during the coating process can also occur if the polyamic acid is crosslinked by the metal ions.

Cobalt and lithium chlorides have been added to 3,3',4,4'-benzophenone tetracarboxylic dianhydrides-4,4'-oxydianiline (BTDA-ODA) polyamic acids to improve the electrical conductivity; the surface conductivities increase, but the ion distribution depends on the processing conditions [1]. Improved adhesion at

high temperatures and high humidity on flexible printed circuit boards was achieved by adding various metallic compounds and gelation inhibitors like acetylacetone to polyamic acids [2]. Silver salts were added to various polyamic acid solutions yielding ~ 75% reflectivity upon thermal imidization [3] or were infused into 3,3',4,4'-biphenyltetracarboxylic dianhydride-4,4'-oxydianiline (BPDA-ODA) polyimides from supercritical CO_2, yielding surface reflectivities between 39% and 61% [4]. Adding metal compounds to BTDA-ODA polyamic acids and subsequent curing at 300°C also improves their mechanical properties [5]. Fluorinated polyimide ionomers have been prepared for single-mode embedded waveguides [6]. So there are a wide variety of applications for polyimide ionomers where this new synthesis procedure may be useful.

Metal ion mediated crosslinking of acrylic and methacrylic acid-containing copolymers has been reported as a promising approach for controlling excessive swelling to maintain high permselectivity in hydrocarbon pervaporation [7, 8]. However, it is shown in Chapter 7 that ionic crosslinking is not as effective as covalent crosslinking in suppressing plasticization in high-pressure CO_2/CH_4 separations.

Most previously reported synthetic procedures for polyimide ionomers involve high-temperature curing of the polyamic acid film because the resulting polyimide is insoluble. With our new technique, however, soluble 6FDA-based polyimides can be made by copolymerizing various amounts of 3,5-diaminobenzoic acid (DABA) into the polymer backbone [9]. Here, the carboxylic acid is a pendant group available for reaction with metal ions. The metal ions may be added to the polyimide solution as Al, Ag, Co, Cu, Pt, and other metal acetylacetonates. The resulting films do not need to be cured at high temperatures. With aluminum acetylacetonate ($Al(AcAc)_3$) gelation is not a problem, presumably because the acetylacetone inhibits this process [2]. Our synthetic procedure is therefore an attractive approach for making ionomer films

with specific metal contents while retaining the rigid aromatic polyimide backbone that provides excellent mechanical properties.

Ionomers have complex morphologies with ion-rich domains ("aggregates") and ion-poor matrix regions. Typically, the aggregates are assumed to be spherical, monodisperse in size, and randomly distributed in the polymer matrix [10]. Small angle X-ray scattering (SAXS) is widely used to investigate the morphology of ionomers; several models have been used to fit the SAXS data and extract structural parameters. Most commonly, the typical ionomer scattering peak is fitted with the Yarusso-Cooper model [11, 12] and aggregate radii, R_1, closest approach distances between two aggregates, R_{CA}, sample volumes per aggregate, v_P, and electron density differences, ρ, between the matrix and the aggregates are extracted from the fitting curve. Other experimental techniques used to investigate ionomers include dynamic mechanical analysis, EXAFS, infrared (IR) and NMR spectroscopy. All these techniques have in common that to some extent they infer structural aspects from data fitting. In contrast, microscopy is a model-free technique that allows for the determination of the morphology above a certain length scale without data fitting.

Winey and coworkers have recently shown using scanning transmission electron microscopy (STEM) that the assumption of monodisperse spherical aggregates randomly distributed in a polymer matrix is only fulfilled in some cases [13, 14]. Other ionomers exhibit aggregates with a variety of shapes, sizes, and different spatial distributions [15-18]. Furthermore, they have demonstrated by using X-ray energy dispersive spectroscopy (XEDS) that the matrix contains a significant amount of metal-neutralized acid groups [18]. STEM imaging combined with XEDS, therefore, yields valuable information, which cannot be extracted from scattering or spectroscopy alone. As a result, STEM and atomic force microscopy (AFM) [19, 20] are complementary to scattering and spectroscopy techniques.

Here the morphologies of two Al-crosslinked ionomers 6FDA-6FpDA:DABA 2:1 and 1:2 are investigated with STEM, XEDS, and SAXS. These polyimides have significantly different theoretical crosslinking densities and CO_2-induced plasticization behavior. The objective of this work is to compare the ionomer morphology with the CO_2 plasticization of the polymer by permeation and sorption characterization. In particular, we are interested to determine if CO_2 plasticization is related to the membrane morphology, specifically the ion distribution.

6. 2 CROSSLINKING DENSITY BY INFRARED SPECTROSCOPY

IR spectra of the 6FDA-6FpDA:DABA films were recorded on a Nicolet Magnum 550 IR spectrometer with an N_2 purge. The conversion of $Al(AcAc)_3$ to aluminum carboxylate was estimated from Beer's law by taking the ratio of the peak intensity of the Al-O stretch of the acetylacetonate ion at 494 cm^{-1} (I_{494}) to that of the carbonyl bending of the aromatic imide bond at 725 cm^{-1} (I_{725}). This peak was used as the internal standard, since its intensity is invariant with the chemical treatment. The peak intensity can vary between films due to different sample thicknesses. This ratio is then normalized with the ratio (I_{494}/I_{725}) for a film of 6FDA-6FpDA (Hoechst-Celanese, no acid component) where a known concentration of $Al(AcAc)_3$ was added [21],

$$\text{Conversion} = 1 - \frac{\left(I_{494}/I_{725}\right)_{\text{crosslinked 6FDA-6FpDA:DABA}}}{\left(I_{494}/I_{725}\right)_{\text{6FDA–6FpDA w/ same wt\% Al(AcAc)}_3}} \tag{6.1}$$

The maximum crosslinking density is determined by the DABA content in the 6FDA-6FpDA:DABA polyimides. The actual crosslinking density may be lower and was measured via IR spectroscopy. A 6FDA-6FpDA film with 12 wt% $Al(AcAc)_3$ was used to calibrate the IR spectra. Because 6FDA-6FpDA contains no carboxylic acids, there is no reaction of the acid groups of the polymer with the

Al^{3+} cations; the film therefore allows the determination of the IR peaks associated with free $Al(AcAc)_3$ dispersed in the polymer matrix.

Fig. 6.1a shows the IR spectra of the 6FDA-6FpDA with and without dispersed $Al(AcAc)_3$. The peaks at 494 and 417 cm^{-1} are associated with the metal-oxygen vibrational modes of the acetylacetonate ion. They agree well with experimental [22] and theoretical data for pure $Al(AcAc)_3$ [23]. Fig. 6.1b and 6.1c are the IR spectra for the 6FDA-6FpDA:DABA 2:1 and 1:2 films, with and without aluminum. For the 2:1 film, the peaks at 494 and 417 cm^{-1} are barely visible, indicating that most of the aluminum is bonded to the carboxylate anions of the polymer. The spectra of the 6FDA-6FpDA:DABA 1:2 film show clear peaks at 498 and 422 cm^{-1}, indicating residual unreacted $Al(AcAc)_3$ in the film.

Using Eq. 6.1, the conversion of the $Al(AcAc)_3$ in the 2:1 ionomer was determined to be ~ 67% and 52% for the 1:2 ionomer. The conversion calculation is based on the peak intensity and not the area, since the $Al(AcAc)_3$ peaks are not well resolved in the crosslinked ionomers. Because we used a 20% excess of neutralizing agent relative to the carboxylic acid content, full conversion of the carboxylic acid groups from the DABA moieties corresponds to an 83% conversion of the $Al(AcAc)_3$; therefore, the estimated DABA conversion is 80% for the 2:1 and 63% for the 1:2 polyimide, respectively. Therefore, the final crosslinking density of the 1:2 ionomer is 60% higher than that of the 2:1 ionomer.

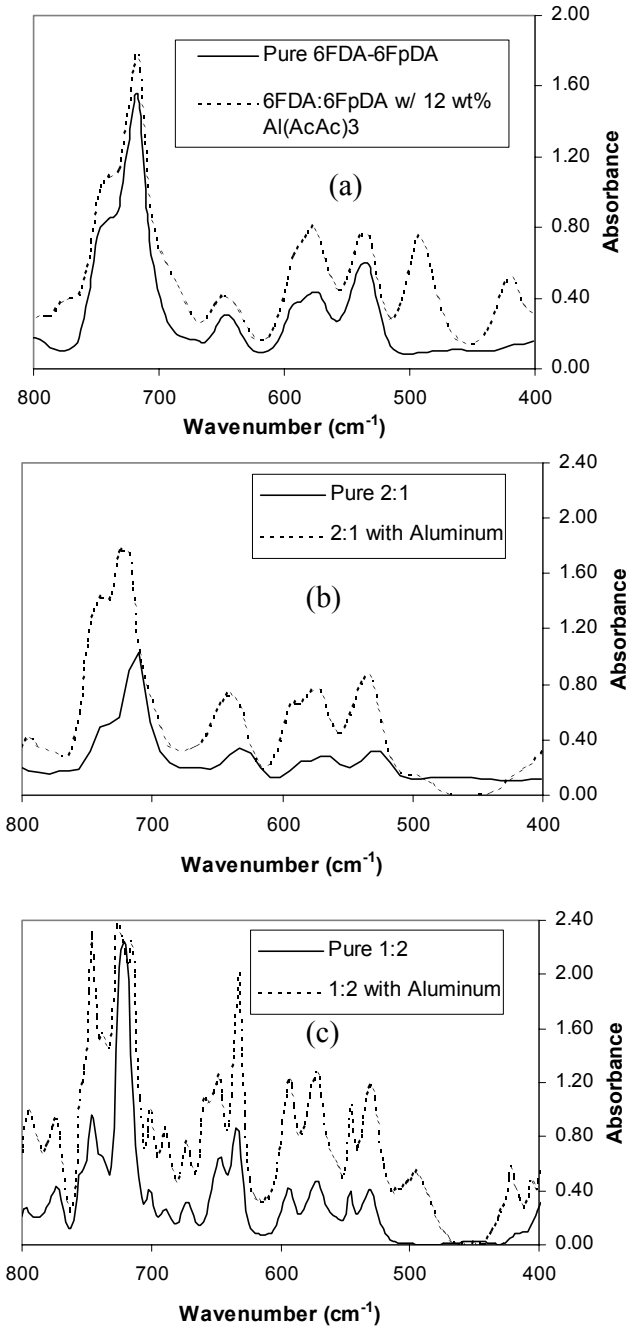

Figure 6.1: IR spectra of polyimides as a function of aluminum and carboxylic acid content.

The presence of unreacted $Al(AcAc)_3$ was further corroborated by TEM and electron diffraction experiments (data not shown). TEM bright field images revealed the presence of large ($\geq \sim 0.5$ μm) polygons that exhibited crystalline diffraction patterns. These particles are probably unreacted $Al(AcAc)_3$ trapped in the film. Due to the limited tilt range of the microscope we were unable to determine the crystallography of the particles.

6.3 GEL FRACTIONS IN THF

The gel fraction of crosslinked polymers in a volatile solvent such as THF can also be used to describe the degree of crosslinking. The gel fractions of the 2:1 and 1:2 ionomer films were 77% and 93% after soaking in THF for five days at 25°C, whereas the unneutralized films are completely soluble. The polymer in the 1:2 ionomer film is essentially insoluble since the 7% that dissolves is likely to be unreacted $Al(AcAc)_3$. This shows that ionic crosslinking has a significant impact on the bulk solubility properties, but its impact on the CO_2-induced plasticization is far less pronounced (see below). The heterogeneity of the ion distribution described later may tend to promote plasticization, whereas the crosslinking should tend to suppress plasticization. We cannot make an unambiguous conclusion about these seemingly competitive forces from the given data, but the implication is that plasticization is more related to the local segmental mobility than to the bulk polymer properties such as gel fraction.

6.4 GLASS TRANSITION TEMPERATURES

The unneutralized 2:1 and 1:2 films have glass transition temperatures of 322°C and 327°C, respectively. However, both Al-crosslinked polymers do not show a T_g when analyzed with DSC up to 450°C. There are some thermal events, but not a definite T_g, as shown in the thermograms in Appendix D. In

comparison, if the same 2:1 and 1:2 polyimides discussed here are covalently rather than ionically crosslinked, they show very little change (< 10°C) in the T_g relative to the uncrosslinked precursor, but they have a significantly better resistance to CO_2 plasticization than the ionomers presented here and the uncrosslinked polymers. Essentially no change in the T_g was observed for crosslinking of poly(methyl acrylate-*co*-acrylic acid)s with $Al(AcAc)_3$ via a similar procedure [8]. However, these polymers were much more flexible than the polyimides, with T_g's of ~ 15-20°C.

In other ionomers, multiple T_g's have been observed. They have been assigned to the glass transitions of the nonionic polymer matrix and the ion-rich aggregates, respectively [24]. The presence of ionic groups in polymers has been shown to restrict the mobility of polymer chains compared to the non-ionic base resin [25, 26]. It has been suggested that the chain immobilization effect is greater the more rigid the unneutralized polymer [10]. The absence of a T_g up to 450ºC in our samples implies that the polymer mobility is drastically reduced by the crosslinking, which normally would be advantageous for inhibition of plasticization. However, this turns out not to be the case, as described below.

6.5 CO_2 AND CH_4 PERMEATION AND SORPTION

6.5.1 CO_2 Permeation Isotherms

The CO_2 permeation isotherms for the 6FDA-6FpDA:DABA 2:1 and 1:2 membranes, with and without aluminum crosslinking are shown in Fig. 6.2. In both cases the ionomers are more stabilized than the uncrosslinked membranes. However, the stability of the ionomers can be misleading because they have long-term increases in the permeability when exposed to high pressure CO_2, as discussed in Sections 6.5.5 and 6.5.6.

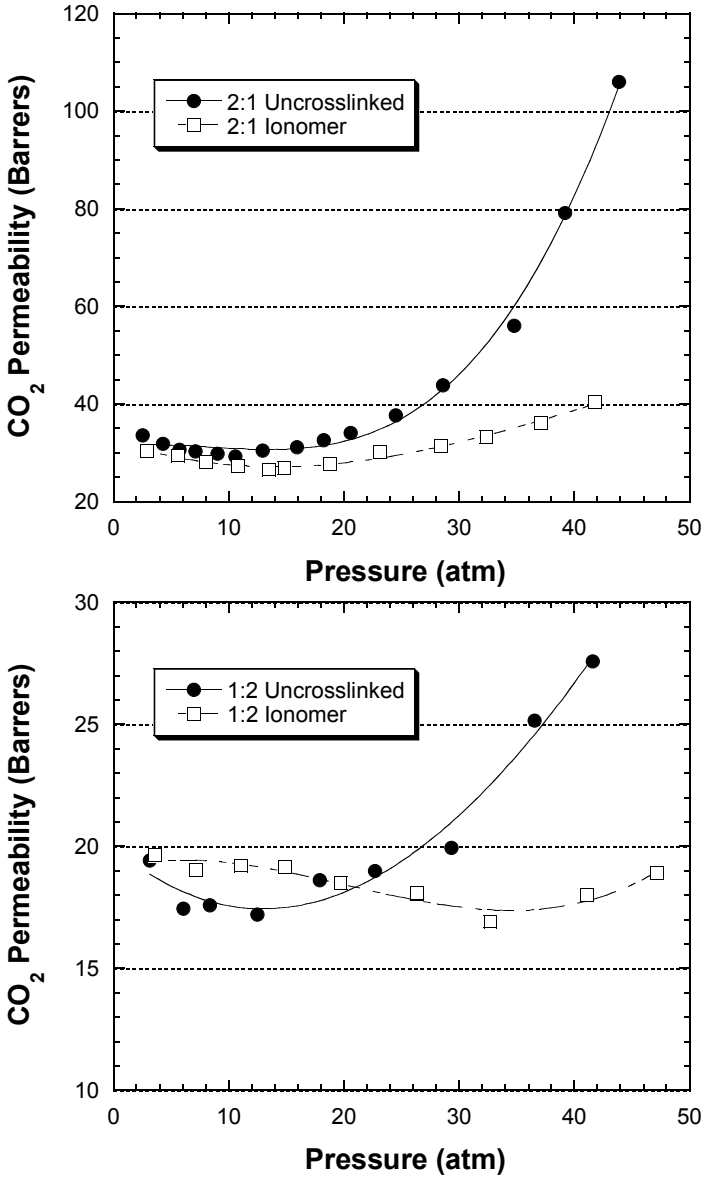

Figure 6.2: CO_2 permeation isotherms for the 6FDA-6FpDA:DABA 2:1 and 1:2 membranes, with and without aluminum crosslinking at 35°C

6.5.2 CO_2 Sorption isotherms

The CO_2 solubility in the 6FDA-6FpDA 2:1 and 1:2 polymers is not significantly different, with and without ionic crosslinking, as shown in Fig. 6.3.

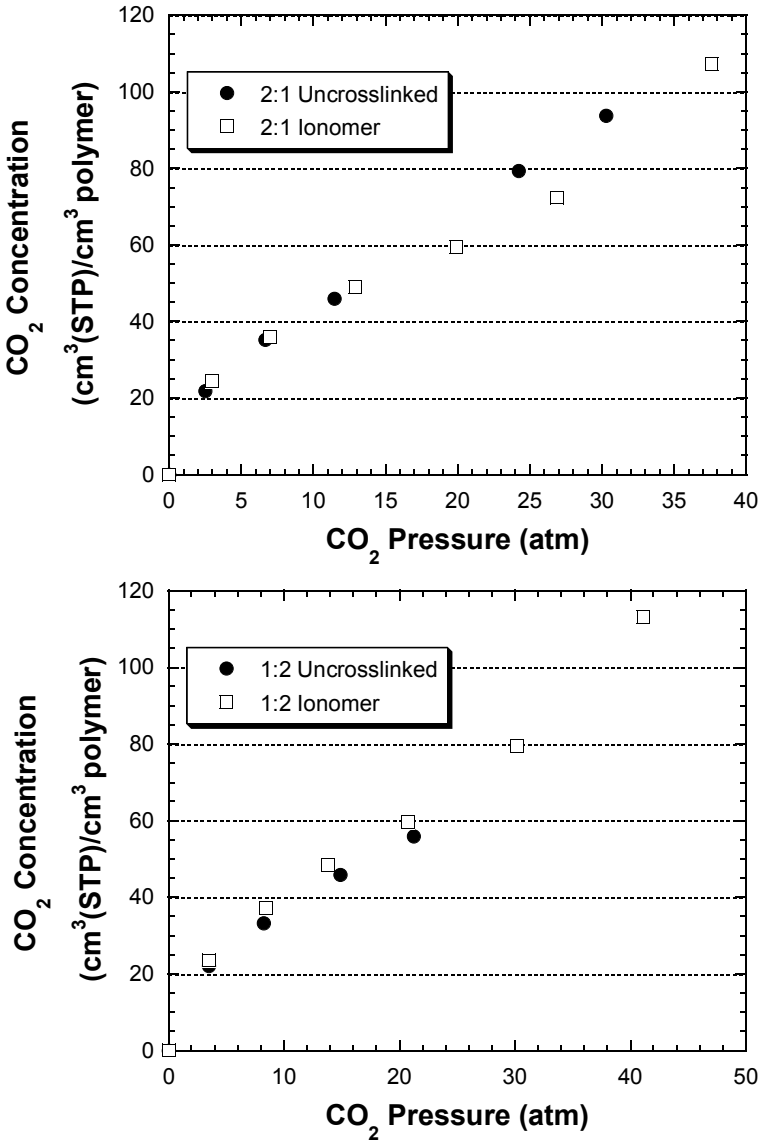

Figure 6.3: CO_2 sorption isotherms in 6FDA-6FpDA:DABA 2:1 and 1:2 copolymers, with and without aluminum crosslinking at 35°C

It is shown in Section 6.5.6 that the long-term kinetic permeation at 40 atm feed pressure is quite different for the all four samples, even though the equilibrium sorption values are very similar. This, along with kinetic sorption data, suggests that the CO_2 diffusion coefficient is affected in different ways between the four polymers.

6.5.3 CH_4 Sorption isotherms

The four polymers studied here also have very similar CH_4 sorption isotherms, as shown in Figure 6.4.

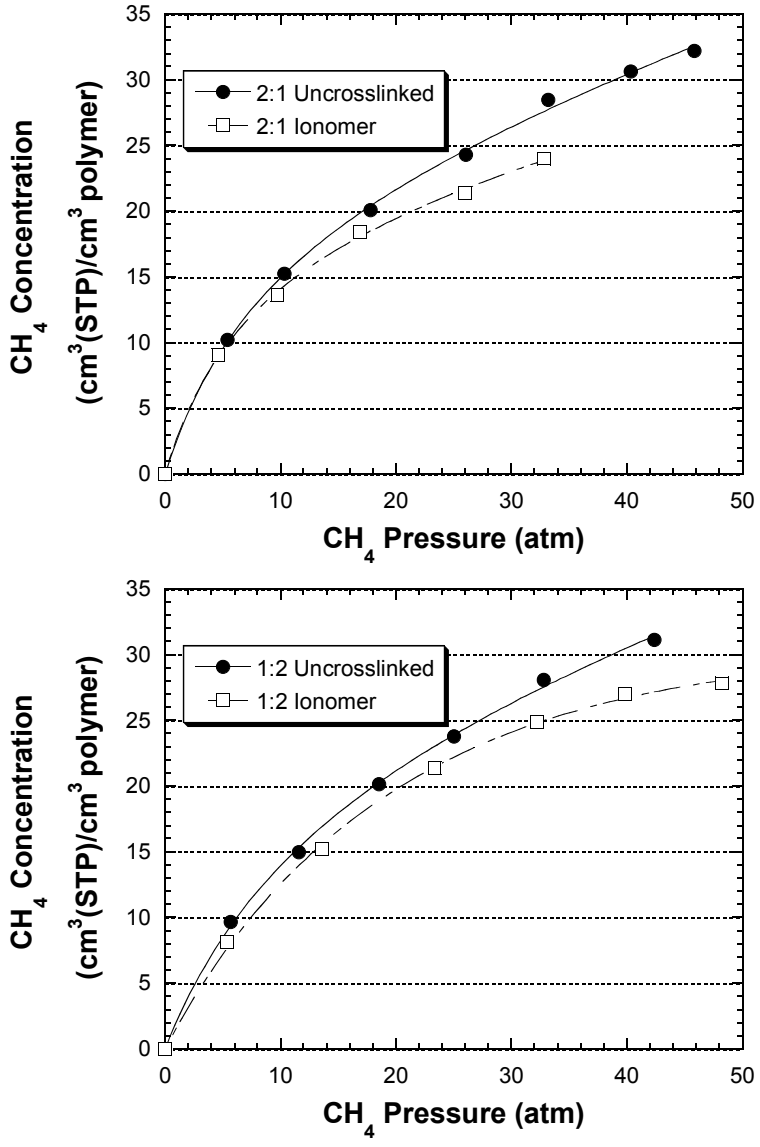

Figure 6.4: CH_4 sorption isotherms in 6FDA-6FpDA:DABA 2:1 and 1:2 copolymers, with and without aluminum crosslinking at 35°C

6.5.4 Summary of CO_2 and CH_4 Permeability and Sorption Parameters

Table 6.1: CO_2 Sorption and Transport properties at 10 atm and 35°C

Polymer	CO_2 Permeability (Barrers)	CO_2 Sorption Coefficient (cm^3(STP)/ (cm^3 atm))	CO_2 Diffusion Coefficient (cm^2/s)	CO_2/CH_4 Ideal Selectivity
Pure 2:1	29	4.2	5.2×10^{-8}	45
2:1 Ionomer	25	4.0	4.8×10^{-8}	46
Pure 1:2	17	3.7	3.5×10^{-8}	50
1:2 Ionomer	19	4.2	3.4×10^{-8}	not measured

6.5.5 Permeation and Sorption Kinetics

Fig. 6.5 shows that both the permeability and sorption increase over long time periods for both the crosslinked (i.e., ionomers) and uncrosslinked membranes when exposed to high-pressure CO_2. This is indicative of non-Fickian polymer relaxations due to CO_2 plasticization [27], even though the sorption and permeation kinetics in membranes are frequently described by standard Fickian models. For Fickian sorption, the permeation time lag (θ) which determines the time to reach steady-state is

$$\theta = \frac{\ell^2}{6D} \tag{6.2}$$

where ℓ is the membrane thickness and D is the average diffusion coefficient of the penetrant in the membrane. The time to reach half of the equilibrium sorption level is [28],

$$t_{1/2} = 0.0492\frac{\ell^2}{D} \tag{6.3}$$

For Fickian sorption uptake, equilibrium is essentially reached within six "half-time" periods. For all of the samples considered here, sorption and permeation equilibrium times based on Fickian models are less than 15 minutes. However, because our membranes are plasticized, there is a relaxation-controlled time-dependent function superimposed onto the Fickian transient functions to describe the sorption and diffusion behavior [27, 29]. Permeability is the product of the sorption and diffusion coefficients, and Fig. 6.5a demonstrates that the diffusion component is much more affected by the plasticization than is the sorption component (Fig 6.5c) for both ionomers. Interestingly, the 1:2 ionomer shows much greater long-term increases in the permeability (or diffusion coefficient) than the uncrosslinked membrane. This is in stark contrast to the solubility behavior in THF, where the unneutralized samples are completely soluble and the ionomers have significant gel fractions.

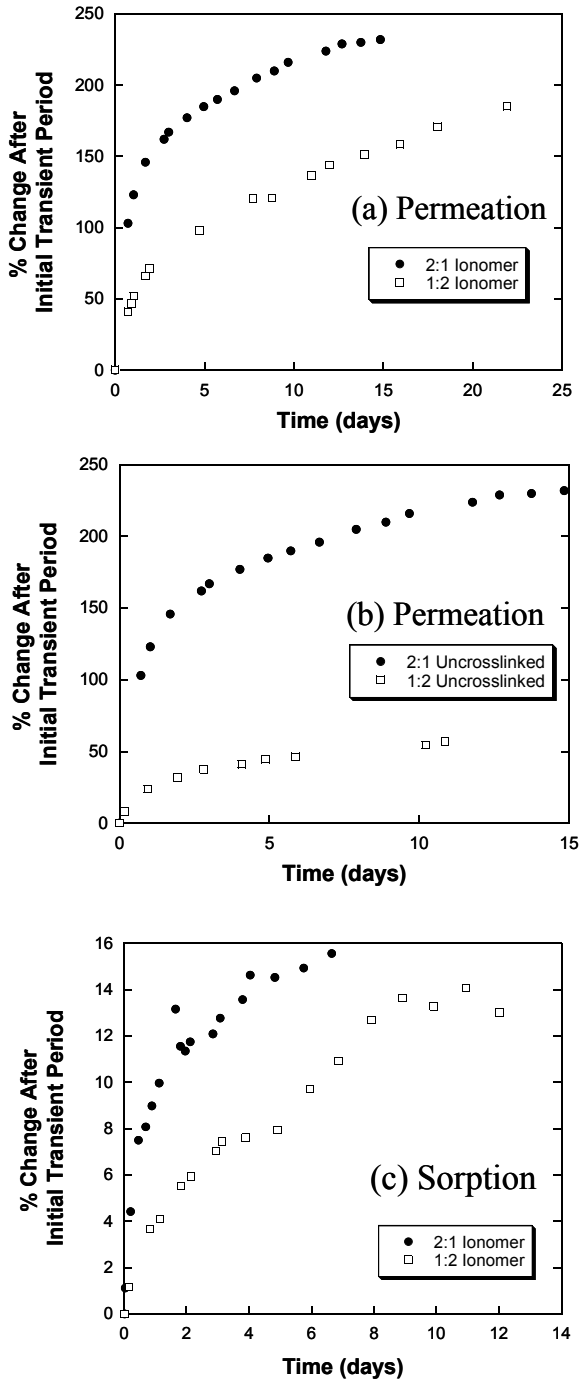

Figure 6.5: Long-term permeation and sorption behavior for crosslinked and uncrosslinked membranes at 40 atm pure CO_2 and 35°C.

Therefore, even though IR spectroscopy shows significant crosslinking, ionic crosslinking is much less effective in suppressing CO_2 plasticization in our polyimide membranes than covalent crosslinking of the same precursor polymers. The sorption and permeation data suggest that the polymer morphology may be different, thereby giving rise to the observed sorption and permeation behavior. In Sections 6.6-6.8, the ionomer morphology is characterized with STEM and XEDS to confirm the presence of different morphologies in the two ionomers.

6.5.6 TIME AND PRESSURE DEPENDENCE OF PLASTICIZATION

Plasticization has been described by the permeability behavior as a function of time and pressure. The sorption and diffusion contributions to the permeability can be analyzed to understand the nature of their coupling. Fig. 6.6 shows the kinetic permeation and sorption under various CO_2 pressures for the 2:1 membrane crosslinked with aluminum. The sorption curves show deviation from Fickian uptake at pressures above the plasticization pressure (~ 19 atm), but the deviation does not grow significantly as the pressure is increased from 20 atm to 40 atm. However, the permeability shows a very significant upward drift as the pressure is increased above the plasticization pressure and the membrane becomes more unstable as the pressure is increased. The data suggest that plasticization is primarily described by increases in the CO_2 diffusion coefficient resulting from increased segmental mobility or free volume.

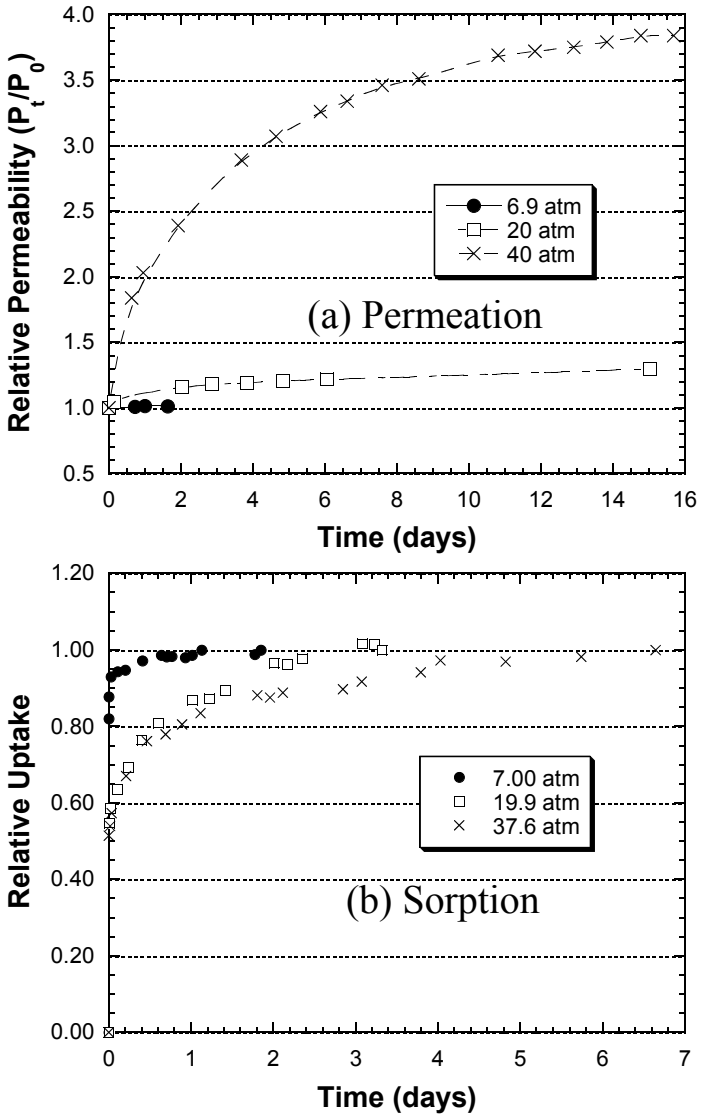

Figure 6.6: Time and pressure dependence of CO_2 permeation and sorption in 6FDA-6FpDA:DABA 2:1 ionomer

6.6 SCANNING TRANSMISSION ELECTRON MICROSCOPY AND X-RAY SPECTROSCOPY

Fig 6.7 is a STEM bright field (BF)/annular dark field (ADF) image pair of the Al-crosslinked 1:2 ionomer. The BF image shows dark features of various shapes and sizes in a bright matrix. The corresponding ADF image shows a contrast reversal where the dark features in the BF images appear bright and the bright matrix appears dark. This behavior indicates that the isolated features contain elements with a higher atomic number Z in a lower Z matrix. Because the Rutherford scattering power of an element scales approximately with Z^2 [30-32], the Al^{3+} (Z = 13) ions in the ionic aggregates scatter more electrons into the annular dark field detector than the polymer matrix, which consists of carbon (Z = 6), nitrogen (Z = 7), oxygen (Z = 8), and fluorine (Z = 9). As a result, the Al-rich aggregates appear bright in STEM ADF and dark in the STEM BF images. Fig. 6.7 also demonstrates that there are rather large regions without visible aggregates on the STEM length scale (STEM resolution is ~ 1 nm).

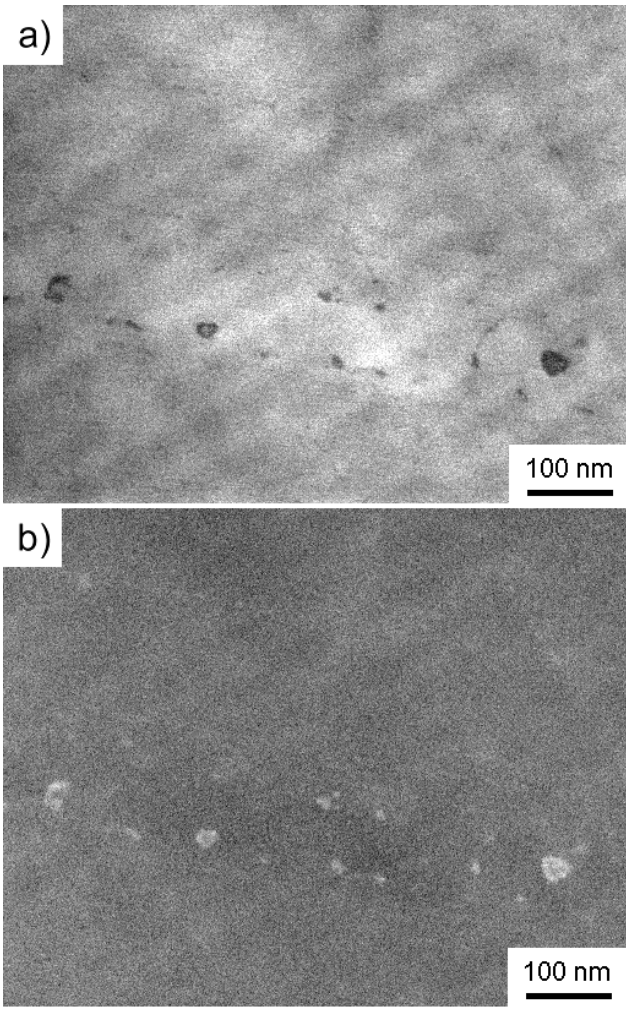

Figure 6.7: STEM BF (a) and ADF (b) image of Al-rich aggregates in the 1:2 Al-crosslinked polyimide ionomer. Contrast reversal confirms that they are Al-rich.

Fig. 6.8 illustrates that the Al-rich aggregates in the 1:2 ionomer vary in size and shape. While some aggregates are spherical and rather small (~ 5 nm), others are on the order of ~ 25 nm in diameter and resemble the vesicular structures previously observed in Zn-neutralized sulfonated polystyrene (Zn-SPS) [15, 16] and Cs-neutralized poly(styrene-ran-methacrylic acid) (Cs-SMAA) [17].

Chainlike assemblies of small spherical aggregates and even extended structures similar to large distorted vesicles and long band-like structures exist in the same sample. Contrast reversal of all dark features occurs between the BF and ADF images suggesting that these structures are Al-rich ionic domains.

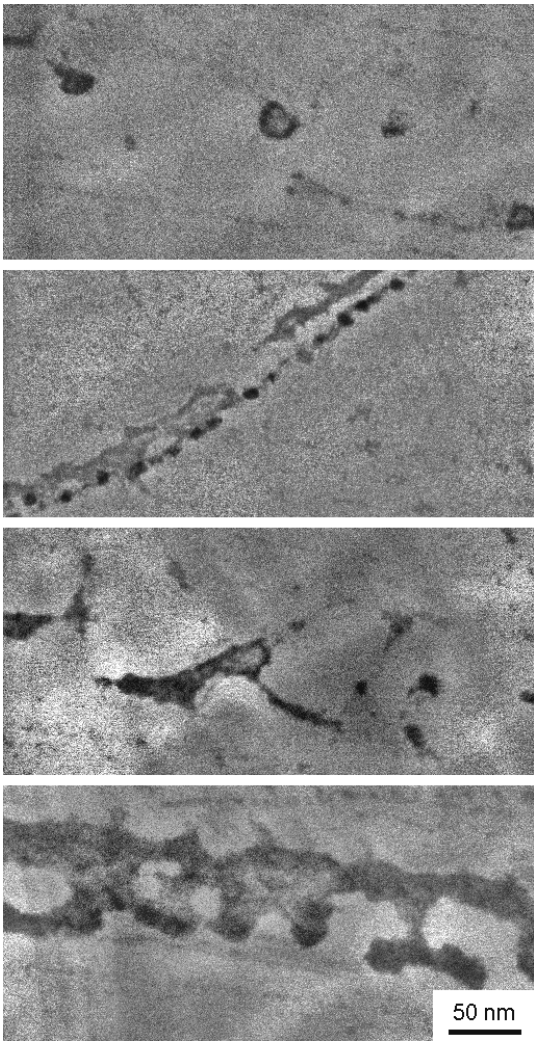

Figure 6.8: STEM BF images of various aggregates in the Al-neutralized 1:2 ionomer. The aggregates have irregular shapes and various sizes.

Fig. 6.9a is a typical image of the 2:1 ionomer and shows that this ionomer is much more homogeneous than the 1:2 ionomer. Large fractions of the material do not exhibit visible aggregates on the STEM length scale. Fig. 6.9b illustrates that some aggregates are still present, but no extended structures resembling the chain-like ion-rich domains in the 1:2 sample. Images with magnifications up to 600,000× confirm the absence of small aggregates on the STEM length scale.

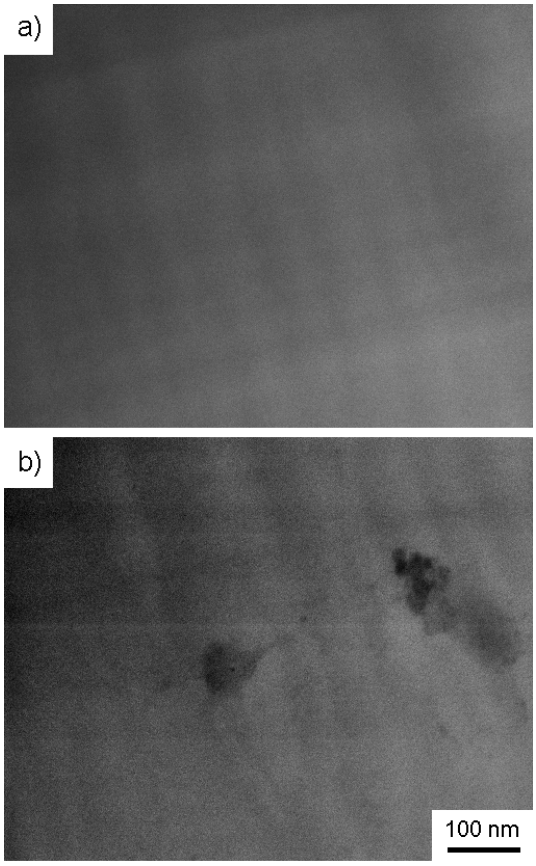

Figure 6.9: STEM BF images of the 2:1 Al-crosslinked polyimide ionomer. Most of the material does not exhibit any aggregates on the STEM length scale (a) but some aggregates are visible (b).

Spot X-ray energy dispersive spectroscopy (XEDS) probes only ~ 1 nm^2 of the sample and, therefore, allows for the determination of the chemical composition of the ionomer on a nanometer level. Spot XEDS data assesses the chemical composition of both the aggregates and the matrix of the 1:2 ionomer. Fig. 6.10 shows spot XEDS data collected from an aggregate and the matrix, both of which exhibit *K* lines for Al along with *K* lines for C, N, and F that are due to the polymer and not the neutralizing cation. The Al *K* lines of the spectra recorded on the aggregates are much more intense than the ones of the matrix spectra.

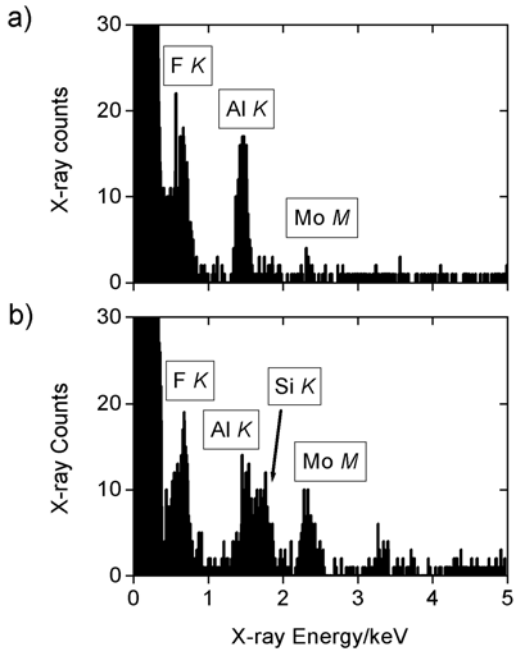

Figure 6.10: Spot XEDS spectra of an aggregate (a) and the matrix (b) of the 1:2 Al-crosslinked polyimide ionomer. The Si *K* line is a detector system peak and the Mo *M* line is due to the support grid.

We also collected overview XEDS spectra that probe ~ 2.5 μm^2 area of the microtomed section. The integrated Al *K* X-ray counts of these spectra exhibit large differences. Some regions exhibit intense Al *K* lines (~14,000 counts), whereas other areas barely show any signal (~ 300 counts). This observed increase in the Al signal correlates with a higher density of aggregates. However, similar to the spot spectra, we also detected Al *K* lines in the absence of aggregates. The presence of *K* lines for N, O, and F along with the Al *K* line, however, clearly confirms that we are probing the ionomer and not erroneously the polystyrene used to stabilize the polyimides. Both the spot and overview XEDS spectra confirm that the aggregates observed by STEM are Al-rich; they furthermore show the presence of Al in the matrix, either as isolated groups or as aggregates too small for the STEM to resolve.

A quantification of the XEDS data is difficult for several reasons. First, the sample cannot be tilted enough to fully determine the 3D shape of the ionic aggregates. While this is no problem for spherical aggregates (Fig. 6.11a), it becomes important for aggregates with irregular shapes (Fig. 6.11b and c). This is because spot XEDS of an aggregate also probes the matrix that is above and below the aggregate [33]. Therefore, if the aggregate is spherical, we can calculate how much of the probed volume is aggregate and how much is surrounding matrix and we can quantify these data. If, however, the aggregate shape is unknown, the contributions from the aggregate and matrix cannot be separated. For example, the aggregates in Fig. 6.8 may span only a fraction of the section (Fig. 6.11b) or the whole section thickness (Fig. 6.11c). The Al *K* line obtained from a spectrum obtained on an aggregate similar to Fig. 6.11b must be separated into the contributions of the aggregate and the surrounding matrix, both of which are probed in the same experiment [33].

Second, we could use the *K* line intensity of N or O to determine the ratio of Al to N or O. However, both the N and O *K* line intensities are small and

overlap with the F and C *K* lines at the lower end of the X-ray spectra. Neither the acid group nor the acetylacetonate ion contains unique elements relative to the bulk polymer that would enable the determination of the aggregate composition (free $Al(AcAc)_3$ versus Al(COO)). Moreover, the F *K* line intensity cannot be quantified because the C-F bond is unstable against electron beam irradiation [34]. We currently do not have an estimate of how much F is lost over the entire acquisition time.

Figure 6.11: Schematic of a cross-sectional view of a STEM sample depicting different possibilities of aggregate locations in the thin section. The aggregates in Fig. 6.11b and c are highly simplified presentations of the large structures shown in Fig 6.7.

6.7 SMALL ANGLE X-RAY SCATTERING

Fig. 6.12 shows the SAXS patterns of the unneutralized precursor polymers and the neutralized 1:2 and 2:1 ionomers; all patterns exhibit a small peak at $q \sim 3.3$ nm^{-1} and only the pattern of the 1:2 crosslinked ionomer exhibits a tiny second peak at ~ 4.4 nm^{-1}. The position, shape, and intensity of the observed scattering peaks for the samples investigated here does not change regardless of the fact that two samples are not neutralized and that the samples vary in their chemical composition. This is in contrast to the STEM images that reveal distinct differences between the two neutralized ionomers. It is interesting to note that even the unneutralized samples exhibit the scattering peak that is typically

characteristic of ionomers. This is similar to early work by Yarusso and Cooper who observed an scattering peak in unneutralized sulfonated polystyrene (SPS) [11, 12].

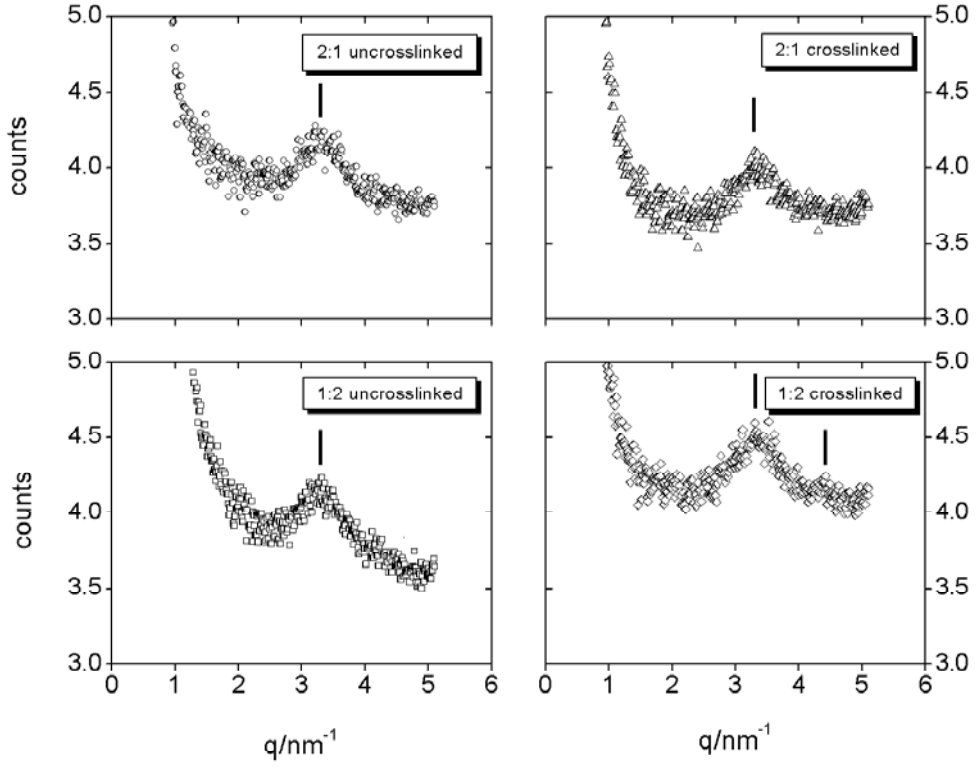

Figure 6.12: X-ray patterns taken in the Intermediate Angle chamber of the MAXS apparatus. The ionomer peaks are located at ~ 3.3 nm^{-1} and have the same shape and intensity. The 1:2 ionomer also exhibits a weak shoulder at ~ 4.4 nm^{-1}.

6.8 DISCUSSION

Ion-rich aggregates are dark in STEM BF and bright in STEM ADF images because STEM is based on atomic number contrast. The contrast reversal observed here therefore implies that the features in the STEM images of the Al-

neutralized polyimide ionomers are Al-rich ionic domains that form in a polymer matrix with a lower average atomic number. This is further supported by overall XEDS because the Al *K* lines are more intense in the presence of many aggregates and by XEDS spot spectra because the spot spectra show a more intense Al *K* line on an aggregate than on the matrix.

STEM images reveal distinct variations in the morphologies of the two ionomers. The 1:2 ionomer has a complex morphology with aggregates that have a range of shapes, sizes, and a heterogeneous spatial distribution. Aggregate shapes include isolated spheres, vesicular aggregates, chains of spheres, and large features that extend up to 1000 nm in length. Furthermore, the aggregate number density varies within one sample: some regions have a high aggregate concentration while others are largely depleted of aggregates visible with STEM.

Aside from the Al-rich aggregates, the matrix also contains Al as determined by XEDS. The Al dispersed in the matrix could be isolated $Al(COO)_3$ or similar sites or aggregates that are too small for the STEM to resolve (i.e. below ~ 1 nm). A structure containing a significant number of cations in the matrix is consistent with STEM and XEDS results on a Na-neutralized poly(ethylene-ran-methacrylic acid) ionomer [18]. It is also consistent with ^{23}Na solid-state NMR (SSNMR) studies by O'Connell et al. [35-38] on Na-neutralized SPS. These authors explain the appearance of two different signals in the NMR spectra with the presence of isolated metal ion sites in the polystyrene matrix and aggregated Na-neutralized acid groups. O'Connell et al. assign this broad peak to variations in the local cation environment due to dimers, trimers, etc., suggesting a heterogeneous structure of the cation environment. This is qualitatively consistent with the STEM and XEDS data presented here, even though the ionomers are very different.

The variety of the aggregate shapes and their heterogeneous spatial distribution in the 1:2 ionomer suggest a non-equilibrium structure or a

composition gradient in the precursor polymer. It could also result from precipitation of the $Al(AcAc)_3$ due to solubility limits. If the polymer has a compositional gradient, it may phase separate into regions with higher and lower acid content, thereby giving rise to aggregate-rich and aggregate-deficient regions. Our STEM experiments have, however, not shown distinct boundaries between regions of high and low aggregate numbers. This is in sharp contrast to previous studies by Winey and coworkers on polystyrene and polyethylene ionomers, where macrophase separation was observed [15-18].

The 2:1 ionomer is more homogeneous on the STEM length scale and only exhibits a few ion-rich aggregates in STEM. This may be due to the lower acid or Al concentration in this polymer, to a structure that is closer to equilibrium, or to a more random copolymer. The copolymers are expected to be random in their sequence distributions because of the equilibrium nature of the polymerization reaction. Even if this polymer is even less random than the 1:2 ionomer, the overall lower acid content may still prevent phase separation into acid-rich and acid-poor regions. The lower acid content and, therefore, the lower amount of added $Al(AcAc)_3$ lead to a lower crosslinking density, which may allow the neutralizing agent to diffuse in the sample more freely. This would prevent the formation of large ionic aggregates like the ones observed in the 1:2 ionomer. Because the 2:1 ionomer has a lower acid fraction but was allowed the same time for neutralization, it may be closer to equilibrium than the 1:2 sample. The high glass transition temperatures of the precursor polymers may also account for the presence of aggregates in some regions and for their absence in others, because the polymer chain flexibility may be insufficient for the polymer to reach an equilibrium morphology upon neutralization.

The ionic aggregates in the 1:2 ionomer range in size from 5 to > 1000 nm. Many aggregates are separated by more than 100 nm from each other. This spacing is much greater than the DABA spacing for an extended chain (2.5 and

1.8 nm for the 2:1 and 1:2 polymers, respectively), as determined by the molecular modeling software HyperChem 7.0® from Hypercube, Inc., with simple bond angle constraints. This suggests that there are multiple DABA groups from many polymer chains participating in the aggregates. This will in turn limit the flexibility of adjacent segments that may contain acid groups: even if these acid groups are neutralized they cannot move freely enough to form an aggregate or an aggregate with an energetically favorable shape. They, therefore, become immobilized by the neighbored ionic groups that are already aggregated. This may lead to the very heterogeneous morphology of the 1:2 ionomer, which has a much higher acid fraction. The polymer between the aggregates may be uniformly crosslinked, especially for the 2:1 polymer, where few aggregates are seen in the STEM images.

Despite the structural differences, both membranes plasticize at high CO_2 pressures. Plasticization may occur due to a weakening of the ionic bond by solvation effects of the quadrupolar CO_2 molecules. It does not appear that heterogeneity in the ion distribution has anything to do with CO_2 plasticization in membrane processes, since the 2:1 and 1:2 both plasticize significantly. The length scales associated with the polymer chain volume fluctuations that control small molecule diffusion are likely to be smaller than the nm-length scale observed in STEM. However, the morphology on the nanometer length scale probably has a direct impact on the Angstrom scale motions that govern CO_2 diffusion through the membrane because the crosslinking density defines the size of the flexible chains in the membrane and so controls the diffusion of the penetrant. This chapter demonstrates that the effects of crosslinking density and aggregate formation may affect the membrane performance in a more complex manner than originally thought. Since plasticization is related to the segmental mobility, it is likely that a uniformly crosslinked polymer is preferred for limiting the segmental mobility uniformly throughout the polymer. The natural tendency

for ions to aggregate makes uniformity inherently less attainable than with covalent crosslinking agents.

6.9 FUTURE WORK

Optimization of the ionomer preparation procedure might change the ionomer morphology and produce more stable membranes. The solvent evaporation rate and the film formation and/or annealing temperature could be varied or the partially crosslinked films could be swollen in a strong solvent to facilitate the mobility necessary for complete neutralization. Additionally, the metal ion in the acetylacetonate compound may affect the morphology and the final crosslinking degree.

6.10 CONCLUSIONS

A novel crosslinking method to produce polyimide ionomers with a controlled carboxylic acid content and crosslinking degree has been developed. These ionomers can be crosslinked at low temperatures and gel formation is inhibited during the casting procedure. IR spectroscopy shows a crosslinking conversion above 60% for both ionomers. The CO_2-induced plasticization in high-pressure permeation leads to unstable membrane performance over long-term operating periods. The 6FDA-6FpDA:DABA 1:2 ionomer exhibits Al-rich aggregates of various sizes and shapes, with a very heterogeneous spatial distribution. The 2:1 ionomer is much more homogeneous and only shows a few aggregates on the STEM length scale. Overall XEDS found a strong correlation between the Al *K* line intensity in the XEDS spectra and the aggregate numbers. Spot XEDS detected Al in both the aggregates and the matrix, similar to observations in other ionomers. IR and TEM show evidence of unreacted neutralizing agent in the ionomers. The comparison of the STEM and XEDS data

with the permeation results suggests that the performance of these materials is much more dependent on the Angstrom-level motions of polymer chain segments than on the morphology on a nanometer-level as revealed by STEM.

REFERENCES

[1] Rancourt, J. D. and L. T. Taylor, Preparation and properties of surface-conductive polyimide films via in situ codeposition of metal salts, *Macromolecules*, **1987**, *20*, 790-795.

[2] Ono, K., M. Nishinaka and R. Akahori, Metal-containing polyamic acid compositions, polyimide films, their manufacture, polyimide moldings, and flexible printed circuit boards thereof, U.S. Patent 6,207,739, Kanegafuchi Chemical Industry Co., Ltd., Japan., 1999.

[3] Thompson, D. W., M. L. Caplan and A. K. St. Clair, Reflective self-metalizing polyimide films, 5,677,418, United States National Aeronautics and Space Administration, USA, 1997.

[4] Rosolovsky, J., R. K. Boggess, A. F. Rubira, L. T. Taylor, D. M. Stoakley and A. K. St. Clair, Supercritical fluid infusion of silver into polyimide films of varying chemical composition, *J. Mater. Res.*, **1997**, *12*, 3127-3133.

[5] Clair, A. K. S. and L. T. Taylor, A comparison of physical and mechanical properties of polyimide films containing different metal ions, *J. Appl. Polym. Sci.*, **1983**, *28*, 2393-2400.

[6] Sawada, T. and S. Ando, Synthesis, characterization, and optical properties of metal-containing fluorinated polyimide films, *Chem. Mater.*, **1998**, *10*, 3368-3378.

[7] Inui, K., T. Noguchi, T. Miyata and T. Uragami, Pervaporation characteristics of methyl methacrylate-methacrylic acid copolymer membranes ionically crosslinked with metal ions for a benzene/cyclohexane mixture, *J. Appl. Polym. Sci.*, **1999**, *71*, 233-241.

[8] Matsui, S. and D. R. Paul, Pervaporation separation of aromatic/aliphatic hydrocarbons by crosslinked poly(methyl acrylate-co-acrylic acid) membranes, *J. Membr. Sci.*, **2002**, *195*, 229-245.

[9] Staudt-Bickel, C. and W. J. Koros, Improvement of CO_2/CH_4 separation characteristics of polyimides by chemical crosslinking, *J. Membr. Sci.*, **1999**, *155*, 145-154.

[10] Eisenberg, A., B. Hird and R. B. Moore, A new multiplet-cluster model for the morphology of random ionomers, *Macromolecules*, **1990**, *23*, 4098-4107.

[11] Yarusso, D. J. and S. L. Cooper, Microstructure of ionomers - interpretation of small-angle x- ray-scattering data, *Macromolecules*, **1983**, *16*, 1871-1880.

[12] Yarusso, D. J. and S. L. Cooper, Analysis of SAXS data from ionomer systems, *Polymer*, **1985**, *26*, 371-378.

[13] Winey, K. I., J. H. Laurer and B. P. Kirkmeyer, Ionic aggregates in partially Zn-neutralized poly(ethylene-ran-methacrylic acid) ionomers: shape, size, and size distribution, *Macromolecules*, **2000**, *33*, 507-513.

[14] Laurer, J. H. and K. I. Winey, Direct imaging of ionic aggregates in Zn-neutralized poly(ethylene-co-methacrylic acid) copolymers, *Macromolecules*, **1998**, *31*, 9106-9108.

[15] Kirkmeyer, B. P., K. I. Winey and R. A. Weiss, Imaging ionic aggregates in Zn-neutralized sulfonated polystyrene ionomers: shape and spatial heterogeneity, *Microsc. Microanal.*, **2000**, *6*, 1112-1113.

[16] Kirkmeyer, B. P., R. A. Weiss and K. I. Winey, Spherical and vesicular ionic aggregates in Zn-neutralized sulfonated polystyrene ionomers, *J. Polym. Sci.: Polym. Phys. Ed.*, **2001**, *39*, 477-483.

[17] Kirkmeyer, B. P., A. Taubert, J. S. Kim and K. I. Winey, Vesicular ionic aggregates in poly(styrene-ran-methacrylic acid) ionomers neutralized with Cs, *Macromolecules*, **2002**, *35*, 2648-2653.

[18] Taubert, A. and K. I. Winey, Imaging and X-ray microanalysis of a poly(ethylene-ran-methacrylic acid) ionomer melt neutralized with sodium, *Macromolecules*, **2002**, *35*, 7419-7426.

[19] McLean, R. S., M. Doyle and B. B. Sauer, High resolution imaging of ionic domains and crystal morphology in ionomers using AFM techniques, *Macromolecules*, **2000**, *33*, 6541-6550.

[20] Sauer, B. B. and R. S. McLean, AFM and X-ray studies of crystal and ionic domain morphology in poly(ethylene-co-methacrylic acid) ionomers, *Macromolecules*, **2000**, *33*, 7939-7949.

[21] Conley, R. T., *Infrared Spectroscopy*, Allyn and Bacon, Inc., Boston, 1972.

[22] Dismukes, J. P., L. H. Jones and J. C. Bailar, Jr., The measurement of metal-ligand bond vibrations on acetylacetonate complexes, *J. Phys. Chem.*, **1961**, *65*, 792-795.

[23] Diaz-Acosta, I., J. Baker, W. Cordes and P. Pulay, Calculated and experimental geometries and infrared spectra of metal tris-acetylacetonates: Vibrational spectroscopy as a probe of molecular structure for ionic complexes. part I, *J. Phys. Chem. A*, **2001**, *105*, 238-244.

[24] Eisenberg, A. and J.-S. Kim, *Introduction to Ionomers.*, John Wiley & Sons, New York, 1998.

[25] Kutsumizu, S., K. Tadano, Y. Matsuda, M. Goto, H. Tachino, H. Hara, E. Hirasawa, H. Tagawa, Y. Muroga and S. Yano, Investigation of microphase separation and thermal properties of noncrystalline ethylene ionomers. 2. IR, DSC, and dielectric characterization, *Macromolecules*, **2000**, *33*, 9044-9053.

[26] MacKnight, W. J., L. W. McKenna and B. E. Read, Properties of ethylene-methacrylic acid copolymers and their sodium salts: Mechanical relaxations, *J. Appl. Phys.*, **1967**, *38*, 4208-4212.

[27] Wessling, M., I. Huisman, T. v. d. Boomgaard and C. A. Smolders, Dilation kinetics of glassy, aromatic polyimides induced by carbon dioxide sorption, *J. Polym. Sci.: Polym. Phys. Ed.*, **1995**, *33*, 1371-1384.

[28] Koros, W. J. and M. W. Hellums, Transport properties, *Encycl. Polym. Sci. Eng.*, **1990**, *Suppl. Vol.*, 724-802.

[29] Berens, A. R. and H. B. Hopfenberg, Diffusion and relaxation in glassy polymer powders: 2. Separation of diffusion and relaxation parameters, *Polymer*, **1978**, *19*, 489-496.

[30] Pennycook, S. J., Z-contrast stem for materials science, *Ultramicroscopy*, **1989**, *30*, 58-69.

[31] Williams, C. E., C. Colliex, J. Horrion and R. Jerome, Scanning-transmission electron-microscopy to observe ionic domains in model ionomers, *ACS Symposium Series*, **1989**, *395*, 439-444.

[32] Williams, D. B. and C. E. Carter, *Transmission Electron Microscopy-a Ttextbook for Materials Science*, Plenum Press, New York, 1996.

[33] Taubert, A. and K. I. Winey, Quantitative determination of the local chemical composition in a Zn-neutralized p(e-ran-maa) ionomer using x-ray energy dispersive spectroscopy, *Polym. Mater. Sci. Eng.*, **2002**, *87*, 182-183.

[34] Lieser, G., S. C. Schmid and G. Wegner, Electrically conducting polymers: Preparation and investigation of oxidized poly(acetylene) by EFTEM, *J. Microsc.-Oxford*, **1996**, *183*, 53-59.

[35] O'Connell, E. M., T. W. Root and S. L. Cooper, Morphological-studies of lightly-sulfonated polystyrene using Na-23 NMR.1. effects of sample composition, *Macromolecules*, **1994**, *27*, 5803-5810.

[36] O'Connell, E. M., T. W. Root and S. L. Cooper, Morphological-studies of lightly sulfonated polystyrene using Na-23 NMR.2. effects of solution casting, *Macromolecules*, **1995**, *28*, 3995-3999.

[37] O'Connell, E. M., T. W. Root and S. L. Cooper, Morphological-studies of lightly sulfonated polystyrene using Na-23 NMR.3. effects of humidification and annealing, *Macromolecules*, **1995**, *28*, 4000-4006.

[38] O'Connell, E. M., D. G. Peiffer, T. W. Root and S. L. Cooper, Morphological studies of lightly sulfonated polystyrene using Na-23 NMR: effects of polydispersity in molecular weight, *Macromolecules*, **1996**, *29*, 2124-2130.

Chapter 7: Separation of Natural Gas Mixtures with Polyimide Membranes

7.1 OVERVIEW

This chapter focuses on the separation of synthetic natural gas mixtures and modeling the separation factor as a function of pressure. A wide range of membrane transport properties can be obtained by varying the copolymer compositions, along with the crosslinking agent and annealing treatment. The following mixtures are being studied, to measure the effect of the feed gas composition on the membrane separation properties.

Table 7.1 Synthetic natural gas mixtures used in this study (component mole %)

Mixture	CO_2	CH_4	C_2H_6	C_3H_8	C_4H_{10}	Toluene
50/50	50.00	50.00	0	0	0	0
1	30.02	62.95	4.00	3.00	0	0.0299
2	30.01	61.00	3.99	2.99	2.01	0

7.2 COMPARISON WITH COMMERCIAL POLYMERS

The above results indicate that a relatively simple covalent crosslinking approach is effective for stabilizing membranes against CO_2 plasticization. These materials are significantly more stable than the commercial membrane materials cellulose acetate [1] and Matrimid® [2], and they have more attractive CO_2/CH_4 separation properties, as shown in Fig. 7.1, an adaptation of Robeson's "Upper Bound" plot [3]. The literature permeabilities are typically measured for pure gases at pressures below 10 atm. The data for the various crosslinked DABA-containing crosslinked polyimides (in the ellipse) as well as Matrimid® and cellulose acetate were measured with 50/50 CO_2/CH_4 mixtures at 25 atm feed

pressure and 35°C. The performance of the crosslinked polyimides (6FDA-DAM:DABA and 6FDA-6FpDA:DABA copolymers) from our laboratory lies near the pure gas upper bound performance line, even though the measurements are for high pressure mixed gas separations, which are much more representative of industrially-relevant feed streams. The covalent crosslinking approach allows one to tailor the transport properties for a wide variety of applications, within the same general procedure.

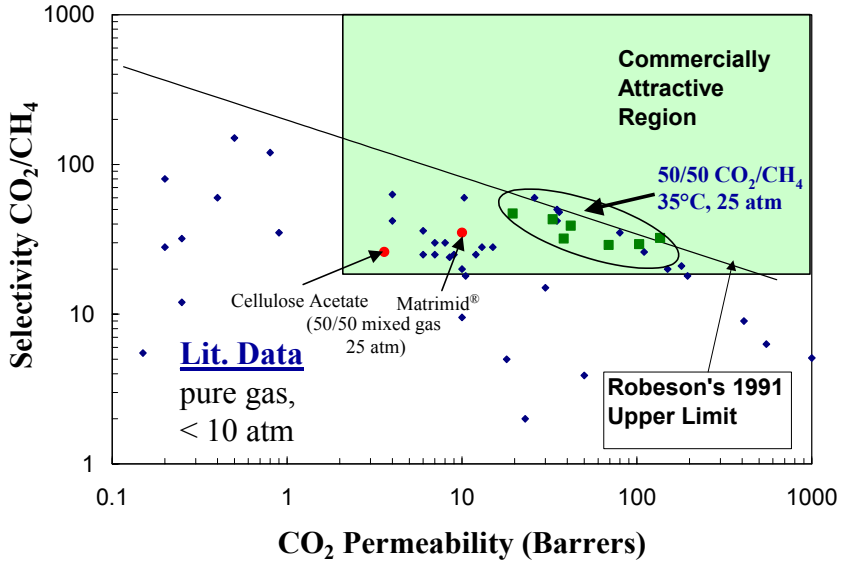

Figure 7.1: CO_2/CH_4 upper bound plot for 6FDA-based polyimides compared to the commercial gas separation polymers cellulose acetate [1] and Matrimid® [2]

7.3 CAUSES OF DECLINES IN SEPARATION FACTORS

7.3.1 Competitive Sorption and Diffusion

In mixed gas permeation, selectivity losses due to sorption competition, bulk flow, non-ideal thermodynamics, and plasticization must be differentiated. The permeabilities of all penetrants are decreased by competition for Langmuir sorption sites for a non-plasticized polymer, according to the dual mode model [4],

$$S_A = \frac{C_A}{p_A} = k_{D\,A} + \frac{C_{HA}^{'} b_A}{1 + \sum_{i=1}^{n} b_i p_i} \tag{7.1}$$

7.3.2 Bulk Flow Effects

Mixed gas selectivities also tend to decrease with increasing feed pressure due to so-called "bulk flow" or frame of reference effects as discussed originally by Ebra-Lima and Paul [5] for pure liquid permeation and extended to multicomponent permeation by Kamaruddin and Koros [6]. For a binary system (i.e. CO_2/CH_4) the flux of each component through the membrane is the sum of the diffusive flux and the bulk flux,

$$n_{CO_2} = \left(n_{CO_2}^{bulk} + n_{CO_2}^{diff} \right) \tag{7.2a}$$

$$n_{CH_4} = \left(n_{CH_4}^{bulk} + n_{CH_4}^{diff} \right) \tag{7.2b}$$

The transport through a membrane is typically attributed to diffusive fluxes (i.e., negligible convection),

$$n_{CO_2}^{diff} = -\rho D_{CO_2} \frac{d\omega_{CO_2}}{dx} \tag{7.3a}$$

$$n_{CH_4}^{diff} = -\rho D_{CH_4} \frac{d\omega_{CH_4}}{dx} \tag{7.3b}$$

where ω is the mass fraction and ρ is the unswollen membrane density. However, at high penetrant concentrations in the membrane, the bulk flow terms may be significant in determining the membrane selectivity.

$$n_{CO_2}^{bulk} = \left(n_{CO_2} + n_{CH_4}\right)\omega_{CO_2} \tag{7.4a}$$

$$n_{CH_4}^{bulk} = \left(n_{CO_2} + n_{CH_4}\right)\omega_{CH_4} \tag{7.4b}$$

For the CO_2/CH_4 separation, since the flux of CO_2 is much greater than the flux of CH_4, the bulk flux and diffusive flux may be on the same order of magnitude for CH_4. This means that the flux of CO_2 can significantly increase the total flux of CH_4 and *thereby reduce the selectivity*. So the practical separation factor is a strong function of the feed conditions, but this behavior may be predicted from pure gas permeation and sorption data if plasticization is eliminated.

7.3.3 Non-ideal Gas Phase Thermodynamics

Partial pressure differences across the membrane are typically used as the driving force to calculate component permeabilities. However, the true thermodynamic driving force is the chemical potential or fugacity difference. Non-ideal thermodynamics can have a significant impact on the separation factor and must be considered when analyzing and predicting membrane performance.

The fugacity coefficients for the mixtures in Table 7.1 were estimated by the commercial process simulator Aspen®, using the Soave-Redlich-Kwong (SRK) equation of state [7], with the interaction parameters given in Appendix A. The predictions for the 50/50 CO_2/CH_4 mixtures agreed well between the SRK, Peng-Robinson [8], and Virial models [9].

For the CO_2/CH_4 separation, the CO_2 fugacity coefficient decreases from unity to a much greater extent than the corresponding fugacity coefficient for CH_4

as the pressure increases at 35°C, as shown in Fig. 7.2. Heavier hydrocarbons behave even more non-ideally than CO_2 (Fig 7.3).

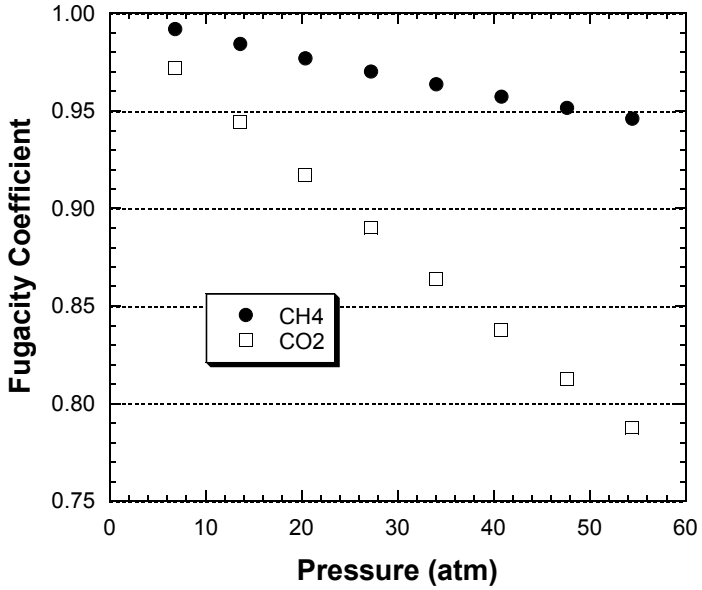

Figure 7.2: Fugacity coefficients for 50/50 CO_2/CH_4 gas mixtures at 35°C

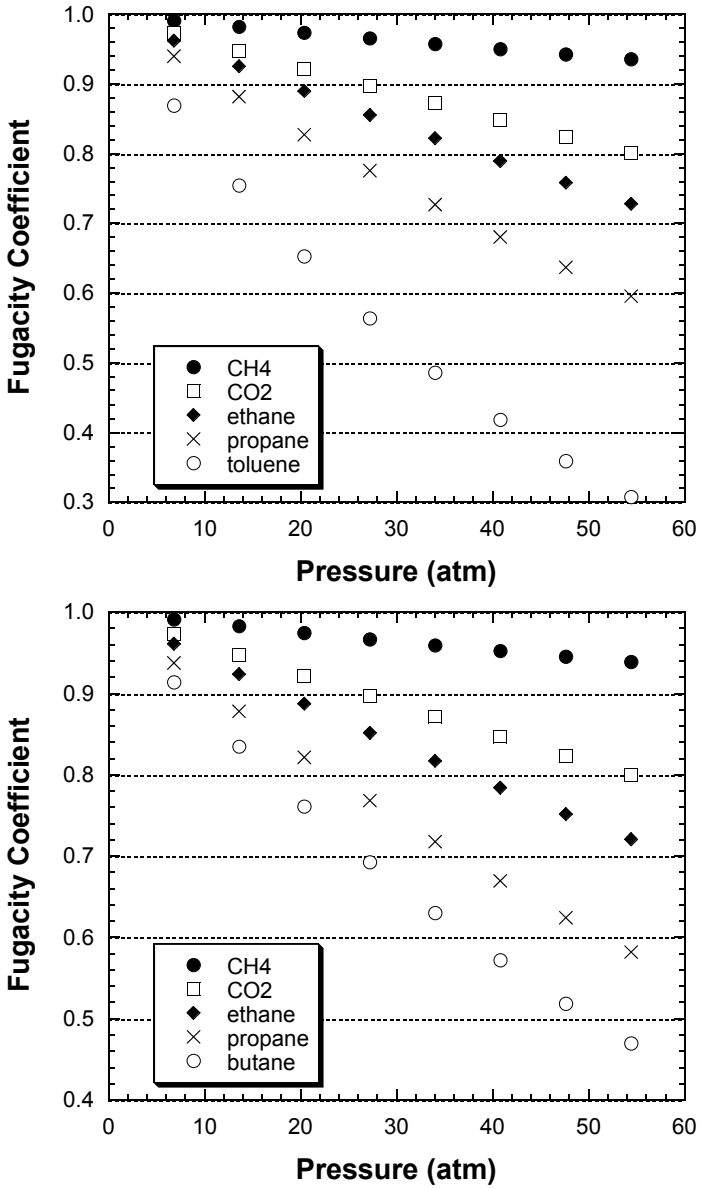

Figure 7.3: Fugacity coefficients for Mix 1 and Mix 2 at 35°C

7.4 6FDA-6FPDA:DABA COPOLYMERS

Fig. 7.4 shows the permeation and separation factor isotherms for the uncrosslinked and covalently (ethylene glycol) and ionically (aluminum) crosslinked 6FDA-6FpDA:DABA 2:1 membranes. For low feed pressures, the mixed gas selectivity is expected to be higher than the pure gas selectivities because CO_2 has a competitive advantage over CH_4 for the Langmuir sorption sites (i.e., a higher affinity constant). For all samples, the selectivity decreases monotonically with increasing feed pressure. However, the uncrosslinked and ionically crosslinked membranes become plasticized at a CO_2 partial pressure of at 17 atm, whereas in pure CO_2 permeation these membranes plasticize at 11 atm and 15 atm, respectively.

It should be noted that **plasticized membranes are inherently unstable** and the **separation factors shown for these membranes will continue to decline over time**, as indicated by the behavior in Chapters 5 and 6. The efficacy of crosslinking towards maintaining the separation factor over long-term operation must be verified experimentally. Field tests show that the typical CO_2/CH_4 separation factor for cellulose acetate membranes is 12-15 [10], even though a value of 26 was reported in the laboratory [1]. The times between measurements for the cellulose acetate and Matrimid® [2] membranes were not reported, so the values are likely to be highly dependent on how long the membrane is exposed to the feed before a measurement is taken. In the data reported in this chapter, for feed pressures above 20 atm, the membranes were exposed to the feed gas for at least 20 h before a measurement was taken at that pressure.

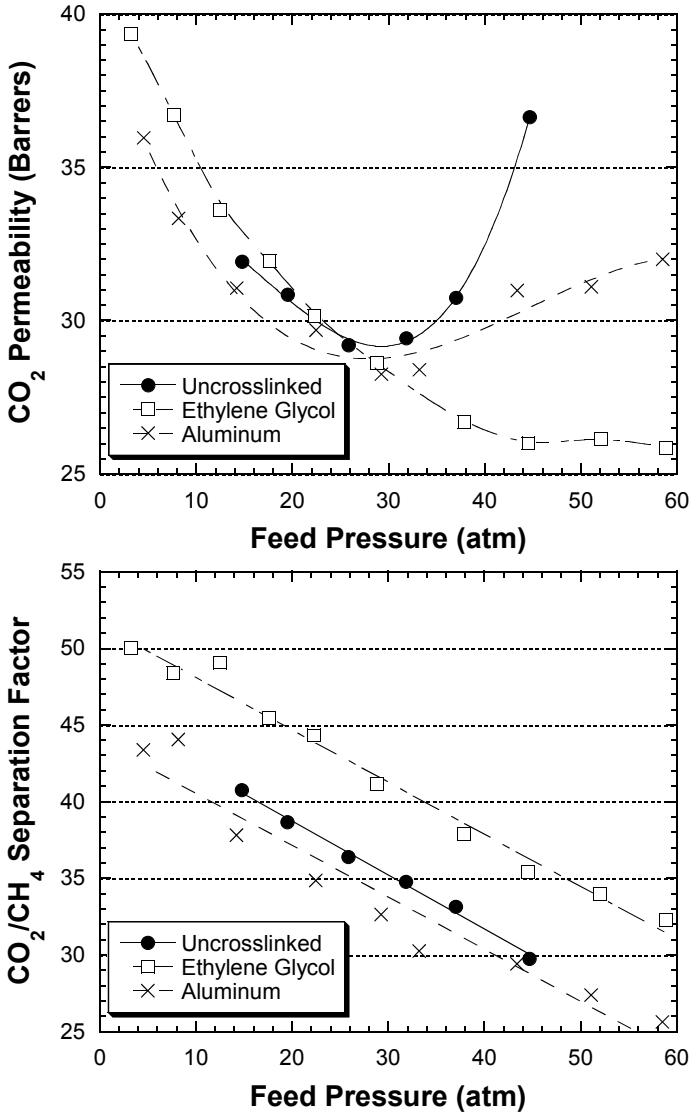

Figure 7.4: Mixed gas CO_2 permeation and separation factor isotherms with 50/50 CO_2/CH_4 at 35°C for 6FDA-6FpDA:DABA 2:1 uncrosslinked, crosslinked with ethylene glycol, and crosslinked with aluminum

From the monotonically decreasing CO_2 permeability with increasing feed pressure it is apparent that the covalently crosslinked sample does not plasticize, even up to CO_2 partial pressures of 29 atm. However, there are still significant selectivity losses with increasing feed pressures. Below 20 atm feed pressure, the drop in separation factor is primarily due to a larger decrease in the solubility coefficient for CO_2 than that for CH_4. At higher pressures, the main two contributions to the performance decline are the bulk flow of CH_4 and a strongly decreasing fugacity coefficient for CO_2. These two effects are separated by the following treatment.

The bulk flow of each component can be estimated by applying the model of Kamaruddin and Koros [6], described by Eq. 7.2-7.4. The pure gas sorption and diffusion coefficients were measured for each component at pressures below 10 atm. These parameters were then put into the model to predict the fraction of the flux of each component due to convection. This model is based on the mixed gas dual mode transport model [4], with the added convection terms. As the feed pressure increases, the components behave more non-ideally with respect to their fugacity coefficients. The effect of these non-idealities on the membrane performance can be quantified by calculating the fluxes based on partial pressure and partial fugacity driving forces. The difference between these two predictions shows the effect of the gas phase thermodynamics on the membrane separation factor.

Fig. 7.5 shows the experimental separation factor compared with the dual mode partial immobilization model (pressure driving force) and bulk flow model predictions, with pressure and fugacity-based driving forces. The fugacity-based model predictions are reasonably accurate. In the absence of plasticization, this model can be used to predict membrane performance over a wide pressure range,

thereby providing a critical tool for designing membrane systems for a wide variety of applications.

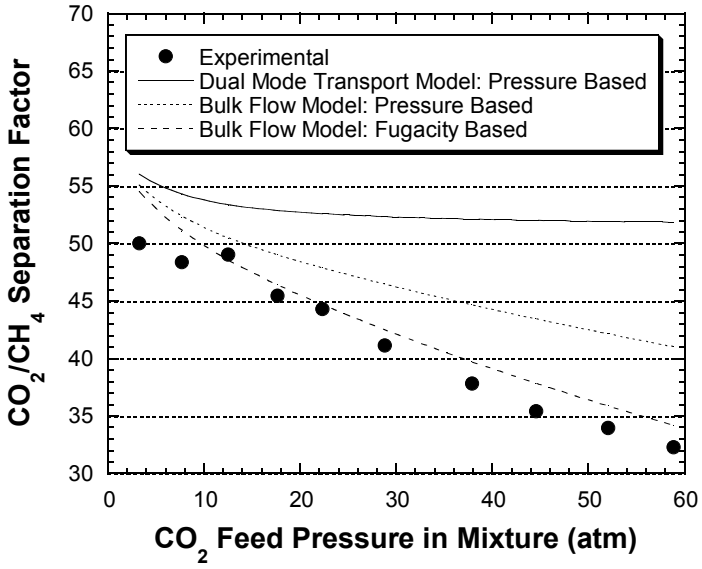

Figure 7.5: Bulk flow model predictions for separation factors of 50/50 CO_2/CH_4 mixed gas at 35°C through 6FpDA:DABA 2:1 crosslinked with ethylene glycol

The contributions of competitive sorption, bulk flow, non-ideal gas phase thermodynamics, and plasticization have been accounted for by the analysis shown in Fig. 7.5. Table 7.2 summarizes the pure and mixed gas membrane properties for the 6FDA-6FpDA:DABA 2:1 copolymers, with various treatments. It is particularly important that the membrane crosslinked with ethylene glycol has a higher permeability and selectivity than the other two. This performance is also expected to be much more stable over long-term operation than the other two.

Table 7.2: Summary of mixed gas (50/50) and pure gas data at 10 atm total feed pressure for 6FDA-6FpDA:DABA 2:1 Membranes

Crosslinking Agent	Pure Gas CO_2 Permeability* (Barrers)	Ideal CO_2/CH_4 Selectivity	Mixed Gas CO_2 Permeability* (Barrers)	Mixed Gas CO_2/CH_4 Selectivity
None	29	45	33	42
Ethylene Glycol	36	42	37	49
Aluminum	25	46	32	42

7.5 6FDA-DAM:DABA COPOLYMERS

7.5.1 50/50 CO_2/CH_4 Mixtures in 6FDA-DAM:DABA 2:1

In Chapter 4 it was shown that the heat treatment and crosslinking had a significant impact on the CO_2 permeability, but a rather small effect on the ideal selectivity. Mixed gas experiments provide insight into how the changes in free volume distribution and polymer chain mobility affect the separation of natural gas mixtures.

Fig. 7.6 shows that the CO_2 permeability decreases with increased annealing temperatures for the untreated membranes, as was seen for the pure gas case in Fig. 5.2. For the films annealed at 130°C, the pure CO_2 plasticization pressure occurs ~ 12 atm feed pressure, whereas in the mixed gas it occurs at a CO_2 partial pressure of 16 atm. This is fairly consistent with the 6FDA-6FpDA:DABA 2:1 data in Section 7.3. The separation factor is not a strong function of the annealing temperature, as has been observed for other polyimides [11]. However, the membrane annealed at 130°C does show a lower separation factor, which may be due to its higher free volume and tendency to plasticize.

Fig. 7.7 shows the effect of annealing temperature on the CO_2 permeation and the CO_2/CH_4 separation factors for feed pressures up to 40 atm at 35°C for the butylene glycol monoester. With similar behavior to that shown in Fig. 4.5, the CO_2 permeability increases **very significantly** after the 295°C annealing. Moreover, the **selectivity increases** for feed pressures below 20 atm, presumably due to the enhanced sorption selectivity from the increased concentration of Langmuir sites. This increase in free volume with higher crosslinking density has a positive effect on *both* the permeability and selectivity in the mixed gas. Similar behavior is seen for the CHDM monoester, in Fig. 7.8.

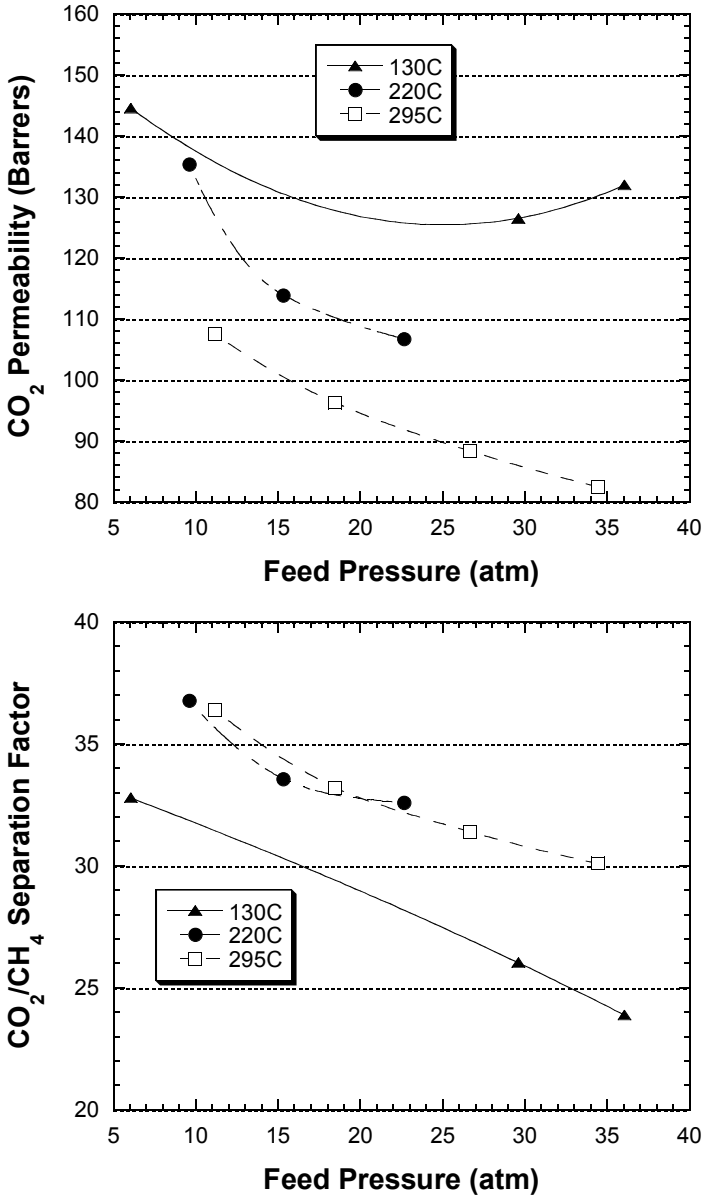

Figure 7.6: Mixed gas CO_2 permeation and separation factor isotherms with 50/50 CO_2/CH_4 at 35°C for 6FDA-DAM:DABA 2:1 untreated, annealed at 130°C, 220°C, 295°C

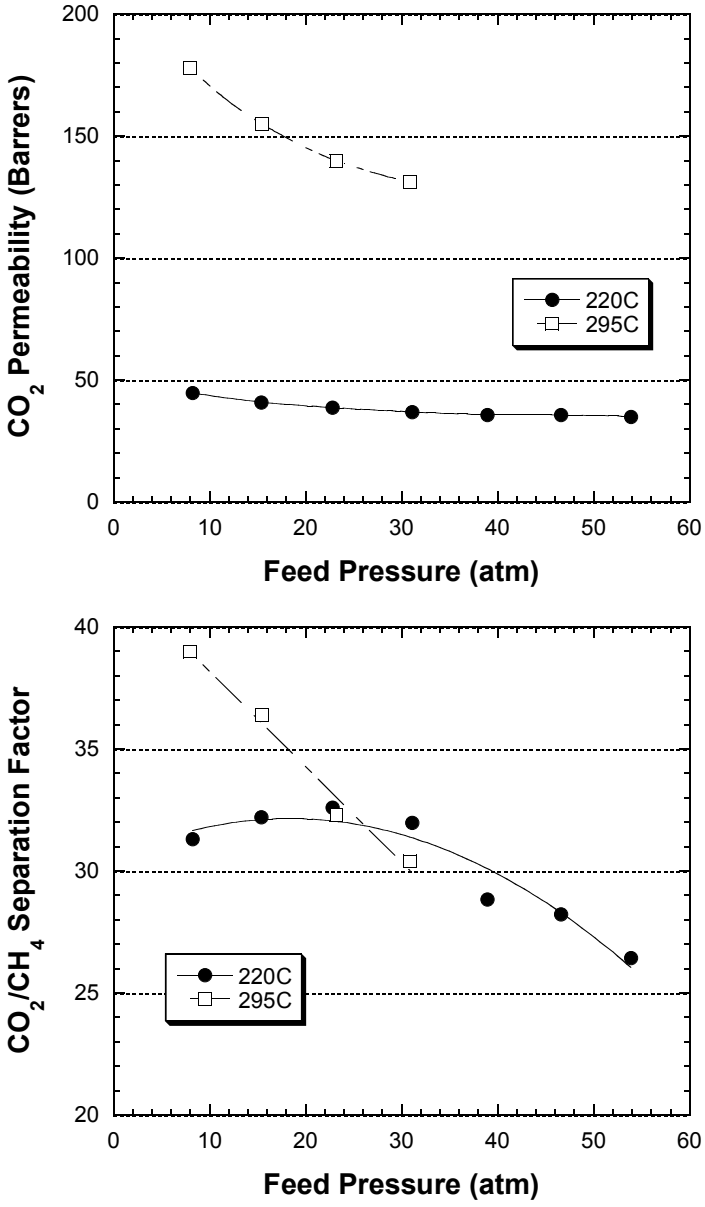

Figure 7.7: Mixed gas CO_2 permeation and separation factor isotherms with 50/50 CO_2/CH_4 at 35°C for 6FDA-DAM:DABA 2:1 BG monoester, annealed at 220°C and 295°C

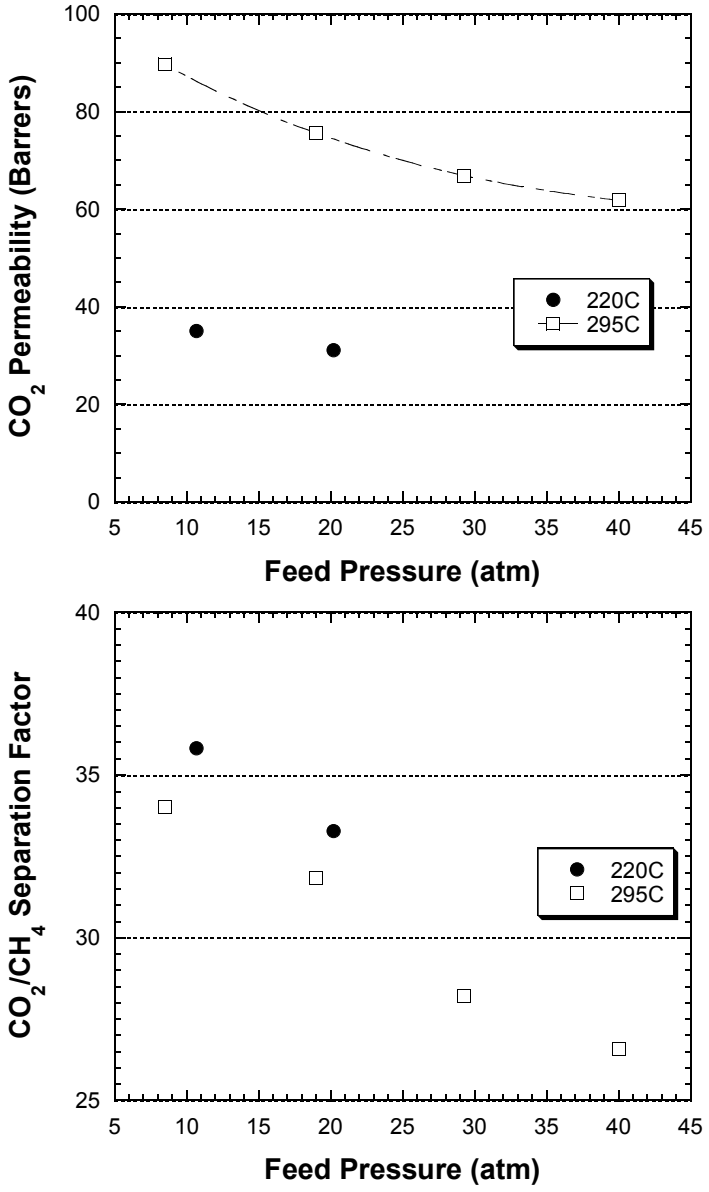

Figure 7.8: Mixed gas CO_2 permeation and separation factor isotherms with 50/50 CO_2/CH_4 at 35°C for 6FDA-DAM:DABA 2:1 CHDM monoester, annealed at 220°C and 295°C

7.4.2 Multicomponent Mixtures

Natural gas compositions and pressures vary widely by geographical location. A few reports exist in the literature of laboratory characterization of hydrocarbon exposure to membranes in CO_2/CH_4 separations, but the CO_2 content of these streams was less than 10% [12, 13]. Some natural gas fields contain as much as 70% CO_2, so it is of interest to test membranes under rigorous feed conditions. The pressure available in the gas cylinder is limited by the dew point of the mixture. A 21°C dew point was specified for the two multicomponent mixtures in Table 7.1 (Section 7.1) and the delivery pressures were at most 42 atm. To obtain higher feed pressures, a pervaporative introduction of the vapors to the feed stream may be desirable [14].

White et al. showed a 34% decrease in the CO_2/CH_4 selectivity when asymmetric polyimide membranes were exposed to feed gas containing 500 ppm toluene (10% CO_2, 90% CH_4, 68 atm, 48°C) [12]. However, the data in Fig. 7.9 indicate a small effect of the toluene (plus other hydrocarbons) on the CO_2/CH_4 selectivity for the 6FDA-DAM:DABA 2:1 membrane annealed at 220°C for 24 h. The highest feed pressure in Fig. 7.9 is 39 atm. Therefore it is necessary to compare the toluene fugacities between White's data and Mix 1. The toluene fugacity can be calculated by,

$$f_i = y_i \phi_i P \tag{7.5}$$

In White's case, the toluene fugacity is 0.20 psia and in this work the maximum fugacity is 0.082 psia. It's unknown if the selectivity decline in their work was due to the higher fugacity toluene, or whether it related to the polymer structure. A recent patent suggests that polar polyimides (e.g. 6FDA-DABA copolymers) are much less affected by toluene than other polyimides [15]. Another reason may be that asymmetric membranes can plasticize at lower pressures than dense

films [16]. In practical applications, aromatic hydrocarbon exposure has caused serious performance declines for cellulose acetate membranes [17].

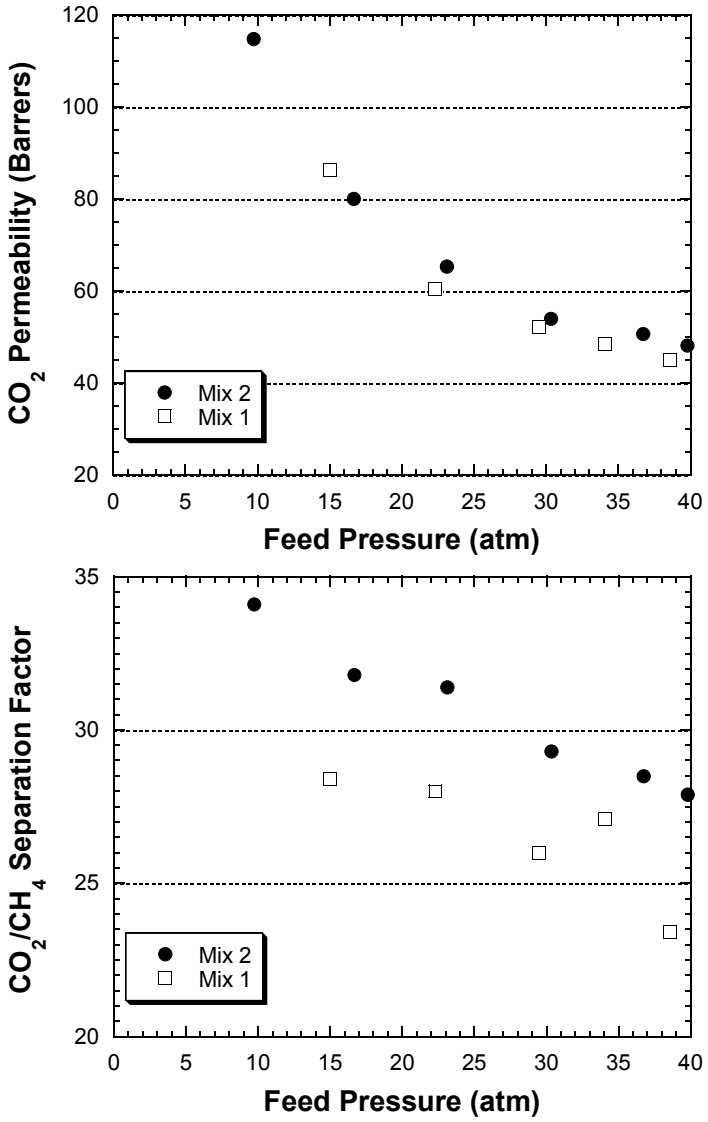

Figure 7.9: Mixed gas CO_2 permeation and separation factor isotherms with synthetic natural gas mixtures at 35°C for DAM:DABA 2:1 annealed at 220°C

The major difference in the separation of binary CO_2/CH_4 mixtures and the multicomponent mixtures is in the magnitudes of the permeabilities, as shown in Fig. 7.10. Here the permeabilities are calculated with a fugacity-based driving force. For Mix 1 and Mix 2, it is believed that the permeabilities are decreased due to competition for Langmuir sorption sites. Differences in the CO_2/CH_4 separation factor are much smaller than differences in the permeabilities.

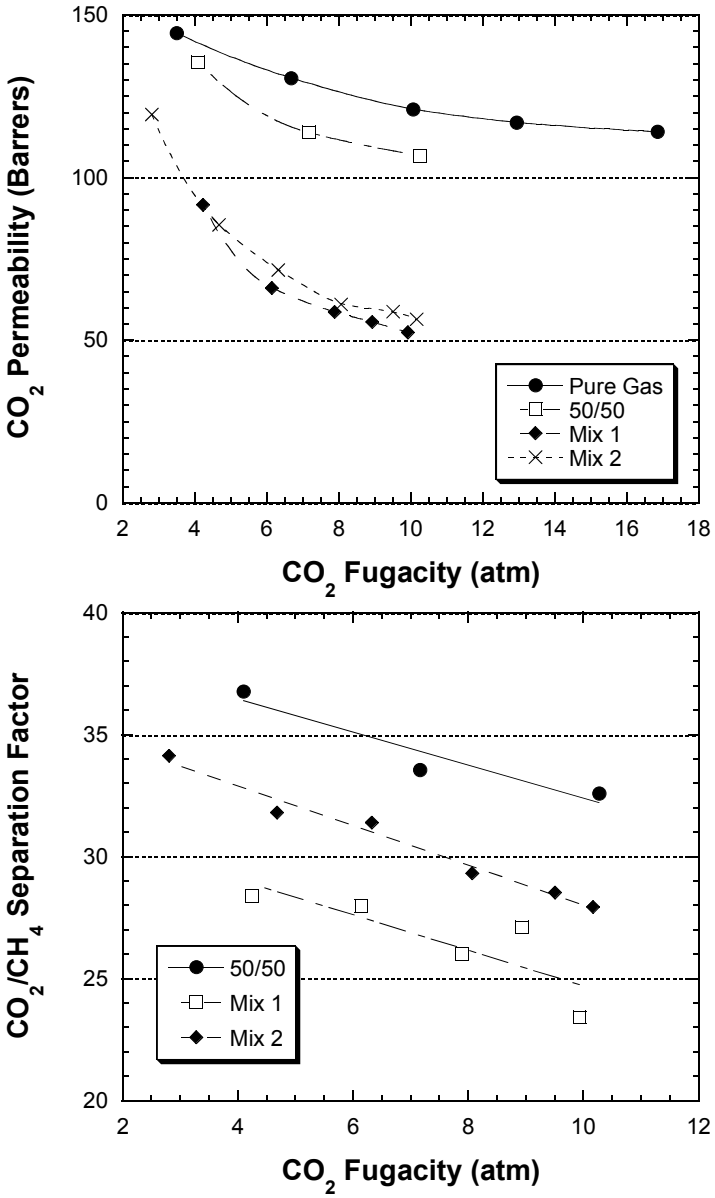

Figure 7.10: Comparison of CO_2 permeabilities pure gas, binary mixtures, and other gas mixtures for 6FDA-DAM:DABA 2:1 membranes.

The C_2H_6/CH_4 selectivity was ~ 0.3 for Mix 1 and 0.5 for Mix 2. The reasons for this difference are not clear at this time. The other components were not present in significant concentrations in the permeate stream in order to calculate their permeabilities.

7.6 CONCLUSIONS

Mixed gas permeation shows many of non-ideal effects that must be accounted for when analyzing membrane performance. Covalent crosslinking is effective at suppressing CO_2-induced plasticization. In the absence of plasticization, membrane performance can be predicted by accounting for competitive sorption, convective flow, and non-ideal gas phase thermodynamics.

Thermal annealing at 295°C affects the transport properties for the 6FDA-DAM:DABA 2:1 untreated and monoester membranes in very different ways. For the untreated membrane, the permeabilities decrease and the selectivity remains unchanged. For the BG and CHDM monoesters, the CO_2 permeabilities increase by factors of 3.7 and 2.5 respectively, at 20 atm feed pressure, without a loss in selectivity. It's hypothesized that CO_2 has enhanced solubility selectivity due to the increased concentration of Langmuir sites as the polymer chain packing is disrupted by the crosslinking.

Separation of more complex synthetic natural gas mixtures results in a decreased CO_2 permeability, but negligible changes in the selectivity relative to the 50/50 feed case.

The 50/50 mixed gas separation performance of the crosslinked polyimides is an improvement over the state-of-the-art polymeric membranes. While these results lie on or near Robeson's 1991 Upper Bound, this boundary is based on pure gas literature data, at feed pressures below 10 atm. The crosslinked polyimide performance is significantly better and they are much more

resistant to CO_2 plasticization than the commercial polymers Matrimid® and cellulose acetate.

REFERENCES

[1] Houde, A. Y., B. Krishnakumar, S. G. Charati and S. A. Stern, Permeability of dense (homogeneous) cellulose acetate membranes to methane, carbon dioxide, and their mixtures at elevated pressures, *J. Appl. Polym. Sci.*, **1996**, *62*, 2181-2192.

[2] Bos, A., I. G. M. Punt, M. Wessling and H. Strathmann, Plasticization-resistant glassy polyimide membranes for CO_2/CH_4 separations, *Sep. and Purif. Tech.*, **1998**, *14*, 27-39.

[3] Robeson, L. M., Correlation of separation factor versus permeability for polymer membranes, *J. Membr. Sci.*, **1991**, *62*, 165-185.

[4] Koros, W. J., R. T. Chern, V. Stannett and H. P. Hopfenberg, A model for permeation of mixed gases and vapors in glassy polymers, *J. Polym. Sci., Polym. Phys. Ed.*, **1981**, *19*, 1513-1530.

[5] Paul, D. R. and O. M. Ebra-Lima, Pressure-induced diffusion of organic liquids through highly swollen polymer membranes, *J. Appl. Polym. Sci.*, **1970**, *14*, 2201-2224.

[6] Kamaruddin, H. D. and W. J. Koros, Some observations about the application of Fick's first law for membrane separation of multicomponent mixtures, *J. Membr. Sci.*, **1997**, *135*, 147.

[7] Bertucco, A., M. Barolo and G. Soave, Estimation of chemical-equilibria in high-pressure gaseous systems by a modified Redlich-Kwong-Soave equation of state, *Ind. Eng. Chem. Res.*, **1995**, *34*, 3159-3165.

[8] Peng, D. and D. B. Robinson, New 2-constant equation of state, *Ind. Eng. Chem. Fund.*, **1976**, *15*, 59-64.

[9] Vu, D. Q., Formation and characterization of asymmetric carbon molecular sieve and mixed matrix membranes for natural gas purification, Ph.D. Dissertation, The University of Texas at Austin, 2001.

[10] Baker, R. W., Future directions of membrane gas separation technology, *Ind. Eng. Chem. Res.*, **2002**, *41*, 1393-1411.

[11] Kawakami, H., M. Mikawa and S. Nagaoka, Gas transport properties in thermally cured aromatic polyimide membranes, *J. Membr. Sci.*, **1996**, *118*, 223-230.

[12] White, L. S., T. A. Blinka, H. A. Kloczewski and I.-f. Wang, Properties of a polyimide gas separation membrane in natural gas streams, *J. Membr. Sci.*, **1995**, *103*, 73-82.

[13] Schell, W. J., C. G. Wensley, M. S. K. Chen, K. G. Venugopal, B. D. Miller and J. A. Stuart, Recent advances in cellulosic membranes for gas separation and pervaporation, *Gas Sep. Purif.*, 1989, *3*, 162-169.

[14] Djoekita, G., D. Q. Vu and W. J. Koros, Pervaporative introduction of organic vapors into high-pressure gas feeds, *J. Appl. Polym. Sci.*, **2001**, *80*, 311-315.

[15] Simmons, J. W., Aromatic co-polyimide hydrophilic membranes for gas separations, especially carbon dioxide and nitrogen from natural gas, U.S. Patent 6,383,258, Air Liquide, Societe Anon. pour l'Etude et l'Exploitation des Procedes Georges Claude, Fr. 2002.

[16] Mikawa, M., S. Nagaoka and H. Kawakami, Gas permeation stability of asymmetric polyimide membrane with thin skin layer: effect of molecular weight of polyimide, *J. Membr. Sci.*, **2002**, *208*, 405-414.

[17] Ratcliffe, C. T., A. Diaz, N. C and G. Munoz, Application of membranes in CO_2 separation from natural gas: pilot plant tests on offshore platforms, presented at Laurence Reid Gas Conditioning Conference, Norman, OK, Feb. 21-24, 1999.

Chapter 8: Summary and Future Work

8.1 SUMMARY

Polyimide membranes have been widely applied for gas separations due to their attractive permeability, selectivity, and processing characteristics. Their use for natural gas and hydrocarbon separations is limited by plasticization-induced selectivity losses in feeds with significant partial pressures of CO_2 and C_3+ hydrocarbons. This project has focused on understanding CO_2-induced plasticization of polyimide membranes and how this can be mitigated by thermal annealing and crosslinking.

Covalent crosslinking has been shown to be an effective approach for stabilizing membranes while retaining very attractive transport properties. The degree of crosslinking can be controlled by the amount of carboxylic acid moieties incorporated into the polymer backbone and the esterification treatments given to the polyimides. The transport properties can be controlled by the monomer stoichiometry. The two-step crosslinking treatment allows for spectroscopic characterization of the reaction yields in the monoesterification and transesterification reactions. These crosslinking reactions occur at temperatures well below the glass transition and no additives are required in the casting solution, making the approach attractive for the eventual production of asymmetric hollow fibers.

When analyzed within the dual mode sorption framework, crosslinking tends to decrease sorption by the Henry's law (dissolution) mechanism and increase the sorption into Langmuir sites (hole-filling). It's envisioned that the insertion of diol molecules between the polymer chains disrupts chain packing and, therefore, increases the free volume. This is particularly evident when the 6FDA-DAM:DABA 2:1 BG and CHDM monoesters are dried at 295°C, when the

permeability increases by more than a factor of 2.5 (relative to values for film dried at 220ºC), and there is no selectivity loss in the mixed gas permeation.

In a plasticized membrane, the sorption, diffusion, and swelling processes are all coupled. The use of *in-situ* spectroscopic ellipsometry to probe the swelling of thin films is an effective way to understand how swelling and sorption are related to plasticization. It appears that the key to controlling plasticization is to control the membrane swelling, since this is related to the increase in polymer chain segmental mobility facilitated by the CO_2 sorption. This increased mobility manifests itself as an increase in the permeability of all components, but a loss in the diffusion selectivity for CO_2 over methane, the primary separation mechanism of the glassy polyimide membranes.

Thermally annealed 6FDA-DAM:DABA 2:1 films are stabilized against plasticization, presumably by formation of charge transfer complexes, crosslinking, or dimerization of the COOH groups, whereas the monoesters are stabilized by covalent crosslinking and possibly charge transfer complexes. The equilibrium sorption coefficient and the kinetics of the sorption process are **not** good indicators of polyimide permeation plasticization, but swelling and permeability are clearly correlated with respect to annealing temperature, for both the untreated and monoester films. An upturn in the swelling isotherm corresponds to an upturn in the permeability isotherm, reflecting an increase in the polymer free volume and the corresponding increase in the CO_2 diffusion coefficient.

The long-term, relaxation controlled (i.e. non-Fickian) kinetics of the swelling and permeation are also correlated. Films annealed at low temperatures become unstable very quickly (with respect to permeability and swelling) and the amplitude of this instability is much larger than that for films annealed at higher temperatures. For practical membranes, thermal annealing and crosslinking is effective at improving the robustness of membranes in being able to handle higher

concentrations of plasticizing agents, both at steady-state and in an "upset condition."

Polyimide ionomers were prepared from 6FDA-6FpDA:DABA 2:1 and 1:2 copolymers. This represents a novel synthesis approach, where the carboxylic acid content of the ionomer precursor can be tuned and the polymer backbone retains its polyimide structure. The 1:2 ionomer shows greater heterogeneity in the ion distribution than the 2:1, as shown by scanning transmission electron microscopy. Small angle x-ray scattering is not effective at characterizing the morphological differences in the samples (i.e., the scattering spectra look the same for the ionomers and uncrosslinked samples), despite the fact that it has been the dominant characterization technique for describing ionomer aggregates. Infrared spectroscopy indicates that the crosslinking reaction proceeds to conversions greater than 60%. Even though both films become largely insoluble in organic solvents, their resistance to CO_2 plasticization is poor. Again, the plasticization is primarily described by the CO_2 diffusion coefficient behavior.

The separation of 50/50 CO_2/CH_4 mixtures up to 55 atm feed pressure at 35°C shows that covalent crosslinking leads to a significant reduction in the methane loss to the permeate from plasticization effects. However, there are still significant reductions in the separation factor at high pressures due to non-ideal gas phase thermodynamics and convective flow of CH_4 due to the flux of CO_2. The separation factor can be predicted in the absence of plasticization by applying the fugacity-based dual mode, bulk flux model. Thermal annealing of the untreated membranes tends to decrease the permeabilities without much effect on the selectivity. Conversely, crosslinking can increase the permeability and selectivity simultaneously. Separation of more realistic natural gas mixtures containing heavy hydrocarbons shows a decrease in the CO_2 permeability with small effects on the CO_2/CH_4 selectivity.

8.2 RECOMMENDATIONS FOR FUTURE WORK

8.2.1 Hydrocarbon Permeation, Sorption, and Swelling

It has been shown that plasticization is a major limitation to applying polyimide membranes in propylene/propane [1], 1,3-butadiene/butane [2], and aromatic/aliphatic separations [3]. The crosslinking approach presented in this work would likely be effective in preserving the diffusion selectivity of polyimide membranes at practically relevant operating conditions. However, it is not clear how crosslinking affects the sorption and diffusion coefficients for penetrants over a wide range of sizes and condensabilities. Research in this area may provide more insight into how the free volume distribution is changed with crosslinking and how this can be tailored for various separations.

Chapter 5 gives a description of the relationship between permeability, swelling, and sorption in a membrane plasticized with CO_2. Conducting *in-situ* ellipsometry measurements with various gas phase penetrants to begin to develop a general model for plasticization based on the polymer and penetrant properties.

8.2.2 High Selectivity Polymers and High DABA Content Polymers

The polymers studied in this work have relatively high permeabilities with moderate selectivities. The increase in permeability with crosslinking is likely to be more pronounced when the starting polymer has a lower permeability and higher selectivity. This work, along with that of Staudt-Bickel and Koros [4] showed that the permeability can be increased without sacrificing selectivity. By working with high DABA contents in the copolymer, the selectivity can be increased and the effect of crosslinking should be greater with respect to the increase in permeabilities. The improved selectivity in mixed gas, due to the increased Langmuir sorption, should be even greater with higher DABA contents.

8.2.3 Charge Transfer Complexes

Polyimide solubility and film color (i.e., UV absorption) is determined by the extent of electron delocalization via charge transfer complexes (CTC). In the solid-state, intermolecular charge transfer is assumed to dominate over intramolecular charge transfer [5].

The charge transfer is promoted by having the donor and acceptor fragments in the same plane. The incorporation of bulky groups that inhibit chain packing tends to increase the solubility of polyimides by limiting their electronic interactions [6]. Typically, incorporation of electron withdrawing groups on the diamine moiety disrupts charge transfer complexes [6]. However, in the 6FDA-DAM:DABA 2:1 copolymer, incorporation of the DABA group (with the electron withdrawing carboxylic acid group) makes these *susceptible* to stabilization against plasticization with heat treatment. Furthermore, annealing these films at 295°C for 24 h causes them to become insoluble in NMP. However, the same treatment for 6FDA-DAM does not cause any solubility changes.

Charge transfer complexes are typically characterized by UV-Vis and fluorescence spectroscopy. Wachsman and Frank claim that the fluorescence emission intensity can be used as a local torsional probe of the nitrogen-phenyl bond to determine the relative degree of ordering in the film [7]. Kawakami et al. showed that the CO_2/CH_4 selectivity at low feed pressures and fluorescence spectrum was a strong function of the annealing temperature for chemically imidized polyimide membranes (6FDA-mDDS) [8]. In the studies presented here, significant intrinsic selectivity changes with thermal annealing of the untreated films have not been observed, but there are huge effects for the plasticization, film solubility, and CO_2 sorption. It would be valuable to understand the polymer structural features that lead to the changes in the transport properties upon annealing, for a variety of separations.

To establish some structure/property relationships regarding polyimide membrane susceptibility to stabilization by heat treatment the following structures should be investigated:

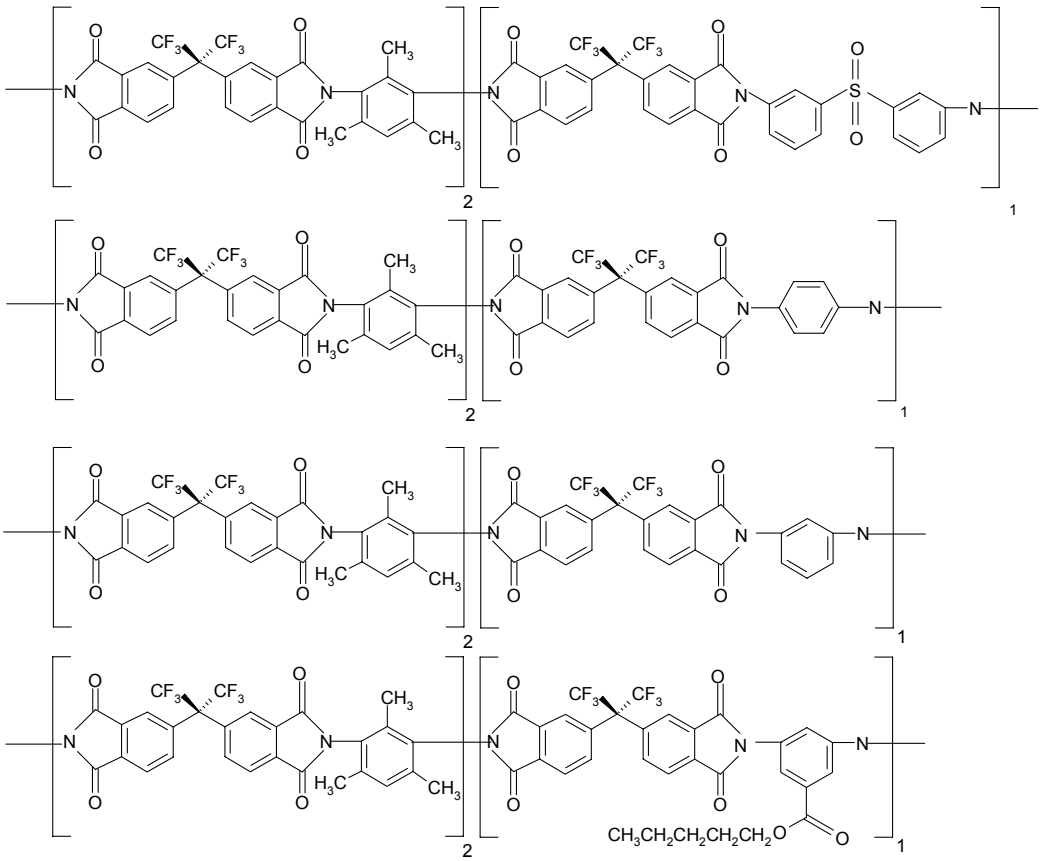

Figure 8.1: Proposed structures for study of charge transfer complex formation. 6FDA-DAM:mDDS 2:1, 6FDA-DAM:pPD 2:1, 6FDA-DAM:mPD 2:1, and 6FDA-DAM:DABA 2:1 n-butanol monoester

For the 6FDA-6FpDA and 6FDA-6FmDA isomers, the *meta* linkage leads to higher packing densities [9], possibly suggesting that intermolecular charge transfer complexes are also promoted by this enhanced packing. The comparison of the *meta* and *para* connected phenylene diamine moieties would lend insight into this relationship. It's also possible that the carboxylic acid group from the

DABA monomer changes the charge distribution to increase the cohesive energy density to provide stabilization against CO_2-induced plasticization, and/or there may be dimerization between the COOH groups. Capping these groups with n-butanol would provide insight into whether these dimers play a major role in determining the solubility and plasticization behavior.

8.2.4 Esterification Reaction Optimization

The ultimate crosslinking degree is a function of the DABA content and the reaction conversions in the monoesterification and transesterification steps. These reactions can be monitored by NMR and IR spectroscopy, respectively, as described in Chapter 4. The monoesterification conversion may be driven to completion through water removal during the reaction, higher catalyst loadings, use of different solvents, or higher reaction temperatures. For the production of asymmetric hollow fiber membranes, it is necessary to minimize the temperature required for the crosslinking reaction, to preserve the delicate morphology and prevent the permeance declines that can accompany heat treatments [10]. This may be achieved by application of microwaves to selectively activate the polar groups involved in the esterification reactions.

There have been reports of the acceleration of chemical reactions in the solid-state by application of microwaves. The activation energy for PET polycondensation reaction was reduced by 27% by the application of microwaves at 2.45 GHz [11]. For the crosslinking of nadic end-capped polyimides, the crosslinking reaction proceeds about ten times faster with the microwaves compared to a simple thermal cure at 230°C [12]. For the curing of Cyclotene™ benzocyclobutene, microwave exposure significantly increased the post-vitrification reaction rates [13]. In another study, the apparent activation energy for ring closure of polyimides in solution was reduced from 105 to 55 kJ/mole by exposure to microwaves [14]. Therefore, it is recommended to

investigate the use of microwave radiation to activate the crosslinking and minimize the time and temperature required for this reaction step.

8.2.5 Mixed Matrix Membranes

Mixed matrix composite membranes consist of molecular sieving domains (e.g. zeolites or carbon) embedded within a polymeric matrix. This approach can produce membranes with superior transport properties relative to pure polymers, while retaining the processability of polymers. One of the biggest challenges in forming these materials has been to obtain good contact between glassy polymeric matrices and the sieves [15]. One attractive approach is to bond the carboxylic acid groups from the DABA to the silanol groups on the zeolite surface [16].

Mixed matrix membranes are being pursued for natural gas separations [17]. With aggressive feed streams, plasticization-induced selectivity losses in the polymer phase are still expected to be problematic. The monoester approach can work to crosslink the matrix to prevent plasticization. The DABA content of the polymer may be tuned to optimize the interfacial bonding. These primed sieves (i.e., covered with a thin layer of polymer) could be blended with a monoester polymer, which should be miscible with the sieve coating. During the crosslinking reaction, the COOH groups that are not bonded with the zeolite surface could participate in the transesterification reaction.

8.2.6 Mixed Gas Separations, Modeling, and Stability

Chapter 7 shows some exciting results for the separation of synthetic natural gas mixtures. The bulk flow model of Kamaruddin and Koros [18] is effective at describing the separation of binary mixtures in the absence of plasticization and it could be extended to an arbitrary number of components in the feed. However, the model is based on the dual mode sorption and transport model, in which the mixed gas sorption in glassy has only been studied for binary

mixtures at pressures below 10 atm [19]. The sorption and diffusion interaction terms are likely to be significant at higher feed pressures, with higher sorbing components such as CO_2 and C_3+ hydrocarbons. Moreover, the bulk flow model cannot explain the results for propylene/propane mixed gas separations [20]. Further research into the mixed gas sorption may provide insight into how the material structure relates to competitive sorption at practically relevant operating conditions.

The Maxwell-Stefan approach to multicomponent transport may offer significant insight into the coupling of diffusion coefficients [21]. This mathematical framework could be combined with experimental investigation of the effect of feed composition and pressure on the CO_2/CH_4 separation.

The long-term stability of polyimide membranes in mixed gas feeds needs to be addressed. Field tests have shown cellulose acetate membranes experienced significant decline in the separation efficiency over long periods of time (8 months), because of exposure to CO_2 and heavy hydrocarbons [22]. The data in Chapter 5 suggest that heat treatment and covalent crosslinking are effective approaches for maintaining membrane stability, but this should be proven with mixed gas feeds over extended periods of time.

REFERENCES

[1] Tanaka, K., A. Taguchi, J. Hao, H. Kita and K. Okamoto, Permeation and separation properties of polyimide membranes to olefins and paraffins, *J. Membr. Sci.*, **1996**, *121*, 197-207.

[2] Okamoto, K., K. Noborio, J. Hao, K. Tanaka and H. Kita, Permeation and separation properties of polyimide membranes to 1,3-butadiene and n-butane, *J. Membr. Sci.*, **1997**, *134*, 171-179.

[3] Jizhong, R., C. Staudt-Bickel and R. N. Lichtenthaler, Separation of aromatics/aliphatics with crosslinked 6FDA-based copolyimides, *Sep. and Purif. Tech.*, **2001**, *22-23*, 31-43.

[4] Staudt-Bickel, C. and W. J. Koros, Improvement of co_2/ch_4 separation characteristics of polyimides by chemical crosslinking, *J. Membr. Sci.*, **1999**, *155*, 145-154.

[5] Salley, J. M. and C. W. Frank, Charge transfer in aromatic polyimides, in *Polyimides: Fundamentals and applications*, Marcel Dekker, Inc., New York, 1996.

[6] St. Clair, A. K. and T. L. St. Clair, Highly optically transparent/colorless aromatic polyimide film, 643,589, (United States National Aeronautics and Space Administration, USA). 1985.

[7] Wachsman, E. D. and C. W. Frank, Effect of cure history on the morphology of polyimide: Fluorescence spectroscopy as a method for determining the degree of cure, *Polymer*, **1988**, *29*, 1191-1197.

[8] Kawakami, H., M. Mikawa and S. Nagaoka, Gas transport properties in thermally cured aromatic polyimide membranes, *J. Membr. Sci.*, **1996**, *118*, 223-230.

[9] Coleman, M. R. and W. J. Koros, The transport-properties of polyimide isomers containing hexafluoroisopropylidene in the diamine residue, *J. Polym. Sci.: Polym. Phys. Ed.*, **1994**, *32*, 1915-1926.

[10] Krol, J. J., M. Boerrigter and G. H. Koops, Polyimide hollow fiber gas separation membranes: Preparation and the suppression of plasticization in propane/propylene environments, *J. Membr. Sci.*, **2001**, *184*, 275-286.

[11] Mallon, F. K. and W. H. Ray, Enhancement of solid-state polymerization with microwave energy, *J. Appl. Polym. Sci.*, **1998**, *69*, 1203-1212.

[12] Liu, Y., X. D. Sun, X. Q. Xie and D. A. Scola, Kinetics of the crosslinking reaction of a bisnadimide model compound in thermal and microwave cure processes, *J. Polym. Sci.: Polym. Chem. Ed.*, **1998**, *36*, 2653-2665.

[13] Tanikella, R. V., S. A. Bidstrup Allen and P. A. Kohl, Variable-frequency microwave curing of benzocyclobutene, *J. Appl. Polym. Sci.*, **2002**, *83*, 3055-3067.

[14] Lewis, D. A., J. D. Summers, T. C. Ward and J. E. McGrath, Accelerated imidization reactions using microwave radiation, *J. Polym. Sci:, Polym. Chem. Ed.*, **1992**, *30*, 1647-1653.

[15] Mahajan, R., R. Burns, M. Schaeffer and W. J. Koros, Challenges in forming successful mixed matrix membranes with rigid polymeric materials, *J. Appl. Polym. Sci.*, **2002**, *86*, 881-890.

[16] Mahajan, R. and W. J. Koros, Mixed matrix membrane materials with glassy polymers. Part 2, *Polym. Eng. Sci.*, **2002**, *42*, 1432-1441.

[17] Vu, D. Q., Formation and characterization of asymmetric carbon molecular sieve and mixed matrix membranes for natural gas purification, Ph.D. Dissertation, The University of Texas at Austin, 2001.

[18] Kamaruddin, H. D. and W. J. Koros, Some observations about the application of Fick's first law for membrane separation of multicomponent mixtures, *J. Membr. Sci.*, **1997**, *135*, 147-159.

[19] Sanders, E. S. and W. J. Koros, Sorption of carbon dioxide, ethylene, nitrous oxide and their binary mixtures in poly(methyl methacrylate), *J. Polym. Sci., Polym. Phys. Ed.*, **1986**, *24*, 175-188.

[20] Burns, R. L., Investigation of poly(pyrrolone-imide) materials for the olefin/paraffin separation, Ph.D. Dissertation, The University of Texas at Austin, **2002**.

[21] Krishna, R. and J. A. Wesselingh, The Maxwell-Stefan approach to mass transfer, *Chem. Eng. Sci.*, **1997**, *52*, 861-911.

[22] Ratcliffe, C. T., A. Diaz, C. Nopasit and G. Munoz, Application of membranes in CO_2 separation from natural gas: pilot plant tests on offshore platforms, presented at Laurence Reid Gas Conditioning Conference, Norman, OK, Feb. 21-24, **1999**.

Appendix A: Thermodynamic Data

The following expressions for the pure gas compressibility factors at 35°C were developed by the National Institute of Standards and Technology [1].

$$CH_4: \mathbf{z} = 1 - 1.049 \times 10^{-4}\, p + 3.818 \times 10^{-9}\, p^2 + 5.202 \times 10^{-12}\, p^3 \quad (A.1)$$

$$CO_2: \mathbf{z} = 1 - 3.375 \times 10^{-4}\, p + 6.169 \times 10^{-8}\, p^2 - 1.686 \times 10^{-10}\, p^3 \quad (A.2)$$

References

[1] Zimmerman, C. M., Advanced gas separation membrane materials: hyper rigid polymers and molecular sieve-polymer mixed matrices, Ph.D. Dissertation, The University of Texas at Austin, **1998**.

Appendix B: Experimental Procedures

B1 PERMEATION VOLUME CALIBRATIONS

The volume of the downstream section of a permeation apparatus (Fig. 3.3) can be measured by expanding a gas from a known volume into the downstream volume. Ultra-high purity N_2 was used for the calibrations. The unknown volume V_1 can be calculated from:

$$V_1 = \frac{V_2}{\left(\frac{p_1 - p_0}{p_2 - p_0}\right) - 1} \tag{B.1}$$

where p_0 is the pressure reading at full vacuum, p_1 is the pressure before expansion, and p_2 is the pressure after expansion.

B2 SORPTION VOLUME/TRANSDUCER CALIBRATIONS

Calibration of pressure-decay sorption cells involves the determination of the volumes and transducer calibration factors for the reservoir and cell. The transducer calibration factors are determined by connecting a Heise® pressure gauge to the sorption system and generating a calibration curve from a pressure range of 0 to 65 atm. The calibration factors are determined from the slope of the power-compensated transducer output to that of the Heise® (true) reading (p),

$$CF(psia^{-1}) = \frac{y(mV)}{Power(mV) * p(psia)} \tag{B.2}$$

The reservoir volumes, V_C and V_R, can be calculated from a system of two equations in two unknowns. In the first set of expansions, UNP N_2 is expanded from the reservoir into an empty cell. Then a steel ball of known volume is

placed into the cell and the expansions are repeated. The values of V_C and V_R are obtained from

$$\frac{V_R}{V_C} = \frac{\frac{V_{C,2}}{z_2} - \frac{V_{C,1}}{z_1}}{\frac{V_{R,1}}{z_1} - \frac{V_{R,2}}{z_2}} \tag{B.3}$$

$$\frac{V_R}{V_C - V_B} = \frac{\frac{(V_C - V_B)_2}{z_2} - \frac{(V_C - V_B)_1}{z_1}}{\frac{V_{R,1}}{z_1} - \frac{V_{R,2}}{z_2}} \tag{B.4}$$

where z is the compressibility factor and the subscripts 1 and 2 refer to the pressures before and after each expansion.

B3 GC CALIBRATIONS

The gas chromatograph should be calibrated to determine the component response factors and retention times. The response factor is defined as (relative to CH_4),

$$\beta_i = \frac{A_i y_j}{A_j y_i} \tag{B.5}$$

The mole fraction can be calculated by

$$y_i = \frac{A_i \beta_i}{\sum_{j=1}^{n} A_j \beta_j} \tag{B.6}$$

The permeate sample is typically injected at pressures greater than 5 torr. The HP 5880A gas chromatograph with thermal conductivity detector, fitted with a Hayesep-R® (Supelco) packed column, was calibrated with several gases from Air Liquide. The calculated response factors were then compared against the literature values [1]. The column temperature was set to 80 and 120°C for the

binary and multicomponent natural gas mixtures (see Table 7.1), respectively. For binary CO_2/CH_4 mixtures of 97.2% and 50% CO_2, the response factors were 0.782. Table B.1 shows the calibration response factors for the components in the synthetic natural gas mixtures.

Table B.1: Response factors for natural gas mixtures

Component	*Mix 1*	*Mix 2*	*Literature Value*
CO_2	0.743	0.742	0.750
C_2H_6	0.710	0.702	0.706
C_3H_8	0.564	0.575	0.554

The n-butane and toluene peaks were not observed during the calibration runs.

B4 DABA RECRYSTALLIZATION

The DABA monomer should be recrystallized if it has a dark gray or brown color that is characteristic of oxidized amino groups. To maintain high purity, it should not be open to air or exposed to light for prolonged periods of time.

1. Assemble glassware using 500 mL three necked flask.
2. Insert a condenser into one neck of a three-neck round bottom flask and insert a purge vent needle pierced through the septum on the condenser.
3. Insert a septum into one neck and introduce a N_2 purge and a thermocouple through this septum.
4. Insert a rubber stopper on the middle neck.

5. Boil distilled water in a flask, equipped with stir bar.
6. Weigh the monomer to be purified and add to the round-bottom flask.
7. Add the appropriate amount of hot water to the flask such that the monomer is almost completely dissolved (~ 20 mL water per gram of DABA)
8. Heat the solution up to ~ 80 – 85°C.
9. Set up a Buchner Funnel into another 500 mL three-neck flask fitted to an aspirator (i.e., slight vacuum). Wet the filter paper and heat it with a heat gun.
10. Pour the solution through the filter and into the new flask. Quickly switch the flask so that it is now under N_2 purge and fitted with a condenser.
11. Allow the solution to cool slowly for ~ 4 h and then put under ice for the 1 h.
12. Again filter the solution on cold filter paper to recover the crystals.
13. Repeat recrystallization procedure until the filtrate from the hot stage is minimized.
14. Dry the product at low temperatures (< 50°C) under vacuum and store the purified monomer in a sealed bottle.

REFERENCES

[1] Rosie, D. M. and E. F. Barry, Quantitation of thermal conductivity detectors, *Journal of Chromatographic Science*, **1973**, *11*, 237-249.

Appendix C: Experimental Reproducibility and Replication

C1 PERMEATION

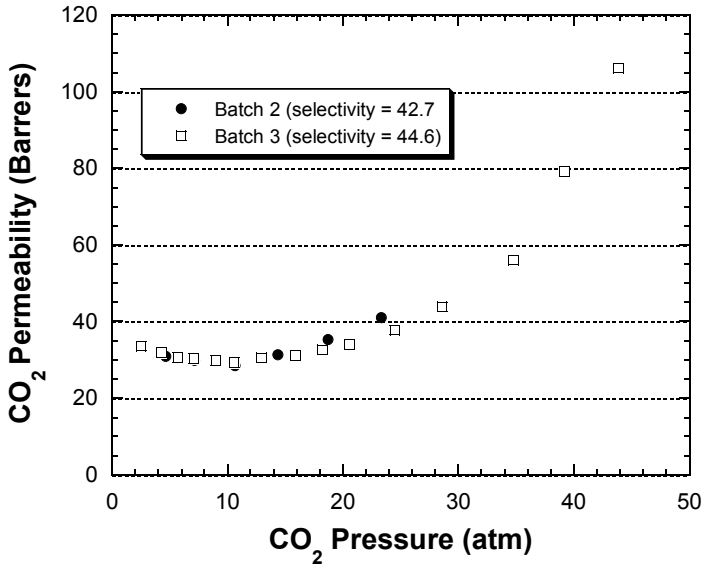

Figure C1: Replicates for CO_2 permeation isotherm at 35°C for 6FDA-6FpDA:DABA 2:1 annealed at 130°C. The CO_2/CH_4 ideal selectivity is measured at 10 atm.

Based on a propagation of error analysis [1], the estimated uncertainty in a permeability measurement is ~ 7%. Table C.1 shows the experimental variability for various permeation measurements.

Table C1: Some representative CO_2 permeability replicate measurements at 35°C

Polymer	Sample 1	Sample 2
6FDA-DAM:DABA 2:1 (220°C)	121	116
6FDA-DAM:DABA 2:1 CHDM (180°C)	30	26
6FDA-DAM:DABA 2:1 CHDM (220°C)	21	23
6FDA-DAM:DABA 2:1 CHDM (295°C)	73	67
6FDA-6FpDA:DABA 2:1 Al Cross (130°C)	25	27
6FDA-6FpDA:DABA 2:1 EG (220°C)	36	35

These replicate values indicate that the theoretical uncertainty of 7% is reasonably accurate.

C2 SORPTION

Fig. C2 shows an example of the reproducibility of the sorption isotherms, where these measurements were made on different films in different systems.

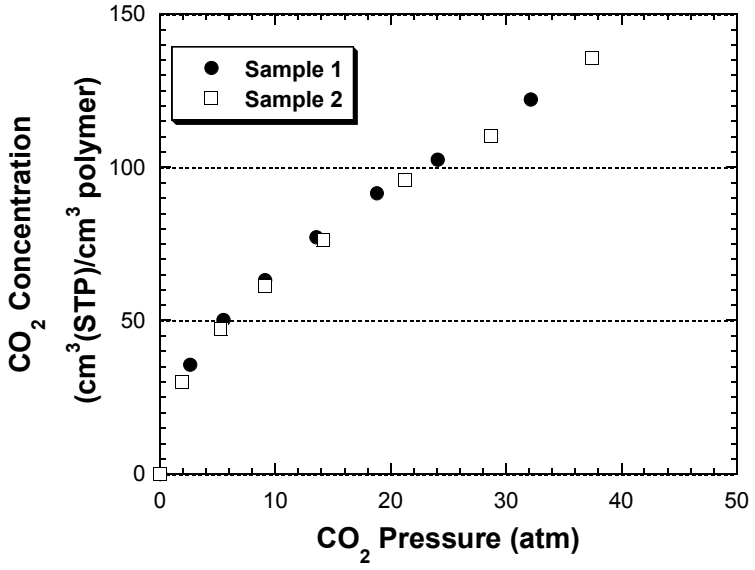

Figure C2: Replicates for CO_2 sorption isotherms at 35°C for 6FDA-DAM:DABA 2:1 annealed at 130°C

The sorption isotherms for CO_2 in 6FDA-DAM (Fig. 2.1) also agree very well with literature values of Tanaka et al [2].

C3 SPECTROSCOPIC ELLIPSOMETRY

The typical uncertainty for measuring film thickness on the order 1200Å is ~ 0.3%.

REFERENCES

[1] Vu, D. Q., Formation and characterization of asymmetric carbon molecular sieve and mixed matrix membranes for natural gas purification, Ph.D. Dissertation, The University of Texas at Austin, 2001.

[2] Tanaka, K., H. Kita and K.-I. Okamoto, Sorption of carbon dioxide in fluorinated polyimides, *J. Polym. Sci.: Polym. Phys. Ed.*, **1993**, *31*, 1127-1133.

Appendix D: Miscellaneous Data

D1 IONOMER DSC THERMOGRAMS

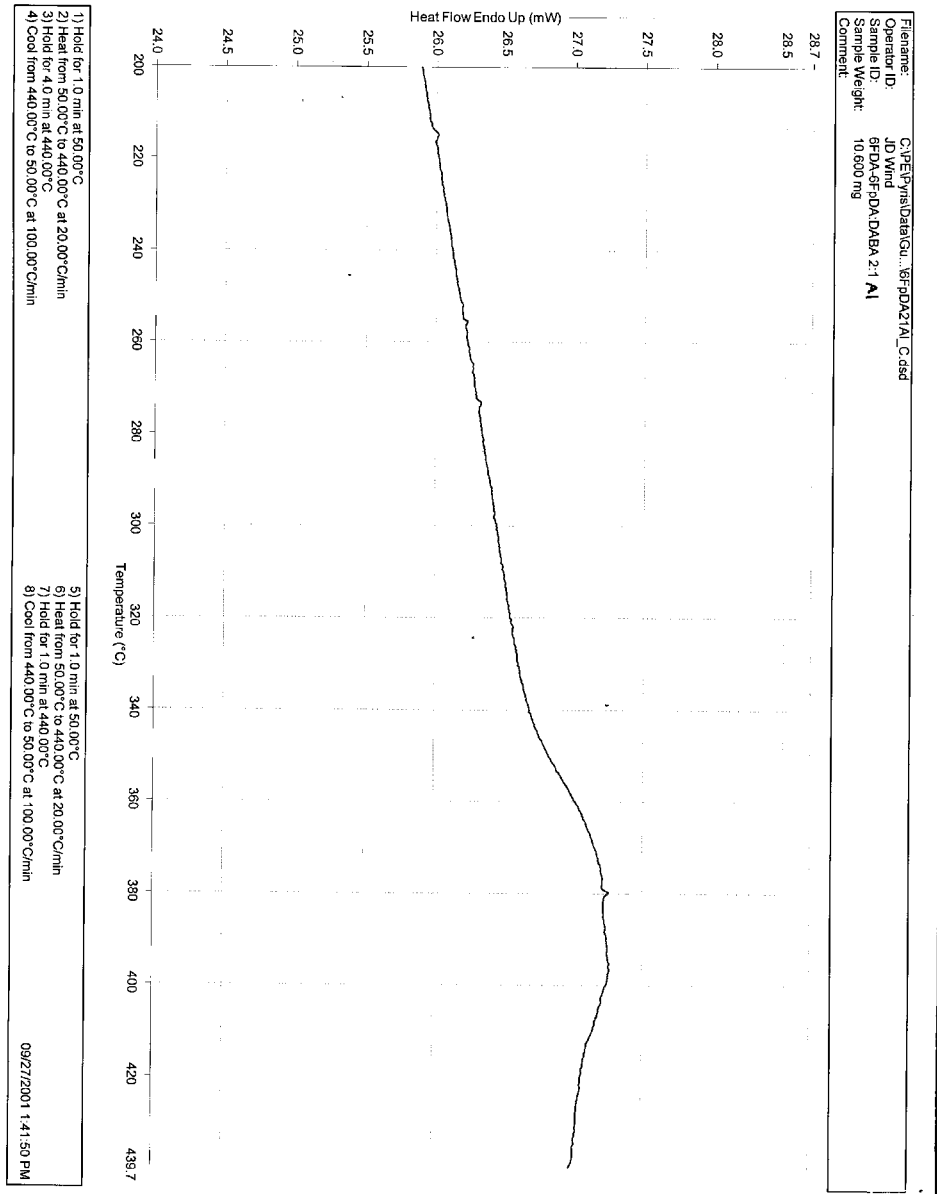

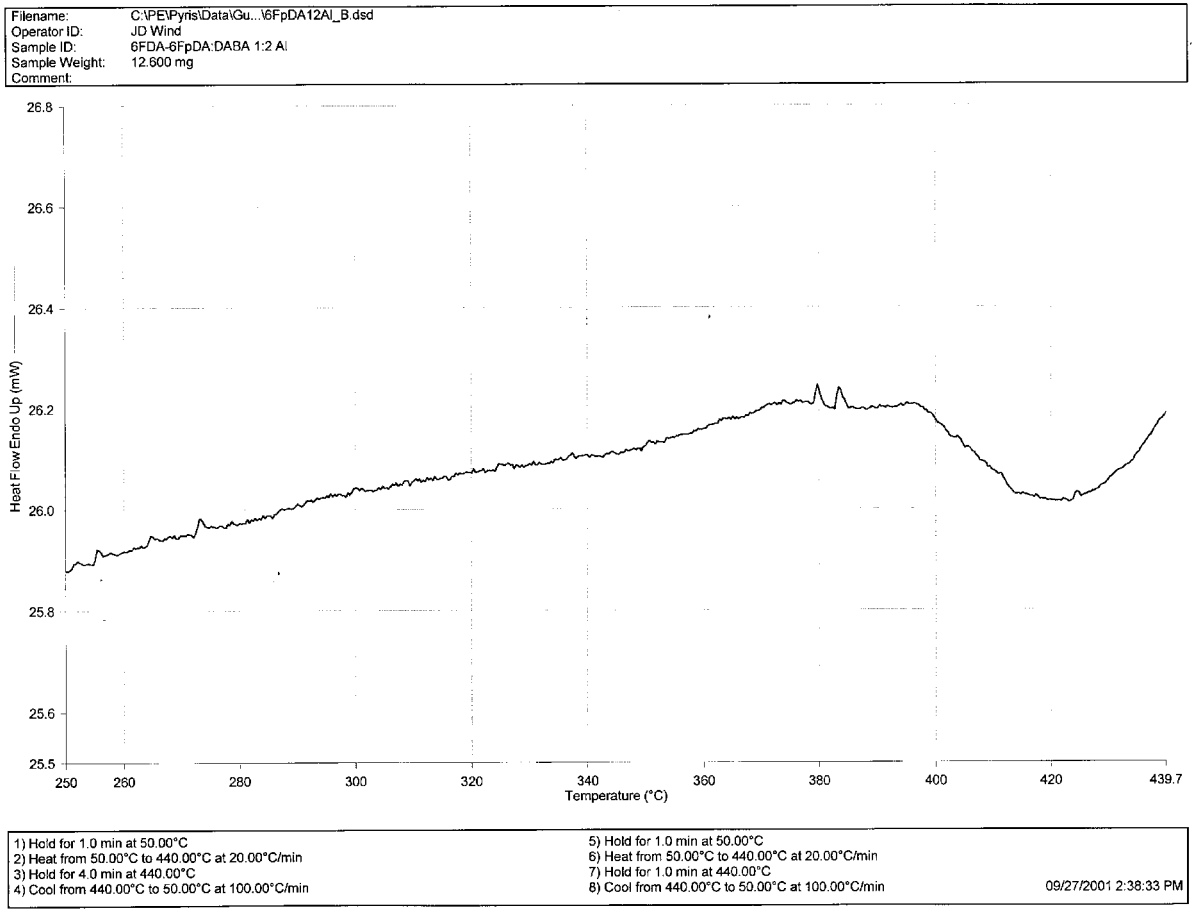
Filename: C:\PE\Pyris\Data\Gu...\6FpDA12Al_B.dsd
Operator ID: JD Wind
Sample ID: 6FDA-6FpDA:DABA 1:2 Al
Sample Weight: 12.600 mg
Comment:
Heat Flow Endo Up (mW)
26.8
26.6
26.4
26.2
26.0
25.8
25.6
25.5
250
260
280
300
320
340
360
380
400
420
439.7
Temperature (°C)
1) Hold for 1.0 min at 50.00°C
2) Heat from 50.00°C to 440.00°C at 20.00°C/min
3) Hold for 4.0 min at 440.00°C
4) Cool from 440.00°C to 50.00°C at 100.00°C/min
5) Hold for 1.0 min at 50.00°C
6) Heat from 50.00°C to 440.00°C at 20.00°C/min
7) Hold for 1.0 min at 440.00°C
8) Cool from 440.00°C to 50.00°C at 100.00°C/min
09/27/2001 2:38:33 PM

Bibliography

Akkerman, J. M., A cross-linking mechanism of poly-acrylics with aluminum compounds, XVIIeme Congres Federation d'Associations de Techniciens des Industries des Peintures, Vernis, Emaux, et Encres d'Imprimerie de l'Europe Continentale (FATIPEC), Lugano, 1984.

Al-Juaied, M., Characterization and analysis of asymmetric hollow fiber membranes for natural gas purification in the presence of heavy hydrocarbon, Separations Research Program, Austin, TX, 2002.

Azzam, R. M. A. and N. M. Bashara, *Ellipsometry and Polarized Light*, North-Holland Publishing Co., Elshevier, 1977.

Baker, R. W., Future directions of membrane gas separation technology, *Ind. Eng. Chem. Res.*, **2002**, *41*, 1393-1411.

Berens, A. R. and H. B. Hopfenberg, Diffusion and relaxation in glassy polymer powders: 2. separation of diffusion and relaxation parameters, *Polymer*, **1978**, *19*, 489-496.

Bertucco, A., M. Barolo and G. Soave, Estimation of chemical-equilibria in high-pressure gaseous systems by a modified Redlich-Kwong-Soave equation of state, *Ind. Eng. Chem. Res.*, **1995**, *34*, 3159-3165.

Bessenov, M. I. and V. A. Zubkov, *Polyamic Acids and Polyimides: Synthesis, Transformations, and Structure*, CRC Press, Boca Raton, 1993.

Bhide, B. D. and S. A. Stern, Membrane processes for the removal of acid gases from natural gas. II. effects of operating conditions, economic parameters, and membrane properties, *J. Membr. Sci.*, **1993**, *81*, 239-252.

Bhide, B. D., A. Voskericyan and S. A. Stern, Hybrid processes for the removal of acid gases from natural gas, *J. Membr. Sci.*, **1998**, *140*, 27-49.

Bolton, B. A., S. Kint, G. F. Bailey and J. R. Scherer, Ethanol sorption and partial molar volume in cellulose acetate films, *J. Phys. Chem.*, **1986**, *90*, 1207-1211.

Bos, A., I. Punt, H. Strathmann and M. Wessling, Suppression of gas separation membrane plasticization by homogeneous polymer blending, *AIChE J.*, **2001**, *47*, 1088-1093.

Bos, A., I. G. M. Punt, M. Wessling and H. Strathmann, CO_2-induced plasticization phenomena in glassy polymers, *J. Membr. Sci.*, **1999**, *155*, 67-78.

Bos, A., I. G. M. Punt, M. Wessling and H. Strathmann, Plasticization-resistant glassy polyimide membranes for CO_2/CH_4 separations, *Sep. and Purif. Tech.*, **1998**, *14*, 27-39.

Bos, A., I. G. M. Punt, M. Wessling and H. Strathmann, Suppression of CO_2-plasticization by semiinterpenetrating polymer network formation, *J. Polym. Sci., Polym. Phys. Ed.*, **1998**, *36*, 1547-1556.

Bueche, F., *Physical Properties of Polymers*, Interscience, Inc., New York, 1962.

Burns, R. L., Investigation of poly(pyrrolone-imide) materials for the olefin/paraffin separation, Ph.D. Dissertation, The University of Texas at Austin, 2002.

Chung, T.-S., E. R. Kafchinski and R. Vora, Development of a defect-free 6FDA-durene asymmetric hollow fiber and its composite hollow fibers, *J. Membr. Sci.*, **1994**, *88*, 21-36.

Cohen, M. H. and D. Turnbull, Molecular transport in liquids and glasses, *J. Chem. Phys.*, **1959**, *31*, 1164-1169.

Coleman, M. R., Isomers of fluorine-containing polyimides for gas separation membranes (glassy polymers), Ph.D. Dissertation, The University of Texas at Austin, 1992.

Coleman, M. R. and W. J. Koros, Conditioning of fluorine containing polyimides. 1. Effect of exposure to high pressure carbon dioxide on permeability, *Macromolecules*, **1997**, *30*, 6899-6905.

Coleman, M. R. and W. J. Koros, The transport-properties of polyimide isomers containing hexafluoroisopropylidene in the diamine residue, *J. Polym. Sci. Polym. Phys. Ed.*, **1994**, *32*, 1915-1926.

Conley, R. T., *Infrared Spectroscopy*, Allyn and Bacon, Inc., Boston, 1972.

Cras, J. J., C. A. Rowe-Taitt, D. A. Nivens and F. S. Ligler, Comparison of chemical cleaning methods of glass in preparation for silanization, *Biosensors & Bioelectronics*, **1999**, *14*, 683-688.

Diaz-Acosta, I., J. Baker, W. Cordes and P. Pulay, Calculated and experimental geometries and infrared spectra of metal tris-acetylacetonates: Vibrational spectroscopy as a probe of molecular structure for ionic complexes. Part i, *J. Phys. Chem. A*, **2001**, *105*, 238-244.

Dismukes, J. P., L. H. Jones and J. C. Bailar, Jr., The measurement of metal-ligand bond vibrations on acetylacetonate complexes, *J. Phys. Chem.*, **1961**, *65*, 792-795.

Djoekita, G., D. Q. Vu and W. J. Koros, Pervaporative introduction of organic vapors into high-pressure gas feeds, *J. Appl. Polym. Sci.*, **2001**, *80*, 311-315.

Doghieri, F. and G. C. Sarti, Nonequilibrium lattice fluids: a predictive model for the solubility in glassy polymers, *Macromolecules*, **1996**, *29*, 7885-7896.

Doolittle, A. K., Newtonian flow. II. the dependence of the viscosity of liquids on free space, *J. Appl. Phys.*, **1951**, *22*, 1471-1475.

Eisenberg, A., B. Hird and R. B. Moore, A new multiplet-cluster model for the morphology of random ionomers, *Macromolecules*, **1990**, *23*, 4098-4107.

Eisenberg, A. and J.-S. Kim, *Introduction to Ionomers.*, John Wiley & Sons, New York, 1998.

Ekiner, O. M., R. A. Hayes and P. Manos, Multicomponent gas separation membranes, U.S. Patent 5,085,676, E.I. du Pont de Nemours and Co., USA. 1992.

Energy Information Administration, *International Energy Outlook 2001*, DOE/EIA-0484, Washington, D.C. March 2001, p. 43.

Fang, J., H. Kita and K.-i. Okamoto, Gas permeation of hyperbranched polyimide membranes, *J. Membr. Sci.*, **2001**, *182*, 245-256.

Fleming, G. K. and W. J. Koros, Comments on measurement of gas-induced polymer dilation by different optical methods, *J. Polym. Sci.: Polym. Phys. Ed.*, **1987**, *25*, 2033-2038.

Fleming, G. K. and W. J. Koros, Dilation of polymers by sorption of carbon dioxide at elevated pressures. 1. Silicone rubber and unconditioned polycarbonate, *Macromolecules*, **1986**, *19*, 2285-2291.

Fleming, G. K. and W. J. Koros, Dilation of substituted polycarbonates caused by high-pressure carbon dioxide sorption, *J. Polym. Sci., Part B: Polym. Phys.*, **1990**, *28*, 1137-1152.

Flory, P. J., *Principles of Polymer Chemistry*, Cornell University Press, Ithaca, 1992.

Fradet, A. and E. Marechal, Kinetics and mechanisms of polyesterifications. I. Reactions of diols with diacids, *Adv. Polym. Sci.*, **1982**, *43*, 51-142.

Freeman, B. D., Basis of permeability/selectivity tradeoff relations in polymeric gas separation membranes, *Macromolecules*, **1999**, *32*, 375-380.

Fried, J. R., H. C. Liu and C. Zhang, Effect of sorbed carbon dioxide on the dynamic mechanical properties of glassy polymers, *J. Polym. Sci., Polym. Lett. Ed.* , **1989**, *27*, 385-392.

Goel, S. K. and E. J. Beckman, Nucleation and growth in microcellular materials: Supercritical CO_2 as foaming agent, *AIChE J.*, **1995**, *41*, 357-367.

Hachisuka, H., T. Sato, T. Imai, Y. Tsujita, A. Takizawa and T. Kinoshita, Glass transition temperature of glassy polymers plasticized by CO_2 gas, *Polym. J. (Tokyo)*, **1990**, *22*, 77-79.

Hayes, R. A., Highly soluble clear polyimides, U.S. Patent 4,912,197, E.I. Du Pont de Nemours and Co., 1990.

Hines, A. L. and R. N. Maddox, *Mass Transfer: Fundamentals and Applications*, Prentice Hall, Englewood Cliffs, NJ, 1985.

Hirayama, Y., T. Yoshinaga, S. Nakanishi and Y. Kusuki, Relation between gas permeabilities and structure of polyimides, in *Polymer Membranes for Gas and Vapor Separations*, American Chemical Society Symposium Series, 1999.

Hong, P. D., C. M. Chou and C. H. He, Solvent effects on aggregation behavior of polyvinyl alcohol solutions, *Polymer*, **2001**, *42*, 6105-6112.

Hong, X., Y. C. Jean, H. J. Yang, S. S. Jordan and W. J. Koros, Free-volume hole properties of gas-exposed polycarbonate studied by positron annihilation lifetime spectroscopy, *Macromolecules*, **1996**, *29*, 7859-7864.

Houde, A. Y., B. Krishnakumar, S. G. Charati and S. A. Stern, Permeability of dense (homogeneous) cellulose acetate membranes to methane, carbon dioxide, and their mixtures at elevated pressures, *J. Appl. Polym. Sci.*, **1996**, *62*, 2181-2192.

Husk, G. R., P. E. Cassidy and K. L. Gebert, Synthesis and characterization of a series of polyimides derived from 6FDA, *Macromolecules*, **1988**, *21*, 1234-1238.

Inui, K., T. Noguchi, T. Miyata and T. Uragami, Pervaporation characteristics of methyl methacrylate-methacrylic acid copolymer membranes ionically crosslinked with metal ions for a benzene/cyclohexane mixture, *J. Appl. Polym. Sci.*, **1999**, *71*, 233-241.

Ismail, A. F. and W. Lorna, Penetrant-induced plasticization phenomenon in glassy polymers for gas separation membrane, *Sep. and Purif. Tech.*, **2002**, *27*, 173-194.

Jellison, G. E., *Optical Materials*, **1992**, *1*, 41.

Jenekhe, S. A. and P. O. Johnson, Complexation-mediated solubilization and processing of rigid-chain and ladder polymers in aprotic organic solvents, *Macromolecules*, **1990**, *23*, 4419-4429.

Jizhong, R., C. Staudt-Bickel and R. N. Lichtenthaler, Separation of aromatics/aliphatics with crosslinked 6fda-based copolyimides, *Sep. and Purif. Tech.*, **2001**, *22-23*, 31-43.

Jordan, S. M. and W. J. Koros, Permeability of pure and mixed gases in silicone rubber at elevated pressures, *J. Polym. Sci.: Polym. Phys. Ed.*, **1990**, *28*, 795-809.

Kamaruddin, H. D. and W. J. Koros, Some observations about the application of Fick's first law for membrane separation of multicomponent mixtures, *J. Membr. Sci.*, **1997**, *135*, 147-159.

Kamiya, Y., K. Mizoguchi, K. Terada, Y. Fujiwara and J. S. Wang, CO_2 sorption and dilation of poly(methyl methacrylate), *Macromolecules*, **1998**, *31*, 472-478.

Kang, C.-K., Modeling of solid-state polymerization of poly(ethylene terephthalate), *J. Appl. Polym. Sci.*, **1998**, *68*, 837-846.

Kawakami, H., M. Mikawa and S. Nagaoka, Gas transport properties in thermally cured aromatic polyimide membranes, *J. Membr. Sci.*, **1996**, *118*, 223-230.

Kawakami, H., M. Mikawa and S. Nagaoka, Gas transport properties of asymmetric polyimide membrane with an ultrathin surface skin layer, *Macromolecules*, **1998**, *31*, 6636-6638.

Kazarian, S. G., Applications of FTIR spectroscopy to supercritical fluid drying, extraction, and impregnation, *Applied Spectroscopy Reviews*, **1997**, *32*, 301-348.

Kazarian, S. G., M. F. Vincent, F. V. Bright, C. L. Liotta and C. A. Eckert, Specific intermolecular interaction of carbon dioxide with polymers, *J. Am. Chem. Soc.*, **1996**, *118*, 1729-1736.

Keyse, R. J., P. Goodhew and G. W. Lorimer (Ed.), *Introduction to Scanning Transmission Electron Microscopy*, Springer-Verlag, New York, 1998.

Kim, T. H., W. J. Koros, G. R. Husk and K. C. O'Brien, Relationship between gas separation properties and chemical structure in a series of aromatic polyimides, *J. Membr. Sci.*, **1988**, *37*, 45-62.

Kirkmeyer, B. P., A. Taubert, J. S. Kim and K. I. Winey, Vesicular ionic aggregates in poly(styrene-ran-methacrylic acid) ionomers neutralized with Cs, *Macromolecules*, **2002**, *35*, 2648-2653.

Kirkmeyer, B. P., R. A. Weiss and K. I. Winey, Spherical and vesicular ionic aggregates in Zn-neutralized sulfonated polystyrene ionomers, *J. Polym. Sci.: Polym. Phys. Ed.*, **2001**, *39*, 477-483.

Kirkmeyer, B. P., K. I. Winey and R. A. Weiss, Imaging ionic aggregates in Zn-neutralized sulfonated polystyrene ionomers: shape and spatial heterogeneity, *Microsc. Microanal.*, **2000**, *6*, 1112-1113.

Kita, H., T. Inada, K. Tanaka and K.-i. Okamoto, Effect of photocrosslinking on permeability and permselectivity of gases through benzophenone-containing polyimide, *J. Membr. Sci.*, **1994**, *87*, 139-147.

Koros, W. J., R. T. Chern, V. Stannett and H. P. Hopfenberg, A model for permeation of mixed gases and vapors in glassy polymers, *J. Polym. Sci., Polym. Phys. Ed.*, **1981**, *19*, 1513-1530.

Koros, W. J. and G. K. Fleming, Membrane-based gas separation, *J. Membr. Sci.*, **1993**, *83*, 1-80.

Koros, W. J. and M. W. Hellums, Transport properties, *Encycl. Polym. Sci. Eng.*, **1990**, *Suppl. Vol.*, 724-802.

Koros, W. J. and D. R. Paul, Design considerations for measurement of gas sorption in polymers by pressure decay, *J. Polym. Sci., Polym, Phys. Ed.*, **1976**, *14*, 1903-1907.

Koros, W. J., D. R. Paul and A. A. Rocha, Carbon dioxide sorption and transport in polycarbonate, *J. Polym. Sci., Polym. Phys. Ed.*, **1976**, *14*, 687.

Krishna, R. and J. A. Wesselingh, The Maxwell-Stefan approach to mass transfer, *Chem. Eng. Sci.*, **1997**, *52*, 861-911.

Krol, J. J., M. Boerrigter and G. H. Koops, Polyimide hollow fiber gas separation membranes: Preparation and the suppression of plasticization in propane/propylene environments, *J. Membr. Sci.*, **2001**, *184*, 275-286.

Kuo, C.-T. and S.-A. Chen, Kinetics of polyesterification: Adipic acid with ethylene glycol, 1,4-butanediol and 1,6-hexanediol., *J. Polym. Sci.: Polym. Chem. Ed.*, **1989**, *27*, 2793-2803.

Kutsumizu, S., K. Tadano, Y. Matsuda, M. Goto, H. Tachino, H. Hara, E. Hirasawa, H. Tagawa, Y. Muroga and S. Yano, Investigation of microphase separation and thermal properties of noncrystalline ethylene ionomers. 2. IR, DSC, and dielectric characterization, *Macromolecules*, **2000**, *33*, 9044-9053.

Laurer, J. H. and K. I. Winey, Direct imaging of ionic aggregates in Zn-neutralized poly(ethylene-co-methacrylic acid) copolymers, *Macromolecules*, **1998**, *31*, 9106-9108.

Lewis, D. A., J. D. Summers, T. C. Ward and J. E. McGrath, Accelerated imidization reactions using microwave radiation, *J. Polym. Sci., Polym. Chem. Ed.*, **1992**, *30*, 1647-1653.

Lieser, G., S. C. Schmid and G. Wegner, Electrically conducting polymers: Preparation and investigation of oxidized poly(acetylene) by EFTEM, *J. Microsc.-Oxford*, **1996**, *183*, 53-59.

Liu, Y., X. D. Sun, X. Q. Xie and D. A. Scola, Kinetics of the crosslinking reaction of a bisnadimide model compound in thermal and microwave cure processes, *J. Polym. Sci., Polym. Chem. Ed.*, **1998**, *36*, 2653-2665.

Liu, Y., R. Wang and T.-S. Chung, Chemical cross-linking modification of polyimide membranes for gas separation, *J. Membr. Sci.*, **2001**, *189*, 231-239.

Loudon, G. M., *Organic Chemistry*, Benjamin/Cummings, Menlo Park, CA, 1988.

MacKnight, W. J., L. W. McKenna and B. E. Read, Properties of ethylene-methacrylic acid copolymers and their sodium salts: Mechanical relaxations, *J. Appl. Phys.*, **1967**, *38*, 4208-4212.

Mahajan, R., R. Burns, M. Schaeffer and W. J. Koros, Challenges in forming successful mixed matrix membranes with rigid polymeric materials, *J. Appl. Polym. Sci.*, **2002**, *86*, 881-890.

Mahajan, R. and W. J. Koros, Mixed matrix membrane materials with glassy polymers. part 2, *Polym. Eng. Sci.*, **2002**, *42*, 1432-1441.

Mallon, F. K. and W. H. Ray, Enhancement of solid-state polymerization with microwave energy, *J. Appl. Polym. Sci.*, **1998**, *69*, 1203-1212.

Matsui, S. and D. R. Paul, Pervaporation separation of aromatic/aliphatic hydrocarbons by crosslinked poly(methyl acrylate-co-acrylic acid) membranes, *J. Membr. Sci.*, **2002**, *195*, 229-245.

Mauze, G. R. and S. A. Stern, The solution and transport of water vapor in polyacrylonitrile: A re-examination, *J. Membr. Sci.*, **1982**, *12*, 51-64.

McCaig, M. S. and D. R. Paul, Effect of UV crosslinking and physical aging on the gas permeability of thin glassy polyarylate films, *Polymer*, **1999**, *40*, 7209-7225.

McCaig, M. S., D. R. Paul and J. W. Barlow, Effect of film thickness on the changes in gas permeability of a glassy polyarylate due to physical aging part II. mathematical model, *Polymer*, **2000**, *41*, 639-648.

McLean, R. S., M. Doyle and B. B. Sauer, High resolution imaging of ionic domains and crystal morphology in ionomers using AFM techniques, *Macromolecules*, **2000**, *33*, 6541-6550.

Meyer, H. S., Volume and distribution of subquality natural gas in the United States, Gas Research Institute, *Gas tips*, 2000.

Michaels, A. S., W. R. Vieth and J. A. Barrie, Solution of gases in polyethylene terephthalate, *J. Appl. Phys.*, **1963**, *34*, 1.

Michels, A. and J. Hamers, The effect of pressure on the refractive index of carbon dioxide, *Physica*, **1937**, *4*, 995-1006.

Mikawa, M., S. Nagaoka and H. Kawakami, Gas permeation stability of asymmetric polyimide membrane with thin skin layer: effect of molecular weight of polyimide, *J. Membr. Sci.*, **2002**, *208*, 405-414.

Nagel, C., K. Guenther-Schade, D. Fritsch, T. Strunskus and F. Faupel, Free volume and transport properties in highly selective polymer membranes, *Macromolecules*, **2002**, *35*, 2071-2077.

National Research Council, *Separations Technologies for the Industries of the Future*, National Academy Press, Washington D.C., 1998.

Nielsen, L. E., Crosslinking - effect on physical properties of polymers, *J. Macromol. Sci., Rev. Macromol. Chem.*, **1969**, *3*, 69-103.

O'Brien, K. C., W. J. Koros, T. A. Barbari and E. S. Sanders, A new technique for the measurement of multicomponent gas transport through polymeric films, *J. Membr. Sci.*, **1986**, *29*, 229-238.

Obriot, J., J. Ge, T. K. Bose and J. M. St-Arnaud, Determination of the density from simultaneous measurements of the refractive index and the dielectric constant of gaseous CH_4, SF_6, CO_2, *Fluid Phase Equilibria*, **1993**, *86*, 315-350.

O'Connell, E. M., D. G. Peiffer, T. W. Root and S. L. Cooper, Morphological studies of lightly sulfonated polystyrene using Na-23 NMR: effects of polydispersity in molecular weight, *Macromolecules*, **1996**, *29*, 2124-2130.

O'Connell, E. M., T. W. Root and S. L. Cooper, Morphological-studies of lightly sulfonated polystyrene using Na-23 NMR.2. effects of solution casting, *Macromolecules*, **1995**, *28*, 3995-3999.

O'Connell, E. M., T. W. Root and S. L. Cooper, Morphological-studies of lightly sulfonated polystyrene using Na-23 NMR.3. effects of humidification and annealing, *Macromolecules*, **1995**, *28*, 4000-4006.

O'Connell, E. M., T. W. Root and S. L. Cooper, Morphological-studies of lightly-sulfonated polystyrene using Na-23 NMR.1. effects of sample composition, *Macromolecules*, **1994**, *27*, 5803-5810.

Ohya, H., T. Higashijima, Y. Tsuchiya, H. Tokunaga and Y. Negishi, Separation of supercritical carbon dioxide and isooctane mixtures with an asymmetric polyimide membrane, *J. Membr. Sci.*, **1993**, *84*, 185-189.

Okamoto, K., K. Noborio, J. Hao, K. Tanaka and H. Kita, Permeation and separation properties of polyimide membranes to 1,3-butadiene and n-butane, *J. Membr. Sci.*, **1997**, *134*, 171-179.

Ono, K., M. Nishinaka and R. Akahori, Metal-containing polyamic acid compositions, polyimide films, their manufacture, polyimide moldings, and flexible printed circuit boards thereof, U.S. Patent 6,207,739, Kanegafuchi Chemical Industry Co., Ltd., Japan., 1999.

Parson, E. A. and D. W. Keith, Fossil fuels without CO_2 emissions, *Science*, **1998**, *282*, 1053-1054.

Paul, D. R. and O. M. Ebra-Lima, Pressure-induced diffusion of organic liquids through highly swollen polymer membranes, *J. Appl. Polym. Sci.*, **1970**, *14*, 2201-2224.

Peng, D. and D. B. Robinson, New 2-constant equation of state, *Ind. & Eng. Chem. Fund.*, **1976**, *15*, 59-64.

Pennycook, S. J., Z-contrast STEM for materials science, *Ultramicroscopy*, **1989**, *30*, 58-69.

Philipp, H. R., Silicon dioxide (sio_2)(glass), in *Handbook of Optical Constants of Solids*, Harcourt Brace Jovanovich, Orlando, 1985.

Punsalan, D. T., A sorption and dilation investigation of amorphous glassy polymers and physical aging, Ph.D. Dissertation, The University of Texas at Austin, 2001.

Rancourt, J. D. and L. T. Taylor, Preparation and properties of surface-conductive polyimide films via in situ codeposition of metal salts, *Macromolecules*, **1987**, *20*, 790-795.

Ratcliffe, C. T., A. Diaz, C. Nopasit and G. Munoz, Application of membranes in co_2 separation from natural gas: pilot plant tests on offshore platforms, presented at Laurence Reid Gas Conditioning Conference, Norman, OK, Feb. 21-24, 1999.

Rezac, M. E. and B. Schoberl, Transport and thermal properties of poly(ether imide)/acetylene-terminated blends, *J. Membr. Sci.*, **1999**, *156*, 211.

Rezac, M. E., E. T. Sorensen and H. W. Beckman, Transport properties of crosslinkable polyimide blends, *J. Membr. Sci.*, **1997**, *136*, 249-259.

Robeson, L. M., Correlation of separation factor versus permeability for polymer membranes, *J. Membr. Sci.*, **1991**, *62*, 165-185.

Rosolovsky, J., R. K. Boggess, A. F. Rubira, L. T. Taylor, D. M. Stoakley and A. K. St. Clair, Supercritical fluid infusion of silver into polyimide films of varying chemical composition, *J. Mater. Res.*, **1997**, *12*, 3127-3133.

Salley, J. M. and C. W. Frank, Charge transfer in aromatic polyimides, in *Polyimides: Fundamentals and applications*, Marcel Dekker, Inc., New York, 1996.

Salley, J. M., C. W. Frank, T. Miwa and R. Roginski, Charge transfer in polyimides, *Adv. Polyimide Sci. Technol., Proc. Int. Conf. Polyimides, 4th*, **1993**, 441-450.

Sanchez, I. C. and R. H. Lacombe, Statistical thermodynamics of polymer-solutions, *Macromolecules*, **1978**, *11*, 1145-1156.

Sanders, E. S., Penetrant-induced plasticization and gas permeation in glassy polymers, *J. Membr. Sci.*, **1988**, *37*, 63-80.

Sanders, E. S. and W. J. Koros, Sorption of carbon dioxide, ethylene, nitrous oxide and their binary mixtures in poly(methyl methacrylate), *J. Polym. Sci., Polym. Phys. Ed.*, **1986**, *24*, 175-188.

Sauer, B. B. and R. S. McLean, AFM and X-ray studies of crystal and ionic domain morphology in poly(ethylene-co-methacrylic acid) ionomers, *Macromolecules*, **2000**, *33*, 7939-7949.

Sawada, T. and S. Ando, Synthesis, characterization, and optical properties of metal-containing fluorinated polyimide films, *Chem. Mater.*, **1998**, *10*, 3368-3378.

Schell, W. J., C. G. Wensley, M. S. K. Chen, K. G. Venugopal, B. D. Miller and J. A. Stuart, Recent advances in cellulosic membranes for gas separation and pervaporation, *Gas Sep. Purif.*, **1989**, *3*, 162-169.

Schultz, J. M., S. Fakirov, *Solid State Behavior of Linear Polyesters and Polyamides*, Prentice Hall, Englewood Cliffs, NJ, 1990.

Schwartz, L. H. and H. B. Cohen, *Diffraction from Materials*, Academic Press, New York, 1977.

Sefcik, M. D., Dilation of polycarbonate by carbon dioxide, *J. Polym. Sci., Polym. Phys. Ed.*, **1986**, *24*, 935-956.

Sefcik, M. D. and J. Schaefer, Solid-state ^{13}C NMR evidence for gas-polymer interactions in the carbon dioxide-poly(vinyl chloride) system, *J. Polym. Sci.: Polym. Phys. Ed.*, **1983**, *21*, 1055-1062.

Shim, J. J. and K. P. Johnston, Adjustable solute distribution between polymers and supercritical fluids, *AIChE J.*, **1989**, *35*, 1097-1106.

Silverstein, R. M. and F. X. Webster, *Spectrometric Identification of Organic Compounds, 6th edition*, John Wiley and Sons, Inc., New York, 1997.

Singla, S., H. W. Beckman and M. E. Rezac, Localized chain mobility and gas transport properties of thermoplastic aromatic polymers, *J. Membr. Sci.*, **2002**, *208*, .257-267.

Sirard, S. M., P. F. Green and K. P. Johnston, Spectroscopic ellipsometry investigation of the swelling of poly(dimethylsiloxane) thin films with high pressure carbon dioxide, *J. Phys. Chem. B*, **2001**, *105*, 766-772.

Sirard, S. M., K. J. Ziegler, I. C. Sanchez, P. F. Green and K. P. Johnston, Anomalous properties of poly(methyl methacrylate) thin films in supercritical carbon dioxide, *Macromolecules*, **2002**, *35*, 1928-1935.

Spillman, R., Economics of gas separation membrane processes, in *Membrane Separations Technology. Principles and Applications*, Elsevier Science, 1995.

St. Clair, A. K. and T. L. St.. Clair, Highly optically transparent/colorless aromatic polyimide film, U.S. Patent 643,589, United States National Aeronautics and Space Administration, 1985.

St. Clair, A. K. and L. T. Taylor, A comparison of physical and mechanical properties of polyimide films containing different metal ions, *J. Appl. Polym. Sci.*, **1983**, *28*, 2393-2400.

Staudt-Bickel, C. and W. J. Koros, Improvement of CO_2/CH_4 separation characteristics of polyimides by chemical crosslinking, *J. Membr. Sci.*, **1999**, *155*, 145-154.

Staudt-Bickel, C. and W. J. Koros, Olefin/paraffin gas separations with 6FDA-based polyimide membranes, *J. Membr. Sci.*, **2000**, *170*, 205-214.

Stern, S. A. and V. Saxena, Concentration-dependent transport of gases and vapors in glassy polymers, *J. Membr. Sci.*, **1980**, *7*, 47-59.

Struk, L. G. F., Segmental mobility model for diffusion of gases in polymers, *J. Polym. Sci.: Polym. Phys. Ed.*, **1990**, *28*, 127-131.

Takekoshi, T., Synthesis of polyimides, in *Polyimides: Fundamentals and Applications*, Marcel Dekker, Inc., New York, 1996.

Tanaka, K., H. Kita and K.-I. Okamoto, Sorption of carbon dioxide in fluorinated polyimides, *J. Polym. Sci.: Polym. Phys. Ed.*, **1993**, *31*, 1127-1133.

Tanaka, K., A. Taguchi, J. Hao, H. Kita and K. Okamoto, Permeation and separation properties of polyimide membranes to olefins and paraffins, *J. Membr. Sci.*, **1996**, *121*, 197-207.

Tanikella, R. V., S. A. Bidstrup Allen and P. A. Kohl, Variable-frequency microwave curing of benzocyclobutene, *J. Appl. Polym. Sci.*, **2002**, *83*, 3055-3067.

Taubert, A. and K. I. Winey, Imaging and X-ray microanalysis of a poly(ethylene-ran-methacrylic acid) ionomer melt neutralized with sodium, *Macromolecules*, **2002**, *35*, 7419-7426.

Taubert, A. and K. I. Winey, Quantitative determination of the local chemical composition in a Zn-neutralized (pe-ran-maa) ionomer using X-ray energy dispersive spectroscopy, *Polym. Mater. Sci. Eng.*, **2002**, *87*, 182-183.

Thompson, D. W., M. L. Caplan and A. K. St. Clair, Reflective self-metalizing polyimide films, U.S. Patent 5,677,418, United States National Aeronautics and Space Administration, USA, 1997.

Tompkins, H. G. and W. A. McGahan, *Spectroscopic Ellipsometry and Reflectometry*, John Wiley & Sons, Inc., New York, 1999.

Vu, D. Q., Formation and characterization of asymmetric carbon molecular sieve and mixed matrix membranes for natural gas purification, Ph.D. Dissertation, The University of Texas at Austin, 2001.

Wachsman, E. D. and C. W. Frank, Effect of cure history on the morphology of polyimide: fluorescence spectroscopy as a method for determining the degree of cure, *Polymer*, **1988**, *29*, 1191-1197.

Wallace, D. W., Crosslinked hollow fiber membranes:implementation challenges and solutions for natural gas processing, Separations Research Program, Austin, TX, 2002.

Wessling, M., I. Huisman, T. v. d. Boomgaard and C. A. Smolders, Dilation kinetics of glassy, aromatic polyimides induced by carbon dioxide sorption, *J. Polym. Sci.: Polym. Phys. Ed.*, **1995**, *33*, 1371-1384.

Wessling, M., M. L. Lopez and H. Strathmann, Accelerated plasticization of thin-film composite membranes used in gas separation, *Sep. and Purif. Tech.*, **2001**, *24*, 223-233.

Wessling, M., S. Schoeman, T. v. d. Boomgaard and C. A. Smolders, Plasticization of gas separation membranes, *Gas Sep. and Purif.*, **1991**, *5*, 222-228.

White, L. S., T. A. Blinka, H. A. Kloczewski and I.-f. Wang, Properties of a polyimide gas separation membrane in natural gas streams, *J. Membr. Sci.*, **1995**, *103*, 73-82.

Williams, C. E., C. Colliex, J. Horrion and R. Jerome, Scanning-transmission electron-microscopy to observe ionic domains in model ionomers, *ACS Symposium Series*, **1989**, *395*, 439-444.

Williams, D. B. and C. E. Carter, *Transmission Electron Microscopy-A Textbook for Materials Science*, Plenum Press, New York, 1996.

Winey, K. I., J. H. Laurer and B. P. Kirkmeyer, Ionic aggregates in partially Zn-neutralized poly(ethylene-ran-methacrylic acid) ionomers: shape, size, and size distribution, *Macromolecules*, **2000**, *33*, 507-513.

Wissinger, R. G. and M. E. Paulaitis, Molecular thermodynamic model for sorption and swelling in glassy polymer-carbon dioxide systems at elevated pressures, *Ind. Eng. Chem. Res.*, **1991**, *30*, 842-851.

Wissinger, R. G. and M. E. Paulaitis, Swelling and sorption in polymer-CO_2 mixtures at elevated pressures, *J. Polym. Sci., Polym. Phys. Ed.*, **1987**, *25*, 2497-2510.

Wright, C. T. and D. R. Paul, Gas sorption and transport in UV-irradiated polyarylate copolymers based on tetramethyl bisphenol-A and dihydroxybenzophenone, *J. Membr. Sci.*, **1997**, *124*, 161-174.

Yarusso, D. J. and S. L. Cooper, Analysis of SAXS data from ionomer systems, *Polymer*, **1985**, *26*, 371-378.

Yarusso, D. J. and S. L. Cooper, Microstructure of ionomers - interpretation of small-angle X- ray-scattering data, *Macromolecules*, **1983**, *16*, 1871-1880.

Yuan, J. P., H. Cao, E. W. Hellmuth and Y. C. Jean, Subnanometer hole properties of CO_2-exposed polysulfone studied by positron annihilation lifetime spectroscopy, *J. Polym. Sci. Polym. Phys. Ed.*, **1998**, *36*, 3049-3056.

Zhou, S. and S. A. Stern, The effect of plasticization on the transport of gases in and through glassy polymers, *J. Polym. Sci. Polym. Phys. Ed.*, **1989**, *27*, 205-222.

Zimmerman, C. M., Advanced gas separation membrane materials: Hyper rigid polymers and molecular sieve-polymer mixed matrices, Ph.D. Dissertation, The University of Texas at Austin, 1998.

Vita

John D. Wind was born on January 13, 1973 in South Bend, IN, as the son of Joseph and Glenda Wind. He graduated from Clay High School in South Bend in May 1991. In May 1996, he obtained a Bachelor of Science in Chemical Engineering from Purdue University and a co-op certificate for working five semesters with Lyondell Petrochemical Co. in Houston, TX. John worked with Air Products and Chemicals, Inc. as a process engineer for two years after Purdue, before entering graduate school at the University of Texas at Austin in August 1998. In December 2000, he completed the requirements for a Master of Science degree in Chemical Engineering. John earned a Doctor of Philosophy degree in Chemical Engineering in December 2002. Following graduation, he began a post-doctoral research position at the University of Washington in the area of photovoltaic polymers for solar power technology.

Permanent address: 17904 Ashmont Place
South Bend, IN 46635-1077

This dissertation was typed by the author.